# Ion Transport Mechanisms in Bipolar Membranes for Electrochemical Applications

Blommaert, M.A.

**DOI**
10.4233/uuid:328a62be-28f0-4f7c-bc91-ee74479adb34

**Publication date**
2021

**Document Version**
Final published version

**Citation (APA)**
Blommaert, M. A. (2021). *Ion Transport Mechanisms in Bipolar Membranes for Electrochemical Applications*. [Dissertation (TU Delft), Delft University of Technology]. https://doi.org/10.4233/uuid:328a62be-28f0-4f7c-bc91-ee74479adb34

# ION TRANSPORT MECHANISMS IN BIPOLAR MEMBRANES FOR ELECTROCHEMICAL APPLICATIONS

# ION TRANSPORT MECHANISMS IN BIPOLAR MEMBRANES FOR ELECTROCHEMICAL APPLICATIONS

## Proefschrift

ter verkrijging van de graad van doctor
aan de Technische Universiteit Delft,
op gezag van de Rector Magnificus Prof.dr.ir. T.H.J.J. van der Hagen,
voorzitter van het College voor Promoties,
in het openbaar te verdedigen op 15 september 2021 om 15:00 uur

door

**Marijn Antoon BLOMMAERT**

Master of Science in Chemical Engineering,
Katholieke Universiteit Leuven, België,
geboren te Delft, Nederland.

This dissertation has been approved by

promotor: Dr. W.A. Smith
copromotor: Dr.ir. D.A. Vermaas

Composition of the doctoral committee:

| | |
|---|---|
| Rector Magnificus, | chairman |
| Dr. W.A. Smith, | Technische Universiteit Delft, promotor |
| Dr.ir. D.A. Vermaas, | Technische Universiteit Delft, copromotor |
| | |
| *Independent members:* | |
| Dr. T.A. Andreu | Universitat de Barcelona, Spain |
| Prof.dr.ir. B. van der Bruggen | Katholieke Universiteit Leuven, Belgium |
| Prof.dr. M.T.M. Koper | Universiteit Leiden |
| Prof.dr. A. Urakawa | Technische Universiteit Delft |
| Prof.dr.ir. J.T. Padding, | Technische Universiteit Delft |

This research received funding from the Netherlands Organization for Scientific Research (NWO) under project number 733.000.008 in the framework of the Solar to Products programme co-funded by Shell Global Solutions International B.V.


*Keywords:* Bipolar membrane, electrolysis, $CO_2$ reduction, ion crossover, electrochemical impedance spectroscopy

*Printed by:* GVO drukkers & vormgevers B.V.

*Front & Back:* Design by Anna Haers, Bruno Bertolina & Marijn Blommaert.



ISBN 978-94-6384-251-8

An electronic version of this dissertation is available at
http://repository.tudelft.nl/.

# CONTENTS

# 1

# GENERAL INTRODUCTION

1

## 1.1. NECESSITY FOR A SHIFT TOWARDS RENEWABLE ENERGY

Imagine a world without fumes from exhausts, no smog, no oil leaks in the ocean. Imagine cars driven on electricity, plastic is completely recycled, airplanes fly on hydrogen or bio-fuels. For the moment no more than aspirations, in the future strongly needed. What all these innovative changes share is that the focus is shifted from fossil fuels as the primary energy source to renewable energy sources. These new energy sources, like wind and solar energy, enable a transition to an electron-based society, where electricity replaces the role of fossil fuels.

For the required chemicals and fuels that cannot be easily electrified, electrochemistry is the ideal technology for the conversion of raw materials powered via electrons to commodity products that are the basis of day-to-day products. While the best known example of electrochemistry are batteries, another example is the production of renewable hydrogen via water electrolysis where water is split into hydrogen and oxygen. While this is currently driven by natural gas, now renewable energy can be used. The hydrogen can then be used for a multitude of applications, ranging from fuel cells, heating devices to production of gasoline from a mixture of carbon monoxide and hydrogen via the Fischer-Tropsch process.

The transition to an electron-based society is already progressing, as 2020 was the first year in Europe where more renewable electricity was produced (38% of the electricity) than energy originating from fossil fuels (37%). [1] This positive news should inspire scientists, engineers, policymakers, businesses and citizens to further accelerate and promote the growth of renewable energy to reduce the carbon dioxide emissions linked to energy production. A reduction in emission of greenhouse gases (of which 80% is $CO_2$) is essential to meet the goals of the Paris treaty on climate change that sets the limit for the global warming at a 2 °C increase compared to pre-industrial level. The Green Deal of the European Union aims to reach net-zero greenhouse gas emissions by 2050.

Currently, half of the renewable electricity production comes from wind and solar and that share increased by 10% in 2020. [1] The amount of electricity that can be produced through wind and sun varies on a daily but also seasonal basis: peak productions are a six-fold of the average production. [2] To be able to ensure continuity and a balance between production and demand on the electricity grid, buffers are needed. The buffering of electricity production should be a combination of different technologies. A part can be covered via household and industry energy management that will use electricity when there is sufficient supply. Other solutions are to store overproduction of electricity via hydro dams. As mentioned before, also electrochemical technologies can help in buffering the volatility by storing electricity in chemical bonds. Batteries (e.g. Li-ion batteries) are suitable for short term storage of electrical energy, while electrolysers are interesting for long-term storage due to the stability of these molecules.

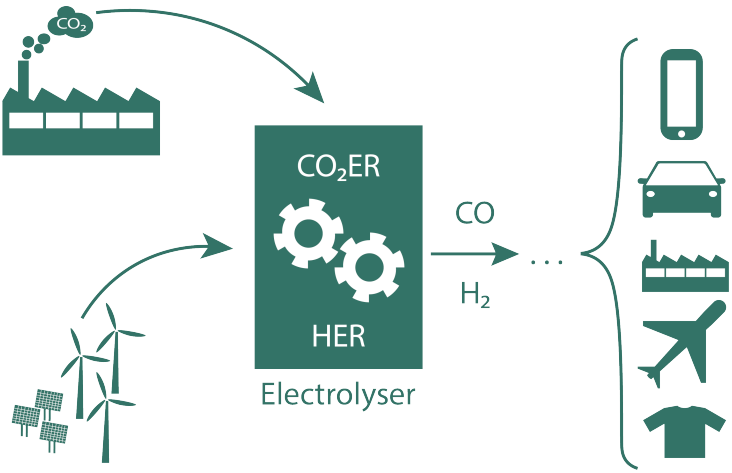


Figure 1.1: Schematic of the role of electrochemistry in an electron-based society powered by renewable electricity, where the required carbon sources come from carbon capture, e.g. from point sources like cement factories. Electrochemical reactions, like the electrochemical reduction of carbon dioxide ($CO_2$ER) and hydrogen evolution reaction (HER), provide commodity chemicals, which can then be used for various products made from plastic (like phone components or fibres for clothing), or fuels for e.g. cars and planes.

Some technologies in electrolysis, like the chloralkali process to produce chlorine, are already a century-old. More recent applications, like water and $CO_2$ electrolysis or ammonia synthesis, focus on the production of commodity products (carbon monoxide, ethylene) or alternative fuels (hydrogen, ammonia) to replace fossil fuels. The commodity products can then be further converted into a wide range of carbon-based products, as can be seen in Figure 1.1. By starting from $CO_2$ electrolysers powered by renewable energy a $CO_2$ neutral process can be achieved, contributing to the goal of becoming climate neutral, therefore the interest in electrochemistry has spiked in recent years.

## 1.2. ELECTROCHEMISTRY

Electrochemistry is performed in an electrochemical cell, which consists of minimally two electrically connected electrodes surrounded by an electrolyte, enabling ionic transport. [3] Electrochemical half-reactions take place at the electrode-electrolyte interface, where often a catalyst is used to enhance the performance. The electrolyte can either be in liquid (e.g., aqueous salt solution or ionic liquids), in solid form (e.g., ion exchange membrane) or a combination of both. Ideally, an electrolyte is highly conductive and does not interfere negatively with the catalyst. In addition, product separation from both electrodes is necessary to have a high purity and avoid potential dangerous mixtures (e.g., hydrogen and oxygen). An ideal

candidate to ensure all these requirements is to implement a membrane with or without a liquid electrolyte. Many different types of membranes exist, which can separate mixtures based on characteristics such as size, affinity, charge, etc of the species. [4] In the next section, we concentrate on the previous mentioned ion exchange membranes that separate mixtures based on charge.

## 1.3. ION EXCHANGE MEMBRANES

Ion exchange membranes are most often made from a polymeric backbone structure given its low price and ease in production. On that backbone structure charged functional groups are placed, which determine its selectivity. A driving force (e.g. concentration gradient or electric field) will enable ion transport through the membrane, and can therefore be considered as a solid electrolyte. Such a membrane has a certain conductivity, depending on the amount of fixed charges on the backbone. [5] Ideally, an ion exchange membrane has a high permeance (i.e. the ability to allow the transport of certain species across the membrane) and selectivity, as well as good chemical, thermal and mechanical stability. In reality, the membranes will not be able to comply to all these requirements, and therefore the following parameters are used to differentiate between akin membranes:

- Membrane material properties:
  - Fixed charge density ($X$): The amount of ion exchange groups bonded to the polymer structure (in $meq./g_{H_2O}$), which can be calculated from the ion exchange concentration over the swelling degree (ratio of extra water uptake weight over the dry membrane weight) [6].
  - Thickness ($\delta$): The length of the membrane perpendicular to the electrode surface. The thicker the membrane, the slower the diffusion which is inversely related to the thickness (Fick's law).
- Membrane benchmark aspects:
  - (Perm)selectivity ($\alpha$): The ability of the membrane to selectively allow ionic species, which depends on the concentration and mobility of those species [7].
  - Conductivity ($\sigma$): The measure of the ability to transport ions through the membrane at a certain driving force, based on the concentration and the mobility of the ions ($\sigma = Fz^2c\mu$) [8].

Further distinction among ion exchange membranes can be made based on the charge sign of the fixed ionic charges, as shown in Figure 1.2. The functional groups are either positive or negative, and selective towards their opposite charge, classifying it as an anion exchange membrane (AEM) or cation exchange membrane (CEM), respectively. A third type of an ion exchange membrane is a combination of a cation exchange layer and an anion exchange layer. When those two membrane

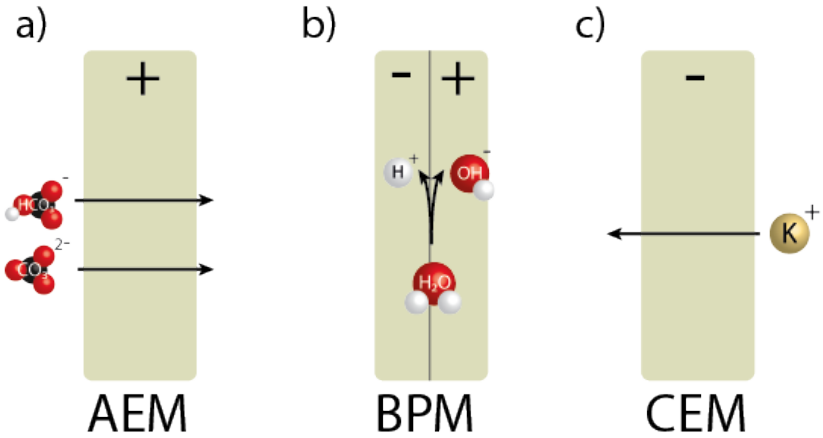


Figure 1.2: Three different types of ion exchange membranes, with (a) anion exchange membrane (AEM), which is selective for negatively charged species like carbonate ($CO_3^{2-}$) and bicarbonate ($HCO_3^-$) ions, (b) bipolar membrane (BPM), which (due to its opposing layer configuration) performs water dissociation into protons ($H^+$) and hydroxide ions ($OH^-$), and (c) cation exchange membrane (CEM), which is selective for cations, like potassium ($K^+$).

layers are laminated together a bipolar membrane (BPM) is formed. This configuration allows the ability to arrange the transport and has several advantages, as will be elaborated further on. In between the two membrane layers is an interface layer (IL), which features an abrupt fixed charge change with a catalyst deposited on it. [9] This bipolar membrane is the main subject of this thesis, and its practical operation is introduced in Chapter 2. The cation and anion exchange membranes are introduced below.

A cation exchange membrane is permselective for positively charged species, like $H^+$ or $Na^+$. When the membrane is selective for protons, it is called proton exchange membrane (PEM). Nafion® is a well-known example, made of a perfluorinated polymer with sulfonic acid groups as functional groups. The main advantage of Nafion membranes is the great stability in a wide range of environments while maintaining a strong proton conductivity. Nevertheless, above 80 °C their performance decreases. Another disadvantage is their high cost. Therefore, currently CEMs are being developed which are made of cheaper materials, hydrocarbon polymers, with a higher thermal stability [10].

An anion exchange membrane is selective for negatively charged species, like $OH^-$ or $Cl^-$. AEMs contain cationic fixed charges covalently bonded with the polymer backbone structure. The backbone structure can be made of several polymers, such as poly(arylene ethers), poly(ether imides) or poly ketones [11]. The fixed cationic species are often N-groups, like quaternary (—$NR_4^+$) or ternary (—$NHR_3^+$) groups,

where $R$ can be an alkyl or aryl group. AEMs have a lower stability and low $OH^-$ conductivity compared to the proton conductivity in their Nafion counterpart. The functional groups can be subject to degradation reactions and have the potential to lower the fixed charge density over time [11]. Recently, progress has been achieved in obtaining an ionic conductivity similar to proton exchange membranes although a good chemical stability still remains a challenge [12].

In electrochemical processes, there are minimally two half-reactions occurring at the two electrodes. Often, half-reactions perform optimally in different conditions in the form of composition, concentration or pH of the electrolyte. However, separation of two electrolytes with different pH or composition is not possible for the monopolar membranes (AEM and CEM). To the contrary, a bipolar membrane is perfectly suited for this task, allowing the ability to optimize each electrode compartment separately.

## 1.4. THESIS OUTLINE AND RESEARCH QUESTIONS

Implementing bipolar membranes in electrochemical applications has multiple advantages, not only does it act as a product separator, it will also ensure a chemical stability between the different compartments in an electrochemical cell. Although the bipolar membrane has a great potential in electrochemical energy applications, it has few applications at industrial scale. Current bipolar membranes are designed for acid/base production and have not been optimized for other applications, such as electrolysis and resource recovery. To be fully deployed in this field further development and knowledge is required. Therefore, the following research questions are addressed in this thesis:

- What are the main challenges to implement BPMs in industrial electrochemical energy systems? (Chapter 2)
- What is the role of the presence of co-ions at the interface of a BPM in performing the water dissociation reaction? (Chapter 3)
- What is the effect of the electrolytes on the stability of a BPM? (Chapter 3)
- What is the relative ion crossover through a BPM in function of current density, pKa, membrane functionality and ion size? (Chapter 4)
- What is the ion transport mechanism in a bipolar membrane electrode assembly configuration for $CO_2$ reduction depending on the orientation of a BPM? (Chapter 5)
- What is the energy required to produce CO via $CO_2$ reduction in a BPM-run cell versus an AEM-run cell? (Chapter 6)

These research questions are addressed throughout the thesis. Firstly, in Chapter 2 an introduction on bipolar membranes is given, as well as its applications. In this

chapter also future requirements are listed to further develop these membranes. The following chapters are focused on the ion transport of the bipolar membrane. In Chapter 3 electrochemical impedance spectroscopy is used as a technique to study the water dissociation reaction in function of the surrounding electrolytes. In Chapter 4, the crossover of these surrounding electrolytes is the subject of the study. For this, several catholytes are tested in function of current density, pKa, valence and ion size. Then, Chapter 5 focuses on the use of a bipolar membrane in a membrane electrode assembly. With this assembly, the effect of the orientation of the BPM was studied on the carbon and ion transport in a $CO_2$ reduction electrolyser. Finally, in Chapter 6 the bipolar membrane is compared with an anion exchange membrane, the current state-of-the-art in this field. The study is performed in a $CO_2$ electrolysis cell, for which the AEM serves as the benchmark. The comparison is based on the required energy to produce carbon monoxide.

1

# REFERENCES


[1] Agora Energiewende and Ember, *The European Power Sector in 2020: Up-to-Date Analysis on the Electricity Transistion*, Tech. Rep. (2021).

[2] H. W. Sinn, *Buffering volatility: A study on the limits of Germany's energy revolution*, European Economic Review **99**, 130 (2017).

[3] A. J. Bard and L. R. Faulkner, *Electrochemistry* (Wiley, 1944) p. 850, arXiv:1011.1669v3 .

[4] B. Van der Bruggen, *Membrane Technology*, in *Kirk-Othmer Encyclopedia of Chemical Technology*, Major Reference Works (2017).

[5] T. Sata, *Ion exchange membranes : preparation, characterization, modification and application* (Royal Society of Chemistry, Cambridge, 2004).

[6] P. E. Dlugolecki, *Mass transport in reverse electrodialysis for sustainable energy generation* (2009) p. 200.

[7] L. Giorno, E. Drioli, and H. Strathmann, *Permselectivity of Ion-Exchange Membranes (Encyclopedia of Membranes)*, (Springer Berlin Heidelberg, Berlin, Heidelberg, 2015).

[8] H.Strathmann, J.J.Krol, H.J.Rapp, and G.Eigenberger, *Limiting current density and water dissociation in bipolar membranes*, Journal of Membrane Science **125**, 123 (1997).

[9] F. G. Wilhelm, *Bipolar Membrane Electrodialysis* (2001) p. 242.

[10] R. S. Yee, R. A. Rozendal, K. Zhang, and B. P. Ladewig, *Cost effective cation exchange membranes: A review*, Chemical Engineering Research and Design **90**, 950 (2012).

[11] J. R. Varcoe, P. Atanassov, D. R. Dekel, A. M. Herring, M. A. Hickner, P. A. Kohl, A. R. Kucernak, W. E. Mustain, K. Nijmeijer, K. Scott, and L. Zhuang, *Anion-exchange membranes in electrochemical energy systems*, Energy & Environmental Science **7**, 3135 (2014).

[12] C. G. Arges and L. Zhang, *Anion Exchange Membranes' Evolution toward High Hydroxide Ion Conductivity and Alkaline Resiliency*, ACS Applied Energy Materials **1**, 2991 (2018).

# 2

# INSIGHTS AND CHALLENGES FOR APPLYING BIPOLAR MEMBRANES IN ADVANCED ELECTROCHEMICAL ENERGY SYSTEMS

*Bipolar membranes (BPMs) are gaining interest in energy conversion technologies. These membranes are composed of a cation and anion exchange layer, with an interfacial layer in between. This gives the freedom to operate in different conditions (pH, concentration, composition) at both sides. Such membranes are used in two operational modes, forward and reverse bias. The BPM has been implemented in various electrochemical applications, like water and $CO_2$ electrolyzers, fuel cells and flow batteries, while BPMs are historically designed for acid/base production. Therefore, current commercial BPMs are not optimized as the conditions change per application. Although the ideal BPM has highly conductive layers, high water dissociation kinetics, long lifetime and low ion crossover, each application has its own priorities to be competitive in its field. We describe the challenges and requirements for future BPMs, and identify existing developments that can be leveraged to develop BPMs towards the scale of practical applications.*

Parts of this chapter have been published as 'Insights and Challenges for Applying Bipolar Membranes in Advanced Electrochemical Energy Systems' by Marijn A. Blommaert, David Aili, Ramato Ashu Tufa, Qingfeng Li, Wilson A. Smith, David A. Vermaas. ACS Energy Lett. 2021, 6, 2539-2548.

## 2.1. INTRODUCTION: CHALLENGES AND DEVELOPMENTS



Renewable energy conversion technologies, including water electrolyzers, fuel cells and photo-electrolytic cells, have rapidly gained interest in the past decades. These electrochemical technologies often use ion-exchange membranes as an electrolyte that has three main functions: 1) allowing passage of ionic charge carrier species, 2) separating reactants and/or products between the anode and cathode, and 3) providing a controlled environment for electrode reactions. [1, 2] An ion-exchange membrane contains immobilized ionic groups facilitating the transport of e.g. proton cations in the case of cation exchange membranes (CEM) or hydroxide anions in the case of anion exchange membranes (AEM). A third category of ion exchange membranes are bipolar membranes, which were first introduced in the electrochemical field by Frilette (1956) [3] and have been receiving increasing attention in the last decennia for various applications, while before there was a strong focus on electrodialysis applications [4, 5]. A bipolar membrane (BPM) is composed of a cation exchange layer (CEL, transporting e.g. $H^+$) and an anion exchange layer (AEL, transporting e.g. $OH^-$), which are laminated together. The abrupt transition from CEL to AEL at the interface of the BPM involves a chemical process e.g. dissociation or association of the two active charge carriers, $H^+$ and $OH^-$. The BPM makes it obsolete to transport either cations or anions across the entire BPM, which provides the freedom to operate in distinct electrolyte at either side. [6, 7] The interface layer (IL) in between the two membrane layers features a catalyst to promote the dissociation/association process in order to maintain the supply or consumption of the ionic charge carriers from either layer of the BPM.

Several applications in electrochemical energy conversion technologies have implemented a BPM as electrolyte, such as $CO_2$ reduction [8, 9], fuel cells [10], water electrolyzers [11], photo electrochemical cells [12, 13], flow batteries [14] and resource recovery, e.g. ammonia and carbon dioxide via bipolar membrane electrodialysis [15, 16]. The choice for a bipolar membrane is made for intrinsic advantages compared to a monopolar membrane (stability of electrolytes as total charge is maintained, improved separation of products and/or reactant), but often the available bipolar membranes have some imperfections leading to unwanted behavior (ion crossover, blistering, high resistance, slow kinetics; see further on). An ideal BPM should feature: 1) high conductivity of the individual bulk layers, 2) if applicable, fast chemical (dissociation or association of water) kinetics at the interface, 3) high water permeability, 4) long lifetime under operational current densities, and 5) low parasitic (ion) crossover. As the BPM has been originally developed for producing acid and base chemicals in e.g. bipolar membrane electrodialysis, the membrane properties have not been geared towards optimization in energy technologies. Hence, embedding a bipolar membrane to electrochemical cells for energy conversion is limited to the lab-scale stage.

At the same time, a BPM can offer a unique advantage to emerging energy tech-

nologies, as it allows passage of protons through the cation exchange layer (CEL) on one side and hydroxide through the anion exchange layer (AEL) on the other. In this way, the BPM is capable of solving incompatibility issues: as for electrochemical applications, like water and $CO_2$ electrolysis, the optimal pH differs for the two electrodes, the BPM can bridge these variations, allowing optimal conditions. Adding this degree of freedom to the process setup, favors individual optimization of separate compartments and tuning of electrode chemistries, and will in the end speed up the development of industrial applications.

Even though an ideal BPM for energy technologies complies with the same five characteristics as an ideal BPM for acid/base production, the optimized realistic BPMs can be quite different. For example, water electrolyzers typically operates in a current density range of 200-400 mA $cm^{-2}$ for alkaline and 1000-2000 mA $cm^{-2}$ for PEM type technology. This high current density demand sets extremely high standards for the water dissociation activity, water diffusion rate and ion conductivity, while these parameters are less stringent for resource recovery that operates typically at an order of magnitude lower current density. Similarly, reducing (cat)ion crossover is key to mitigate salt formation and ensure operational stability in case of $CO_2$ electrolysis [17], while a few percent ion crossover would be acceptable for BPM-facilitated water electrolysis and resource recovery. For example, at 100 mA $cm^{-2}$ it would take 13.4 years for a 1M phosphate buffer at pH 7 before 1 mol of phosphate has exchanged through the BPM based on a crossover flux of 8.5 µmol $hr^{-1}$ $cm^{-2}$ (0.2% of the ion transport) for a 1 $cm^2$ surface area. [18]

The recent reviews on bipolar membranes by Pärnamäe *et al.* (2021) [19] and Giesbrecht & Freund (2020) [20] provide an excellent overview of the recent achievements in the field, but do not address the improvements that are required to implement BPMs in energy conversion technology applications at industrially relevant conditions. In this perspective, we analyze what developments in bipolar membrane material are already available, and what will be still needed to successfully apply a BPM in electrochemical energy technologies. We outline the BPM modes as applied in energy technologies, and provide a roadmap for improvements from a materials point of view and in terms of operational conditions. Having established that conditions and requirements of BPMs are strongly application-dependent, we apply the outlined opportunities for improvement to the applications of water electrolysis, $CO_2$ electrolysis, resource recovery, fuel cells, and batteries.

## 2.2. BIASING FUNCTIONALITY - DISSOCIATION AND ASSOCIATION

The bipolar membrane, being made of two opposite charged layers, can be operated at two modes of operation, depending on the direction of the ion flow (Figure 2.1). When the transport of cations and anions is directed towards the interfacial layer, the operational mode is called forward bias. In opposing mode, a

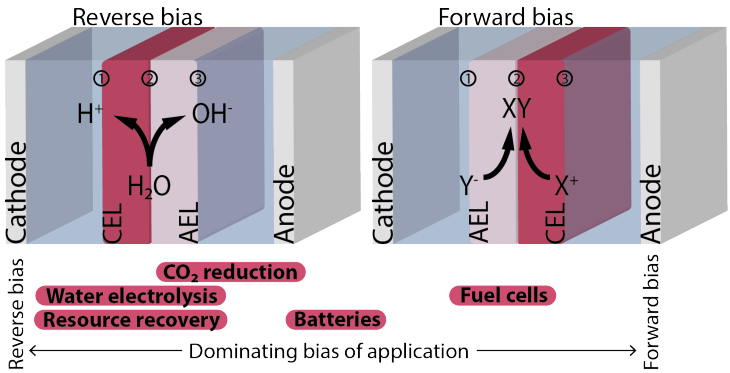


Figure 2.1: The bipolar membrane can operate in two modes: reverse and forward bias. A BPM comprises three interfaces of interest, two with the electrolyte/electrode and membrane layer (1 & 3) and one between the membrane layers (2) where a catalyst layer is deposited to enhance kinetics. At each interface a potential difference is created due to the change in charge density, as described in literature. [21, 22] A BPM can also be used in a zero gap configuration (not shown here), then the membrane layer is in contact with the electrode. The bars at the bottom indicate the different applications and their relative usage of each orientation (e.g. water electrolysis is only performed in the reverse bias orientation, while $CO_2$ reduction is predominantly used in reserve bias but has also been studied in forward bias).

reverse bias is applied across the BPM with an outward transport of cations and anions. The terms of forward and reverse bias were, in analogue to the n-p junction, adopted for electrodialysis referring to the enrichment and depletion of ions in the IL, respectively. For energy conversion technologies the concerned cations and anions are most of the time protons and hydroxides, respectively. The two operating modes are hence accompanied with water formation (forward bias) and dissociation (reverse bias) in the IL, as shown in Figure 2.1. In some cases in literature where forward bias is used, other ionic species are transported to the IL and salts are formed. [21] A membrane-membrane potential similar to the Donnan potential is developed for separation or recombination of the protons and hydroxides. At a pH difference of 14 units across the BPM interface, i.e. separation of protons of a unit activity in the CEL and hydroxide of a unit activity in the AEL, the interfacial potential is 0.83 V according to the Nernst equation. However, the total thermodynamic equilibrated potential of the membrane depends on the surrounding electrolytes, as Donnan potentials exist at each membrane interface (electrode/electrolyte-membrane layer twice and interface layer). [23] The underlying thermodynamics has been recently rationalized for the use of BPM in water electrolysis [24] and for fuel cells [25].

A reverse bias is traditionally applied to bipolar membranes, as this leverages the enhanced water dissociation. In the reverse bias mode, ions are removed from the interface layer, depleting the membrane of the mobile charges. In order to main-

tain charge neutrality and to supply the required ion current, the depletion of ions (proton and hydroxide) triggers further water dissociation in line with Le Chatelier's principle. The reverse bias has been demonstrated in acid/base production [4], water electrolysis [23], $CO_2$ electrolysis [8], and resource recovery via pH swing [16, 26]. The ion transport mechanism in reverse bias has been well studied, in particular for extreme pH gradients (i.e., pH 0 vs pH 14) and unbuffered (initially neutral) solutions. [22, 23]

In forward bias mode, an energy gain in the cell voltage can be acquired due to recombination reactions at the interface layer, with products like salt formation [21] or water [25, 27, 28]. Potentially, the membrane voltage obtained from water recombination is the same as the thermodynamic potential for water dissociation, and can be harvested as electrical energy, in e.g. fuel cells or acid/base batteries. [14, 25, 29] Other studies opted for the forward bias mode to mitigate $CO_2$ crossover in water/$CO_2$ electrolysis cells. [30] Potential challenges in forward bias mode are reduced stability (blistering), particularly in case of gas evolution at the interface, and decreasing ionic strength in the electrolyte as charged species neutralize each other. [13]

## 2.3. DESIGN CRITERIA OF INDIVIDUAL CEL AND AEL FROM A MATERIALS POINT OF VIEW

One component of the ideal BPM features a high ion conductivity of the CEL and AEL, which for commercially available membrane layers in pH neutral electrolytes is moderate. Under reverse bias the conductivity increases due to the formation and outward flux of $H^+$ and $OH^-$ ions. At 60-80 °C the ion conductivity of fully hydrated state-of-the-art CEL (e.g. perfluorosulfonic acid membranes) in the $H^+$ form is typically above 0.1 S $cm^{-1}$, [31] while that of AEL (e.g. quaternary ammonium functionalized membranes) in the $OH^-$ form is slightly lower [32]. Assuming a thickness of 25 µm of the individual layers and a conductivity of 0.1 S $cm^{-1}$ for both layers, it translates to a total area specific resistance for the bulk layers of 50 m$\Omega$ $cm^2$. This corresponds to an ohmic voltage drop of 10 mV across the bulk layers of the BPM at a current density of 100 mA $cm^{-2}$. Further increasing the current density to 500 and 1000 mA $cm^{-2}$ would result in a voltage drop of 50 and 100 mV, respectively. However, commercial bipolar membranes demonstrate typical area specific resistances of 3-10 $\Omega$ $cm^2$, i.e. two orders of magnitude higher than the total area specific resistance of the individual layers. [33] One of the explanations for this discrepancy is that the thickness of commercial BPMs is almost an order of magnitude larger than 25 µm. Also, there is partial neutralization of the ionic groups due to support electrolyte entering the membrane, which seems supported by the observation that the area specific resistance under reverse bias decreases with increasing current density as a result of the higher rate of $H^+$ and $OH^-$ formation at the interface. [33] A third explanation is that additional contributions to the resis-

tance plays in, that appear ohmic from the linearity of the polarization curve, but are connected to e.g. kinetic losses or mass transport limitations related to the water dissociation reaction under reverse bias operation. Electrochemical impedance spectroscopy studies have shed light on the complexity of the polarization losses associated with the water dissociation and ionic separation. [33, 34] From an engineering point of view, making thinner CEL and AEL using the latest technologies with high conductivity and selectivity for $H^+$ and $OH^-$, respectively, would be readily available to boost the BPM performance.

As a result of the electric field across the BPM interface, the rate of water dissociation is enhanced by several orders of magnitude as compared with the autoionization of water. This is a well-described phenomenon commonly referred to as the second Wien effect. [35] However, in order to obtain a BPM that can support currents in a technologically relevant range (>100 mA $cm^{-2}$) at a reasonable cell voltage, introduction of water dissociation catalysts at the IL is necessary to further improve the kinetics. This is clearly demonstrated by Oener *et al.* (2020), based on a screening of a large number of different metal oxides. [36] Both membrane layers at the interface layer have their own local pH and therefore optimal catalyst in the form of metal-oxide nanoparticles (e.g. $IrO_2$ at CEL and NiO at AEL interface side). This then lowered the water dissociation overpotential to 10 mV at 20 mA $cm^{-2}$. [36]

At higher current densities, the diffusion rate of water has to be sufficient in order to avoid mass transfer limitations (to reach 1 A $cm^{-2}$ a rate of 10.4 µmol $s^{-1}$ $cm^{-2}$ is needed), requiring a high water permeability. Commercial BPMs show a limiting current density of 600 mA $cm^{-2}$. [37] As applications like water electrolysis operate at higher current densities, new designed BPMs require a higher cut-off. The water permeance can be tuned by the membrane thickness. In addition, a combination of highly hydrophilic membrane surfaces combined with highly active membrane interface could alleviate the water transport limitations.

To improve the lifetime of BPMs, the AEL presents significantly more challenges than the CEL because of the intrinsic instability of common quaternary ammonium groups in alkaline environment. The challenge originates from the basicity and nucleophilicity of the hydroxide ion, which lead to different degradation mechanisms depending on conditions and particular structure. Hoffmann β elimination and different substitution or rearrangement reactions are commonly reported. [38] This has triggered tremendous research towards stable quaternary ammonium head groups within the AEM community. The most successful degradation mitigation strategies include steric hindrance [39] and integration of cyclic configurational or geometric features that increase the activation barrier of common degradation pathways. [40, 41] Backbone stability is another concern, particularly for AEL based on poly(arylene ethers) or other ether linked backbone chemistries. [42] The recent development in the field is therefore focusing on all-carbon linked struc-

tures devoid of labile ether linkages, such as polyphenylenes [43], polycarbazoles [44], polyfluorenes [45], poly(arylene alkylenes) [41] or aliphatic polymers [46].

Another aspect of the chemical stability of the BPM is the interfacial compatibility between the AEL and CEL, which is an essential factor that needs to be considered in the design phase of novel BPM structures. First of all, good adhesion between the layers is needed to avoid delamination and blistering. Interfacial compatibility is also needed to be able to control and tune the depth, morphology and composition of the boundary region where the water dissociation reaction occurs, which is the key to develop high-performing BPMs. [36, 37] As discussed above, the AEL represents the biggest challenge from a polymer electrolyte stability perspective and a rational way forward to improve the interfacial properties is therefore to develop CEL that are compatible with the most promising AEL chemistries that are available. Using CELs based on perfluorosulfonic acid derivatives is indeed attractive from a conductivity and stability point of view, but interfacial compatibility and adhesion to high performing AEL chemistries is a challenge. One way to further mitigate adhesion limitations is the development 3D CEL-AEL interfaces, which not only increases the active contact area and overall water dissociation rate, but also physically anchors the individual layers and thereby improves interfacial stability. [37, 47]

The final important feature of an ideal BPM is low ion crossover, i.e. unwanted transport of ionic species present in the support electrolytes across both membrane layers. This lowers the selectivity of the water dissociation reaction (WDR) and, therefore, reduces the chemical potential of the surrounding electrolytes. [18] However, this feature cannot be tuned independently from the previously discussed material properties, in particular the catalyst (favoring WDR), morphology of the interface and thickness of the BPM. Tuning e.g. ion exchange capacity, swelling and nanomorphology will therefore also impact the other components of an ideal BPM. In addition, operational parameters (like surrounding environment, current density) also have a great impact, and the selectivity of ion exchange membranes is known to diminish in contact with aqueous solutions of high ionic strength. [48] A rational development strategy would thus be to tailor the morphology of the layers and the dimensions of the conducting domains balancing undesired migration/diffusion of certain species and conductive membrane layers in a tradeoff that is specific to the application.

## 2.4. TUNING PERFORMANCE BY OPERATIONAL PARAMETERS

Lowering the thickness of the membrane layers increases the conductance and water permeance towards the IL, both enhancing the performance the BPM at high current densities. However, a thin membrane layer also increases the ion crossover. [49] If the thickness is doubled, the ion crossover through BPMs is more than halved. [50] This requires a trade-off, as shown in Figure 2.2. The trade-off can be influenced by

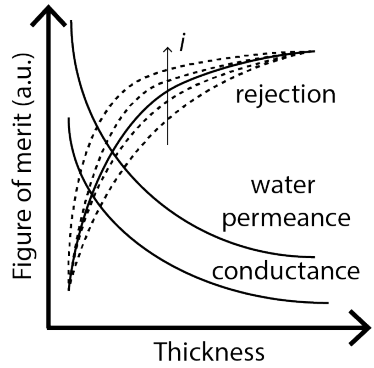


Figure 2.2: Effect of the thickness of the BPM or individual layers. Thicker membranes negatively impact the conductivity and water permeance, while improving the rejection (i.e., selectivity of BPM) in favor of the WDR at the interface layer. As an example, rejection is the only shown parameter that is influenced by current density (i).

a different operational parameter: current density. As increasing the current density reduces the relative ion crossover significantly [18], the optimal trade-off will be favored towards lower thicknesses for applications that run at high current densities. Asymmetry in the membrane layer thickness is a potential method to further balance the water permeance and conductance at one side, and ion crossover at the other side. In particular, the CEL can be made very thin while still maintaining a high performance in terms of ion crossover, as recently demonstrated via simulations. [22] The thickness of the AEL can also be reduced to boost the current density [51], but that affects the rejection of the BPM [22]. Asymmetric BPMs have therefore been suggested, but that requires extra attention for the membrane properties as delamination occurs more easily. [22, 52]

Another operational parameter is the environment surrounding the membrane. Depending on the application, the membrane is contacted with a support electrolyte on zero, one or both sides of the membrane. If no support electrolyte is used, substantial humidification of feed gases is needed to provide enough water for the cell reactions (e.g. $CO_2$ reduction) and to keep conducting ionic groups dissociated. The type of electrolyte (or the absence of it) determines the local environment and has a major influence on the membrane potential. While neutral pH electrolytes result in a low thermodynamic potential, a high overpotential for the WDR is generally created. [23] A high concentration of ions that interact with $H^+$ and $OH^-$ or the fixed charges of the membrane result in a complex distribution of ionic species across the membrane, which compromises the Donnan potentials at the membrane-electrolyte interface. Moreover, these additional electrolytes also affect the ion conductivity of the individual layers of the membrane, and the transference number for the different ionic species. [23, 48]

To mitigate the high overpotentials at near-neutral pH of the surrounding electrolyte, two strategies can be applied: 1) the diffusion of ionic species into the membrane layers can be accepted, if catalysts at the BPM interface are geared towards near-neutral pH conditions, for instance, using catalysts based on graphene oxide [53] or metal organic frameworks [54]. Depending on the electrolyte composition and speciation, ionic species with a higher diffusion coefficient would trigger co-ion leakage which requires an optimal choice of electrolytes and design of membrane materials; 2) alternatively, efforts should be directed towards maintaining a sudden jump in pH at the membrane-electrolyte interfaces, which directly yields a Donnan potential that compensates the WDR potential. This sudden pH-jump at the membrane-electrolyte interface requires flow strategies to reduce the concentration polarization and membrane material with extremely high affinity for protons and hydroxide ions over other ions. In principle, such membrane material exists in the form of an ice-based proton membrane, but has obviously limited practical (liquid) water possibilities. [55] However, the recent pioneering work by Mayerhöfer *et al.* (2020) [51] and Oener *et al.* (2021) [56] show that highly asymmetric BPM can support remarkably high currents even in pure water when the BPM junctions are installed near the electrodes. This mitigates mass transport limitations related to slow water diffusion, and sufficiently high water dissociation rates can thus be reached to maintain the steep pH gradient across the BPM interface even in pure water.

Compared to monopolar membranes, the membrane potential of a BPM can be substantially higher. This is due to the required potential to perform the WDR, as well as the earlier mentioned higher thickness. By selecting certain electrolytes (e.g. acidic catholyte and alkaline anolyte in water electrolyzers), the total cell voltage can be reduced in comparison to a setup with monopolar membranes. The membrane potential can be quantified and different resistance contributions can be decoupled by chronopotentiometry or electrochemical impedance spectroscopy [33], but there is a large gap in the literature that remains to be filled. For example, the diffusion and migration behavior of different ionic species and the dependence of their transference numbers on current, temperature and electrolyte composition remains largely unexplored except the early efforts. [7, 34]

The surrounding electrolytes do not only affect the membrane potential, but also the ion crossover across the membrane. This exchange of ionic species negatively affects the kinetics of the water dissociation, as the WDR occurs due to the lack of transportable ionic species. Therefore, the higher the ion crossover, the lower the water dissociation efficiency. This co-ion transport can be reduced by the type of electrolytes based on their ionic properties (valence, diffusion coefficient, size etc.). Ions with higher valence or ionic size show significant lower crossover, but the electrolytes with a higher ionic size typically feature a lower conductivity and

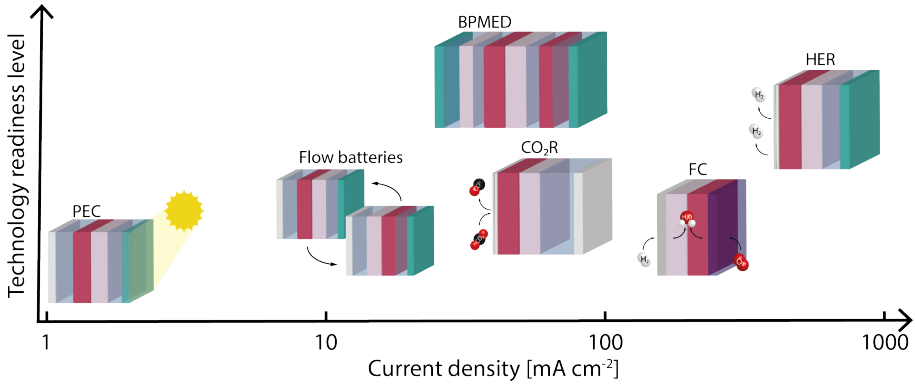


Figure 2.3: Schematic of the different applications in function of the current density and technology readiness level. The applications are, in order of increasing current density, photoelectrochemistry (PEC), flow batteries, bipolar membrane electrodialysis (BPMED, resource recovery), $CO_2$ electrochemical reduction ($CO_2R$), fuel cells (FC), and water electrolysis (HER).

solubility. [18]

## 2.5. BIPOLAR MEMBRANES IN ADVANCED ENERGY APPLICATIONS

As the current density is one of the most influencing operational parameters for tuning the BPM crossover and conductance, we have mapped the different BPM-applications on their typical current density. Figure 2.3 shows the different applications using a BPM with their relative current density and technology readiness level (TRL), which is determined based on number of publications and size and conditions of BPM-facilitated systems in literature and industry. For the latter, only bipolar membrane electrodialysis qualifies as industrial developed technology. The highest applied current densities are found in water electrolysis (>500 mA cm$^{-2}$) [37], while photo-electrochemistry operates typically at two orders of magnitude lower [57].

### 2.5.1. WATER ELECTROLYSIS

The motivation of using a BPM in water electrolysis is directly associated to the lack of consensus about the optimal pH in electrolyzers; both acidic (PEM) and alkaline electrolysis are developed, each with corresponding electrocatalysts. In the realm of earth abundant materials, highly active oxygen evolution catalysts (e.g., Ni-based) are almost exclusively operating in alkaline media. For the hydrogen evolution reaction in acidic environment, platinum remains the state-of-the-art material, although transition metal phosphides, for example, have been demonstrated as potential substitutes. [58] BPM-based electrolyzers have successfully been demonstrated to combine hydrogen evolution catalysts in acidic envi-

ronment with oxygen evolution catalysts in alkaline environment at lab scale. However, as industrial electrolyzers typically operate between 100 and 1000 mA $cm^{-2}$, the commercial BPMs fail to provide sufficient water dissociation kinetics to operate energy-efficient water splitting. With thinner and highly asymmetric BPMs, an opportunity is available for BPM development for electrolysis, as demonstrated by Mayerhöfer *et al.* (2020). [51] A cell equipped with a bipolar membrane with the interface placed directly at the high pH anode by pressing a Nafion membrane onto an anode containing an anion exchange ionomer, current densities as high as 8 A $cm^{-2}$ at 2.2 V were achieved, pointing at further exploration of highly asymmetric BPMs as a rational way forward. [51]

As an alternative to targeting high current density electrolysis, photo-driven systems can be considered, which usually operate at a low current density (typically 10 mA $cm^{-2}$) due to the limited solar radiation flux. For those cases when the operating currents are very small, the high internal resistance of the BPMs is no longer troublesome. However, three other challenges appear. First, when making use of photo-electrodes in the system, a near-neutral pH is often required to provide realistic electrode lifetime. As explained before, a near-neutral pH compromises the WDR efficiency and membrane conductivity. Moreover, to allow the use of both photo-cathode and photo-anode, or a single photo-electrode with a non-transparent photovoltaic cell behind, a frontal illumination is needed, which requires a transparent BPM. Such transparent membrane has been presented in literature already, with a transmission of 75%. [59] Third, at these low current densities the ion crossover can be up to 10% of the charge for near-neutral pH electrolytes, which can be reduced by selecting electrolytes with high ionic sizes as the low conductivity has a limited effect on the performance. [18]

### 2.5.2. $CO_2$ ELECTROLYSIS

Under $CO_2$ electrolysis conditions, the electrochemical setup is similar to a water electrolyzer (including the benefit of the anode catalyst optimization), with the addition of the mixed liquid-gas feed (allowing to overcome the mass transport limitations in aqueous conditions) at the cathode requires modifications of the cell configuration. [60] One of the biggest challenges with $CO_2$ electrolyzers using traditional anion exchange membranes in combination with bicarbonate support electrolytes is the parasitic $CO_2$ crossover. This is an unavoidable effect when the current through the membrane is carried by bicarbonate ions. The bicarbonate ions are continuously generated at the cathode from hydroxide ions (released from the electrochemical reaction) and $CO_2$ (from cathode feed). After migrating towards the anode, $CO_2$ release is driven by the oxygen evolution reaction. In $CO_2$ electrolyzers constructed around BPM, on the other hand, parasitic $CO_2$ transport can be completely eliminated since the current is supported by the water dissociation and ionic separation, as shown experimentally in a liquid-liquid environment. [1] The use of a (bicarbonate) buffer in the catholyte improves the $CO_2$ reduction effi-

ciency by suppressing the HER, but increases the thickness of the reactor. Recent work shows that by reducing the acidity of the CEL, the buffer can be omitted as the HER is suppressed (up to 40% increase in efficiency). [61] This is a step in the right direction, but to reach similar faradaic efficiencies as in systems with an AEM, further optimization of the CEL is required. While attempts of direct depositing the catalyst on the membrane layer report a FE above 60% for CO at 25 mA $cm^{-2}$, the system suffered from high membrane voltages due to a poor conductivity of the catalyst layer. [21] To overcome these conductivity issues, a few MEA designs implemented a buffer (aqueous or ionic liquid), reaching similar FEs at current densities above 100 mA $cm^{-2}$. [62] Others showed a similar setup, reaching 90% FE towards formate at 500 mA $cm^{-2}$. [63] Another approach to suppress the competing hydrogen evolution reaction at the cathode side under $CO_2$ reduction conditions is to adjust the local pH of the CEL near the electrode by reducing the activity of the cationic functions. [61] In these designs, the high membrane voltage remains a challenge, similarly as discussed in the resource recovery section.

### 2.5.3. RESOURCE RECOVERY

In addition to usage of BPMs in electrolyzers, BPMs can be utilized for obtaining the raw materials for energy technologies. Bipolar membrane electrodialysis (BPM-ED) processes for recovery of resources like ammonia [15] and capture of $CO_2$ [16, 64] present a promising alternative to the existing technologies. The recovery of ammonia and $CO_2$ ultimately leverage the ability of BPMs to create a different pH in the concentrate stream compared to a diluate stream, which allows to combine concentrating and converting to the desired product (e.g. $NH_3$ and $CO_2$ (g)). At the same time, such a system is limited by the undesired crossover of neutral species and proton/hydroxide crossover, showing a current efficiency barely above 50%. [15] This is mainly associated with poor selectivity of membranes and the necessity to recirculate solutions to reach a high effluent concentration. [26] The diffusion of neutrally charged species like $NH_3$, $H_3PO_4$ and $CO_2$ ($H_2CO_3$) cannot be solved with the same strategy of using asymmetric BPMs like in other applications [65], as charge selectivity is invalid in this case. [15] Although the concentration of ionic species can be larger than that of the neutrally charged species (especially for the mediocre soluble $CO_2$ in aqueous solutions), the unhindered crossover of neutrally charged species via diffusion can exceed the crossover of ionic species for low current densities (<40 mA $cm^{-2}$ for the example of 0.5 M phosphoric acid). [18] As the crossover of such neutrally charged products like $NH_3$ and $CO_2$ is exclusively driven by diffusion, the crossover can be balanced at the expense of permeance by tuning the degree of crosslinking and thickness of the BPM. [49]

Although the energy consumption is another issue in BPM-ED systems, promising developments have been recently shown to improve energy consumption both for NH3 recovery and $CO_2$ capture systems. [26, 64] Energy consumption down to 19 $kJ/g_N$ was reported for $NH_3$ [15, 26] making it competitive with the classical ED

operations (30.6 kJ/$g_N$). [66] However, more advanced developments are still required to reach a decent performance. Strategies would involve improving stack design using thinner flow channels and, to some extent, using BPMs with reduced overpotential at the interface layer for the near-neutral operating pH in resource recovery. In BPM-ED systems for $CO_2$ capture (e.g. from seawater), the extra energy constraint due to undesired water-splitting at the electrodes can be reduced by combined capture and conversion cells [67] or reversible redox-couples (e.g. K3/K4[Fe(CN)6]) at the electrodes [64].

### 2.5.4. FUEL CELLS

With water formation in the IL, the forward bias mode of the BPM is a natural option for fuel cells. BPM fuel cells operating in the reverse bias mode is impractical from electrode kinetics or catalyst material points of view and have also shown much lower performance. [10] For the forward bias mode BPM fuel cells, hydrogen oxidation takes place near the CEL and oxygen reduction near the AEL. The distinct proton concentrations in the CEL and AEL are favorable for both reactions in terms of electrode kinetics and catalyst selection. With the anode side at pH 0 and the cathode side at pH 14, the standard redox potential difference of a fuel cell operating in forward bias mode is 0.4 V, using both the electrode potentials for their respective local pH. On top of that, the potential across the interface within the BPM at a pH difference of 14 is 0.83 V, which constitutes a positive bias to the cell voltage so that the thermodynamic voltage of 1.23 V is obtainable. [25] Fuel cells equipped with BPM membranes have been explored in several publications during the last decade. Open circuit voltages close to what is normally obtained for cells based on monopolar AEM and CEM chemistries (0.9-1.0 V) have been achieved when the BPM interfacial junctions are placed very near the electrode surfaces. [10, 25] In practice, such cell designs have been obtained by e.g. introducing the AEL in the high pH cathode catalyst layer and thereafter assembling the cell with a thick CEL based on a conventional Nafion membrane. [10]

Operation of fuel cells in the forward bias meets an issue of parasitic H2O transport and management. Water is supplied with oxygen on the cathode in order to generate $OH^-$ and with hydrogen on the anode to form hydrated protons (e.g. $H_3O^+$), which are the charge carriers through the AEL and CEL, respectively. As a result, the amount of water produced in the IL is at least three times of the fuel cell reaction product. This, on one hand, opens the possibility to eliminate the humidification when the CEL and AEL membranes are compatible in term of water uptake and transport, as demonstrated by Peng et al. (2015) [68]. On the other hand, ineffectual removal of the water from the IL may cause the flooding and BPM delamination. However, this application has good potential, because there are no other ions that could cross over, as both sides have gas feed. The lack of published fuel cell data with symmetric BPM points towards development of highly asymmetric structures as the most rational way forward.

### 2.5.5. BATTERIES

The first implementation of a BPM in flow batteries was demonstrated in Vanadium-metal hydride semi-flow systems. [69] Such systems benefited from the unique operability of BPMs in maintaining pH gradient resulting in higher operating voltages of up to 2.4 V compared to the conventional all vanadium redox flow battery systems utilizing monopolar membranes (~1.2-1.3 V). [70] However, the current density is low (<10 mA $cm^{-2}$), which results in leakage of current due to ion crossover across the BPM calling for highly selective membrane designs. Moreover, aqueous redox flow batteries sometimes produce highly oxidative species, such as $VO^{2+}$, $Ce^{4+}$ and $Br^2$, which directly oxidize the functional groups in membranes, particularly the AEMs. As such, highly stable Nafion membranes have been utilized in batteries as a separator but this pertains to a high capital cost for large-scale implementation. The use of hydrocarbon BPMs with highly functional and stable AELs can essentially enhance the cycle life and bring down the capital cost.

A more recent route for BPM-based batteries is the acid base flow battery system, using a BPM in reverse bias to charge the fluids and in forward bias for discharging. [14, 29, 71, 72] Being charged from a neutral NaCl solution into HCl and NaOH, the acid base flow batteries benefit from more abundant resources compared to the vanadium redox flow batteries. [71] However, such a systems are limited by low voltage efficiency as well as co-ion leakage particularly when working at high acid-base concentrations, leading the self-discharge of the battery. The discharge mode (in forward bias) requires a membrane that is prone to water formation at the BPM interface, similar to the conditions in fuel cells. However, as the current densities in acid base flow batteries are typically at least an order of magnitude smaller than in fuel cells (Figure 2.3), and opportunities for membrane thickness tuning exist, this seems realistic for future BPM architectures. More specific to this technology is the relatively low power density of acid base flow batteries (4-200 W $m^{-2}$) compared to other flow battery systems [14, 29], which means this technology is calling for highly conductive and low-cost BPM materials.

## 2.6. CONCLUSION AND OUTLOOK

The versatile bipolar membrane (BPM) can be implemented in various electrochemical energy applications. A bipolar membrane, composed of a cation and anion exchange layer with a catalyst deposited on the interfacial layer, is ideally suited to optimize individual compartments in an electrochemical cell as it can separate different electrolytes. However, although BPMs are used for decades in acid/base production, no single energy conversion technology with BPM has reached industrial application. For every application in this field, specific requirements towards the BPM exist. In general, the BPM should feature highly conductive individual bulk layers, fast water dissociation or recombination kinetics at the interface, a long lifetime, high water permeability and a low ion crossover. For each of these membrane characteristics, improvement strategies are already available, via material en-

hancements or tuning operational conditions, albeit often compromising another parameter. However, the priority for each membrane characteristic strongly differs per application, due to different electrolyte conditions and typical current densities that vary more than 2 orders of magnitude. While fuel cells, water and $CO_2$ electrolysis require fast kinetics at the interface layer, low ion crossover is more important to batteries and resource recovery. Hence, a dedicated approach to design BPMs for each application is needed, to fabricate new BPM designs in order to be successfully implemented in industrial applications.



## REFERENCES


[1] M. Ma, S. Kim, I. Chorkendorff, and B. Seger, *Role of ion-selective membranes in the carbon balance for CO2 electroreduction via gas diffusion electrode reactor designs,* Chemical Science **11**, 8854 (2020).

[2] T. Luo, S. Abdu, and M. Wessling, *Selectivity of ion exchange membranes: A review,* Journal of Membrane Science **555**, 429 (2018).

[3] V. J. Frilette, *Preparation and characterization of bipolar ion-exchange membranes,* Journal of Physical Chemistry **60**, 435 (1956).

[4] F. G. Wilhelm, I. Pünt, N. F. A. Van Der Vegt, M. Wessling, and H. Strathmann, *Optimisation strategies for the preparation of bipolar membranes with reduced salt ion leakage in acid-base electrodialysis,* Journal of Membrane Science **182**, 13 (2001).

[5] P. Ramírez, H. J. Rapp, S. Mafé, and B. Bauer, *Bipolar membranes under forward and reverse bias conditions. Theory vs. experiment,* Journal of Electroanalytical Chemistry **375**, 101 (1994).

[6] R. Simons and G. Khanarian, *Water dissociation in bipolar membranes: Experiments and theory,* The Journal of Membrane Biology **38**, 11 (1978).

[7] F. G. Wilhelm, N. F. A. Van Der Vegt, H. Strathmann, and M. Wessling, *Current-voltage behaviour of bipolar membranes in concentrated salt solutions investigated with chronopotentiometry,* Journal of Applied Electrochemistry **32**, 455 (2002).

[8] D. A. Vermaas and W. A. Smith, *Synergistic Electrochemical CO2 Reduction and Water Oxidation with a Bipolar Membrane,* ACS Energy Letters , 1143 (2016).

[9] Y. C. Li, D. Zhou, Z. Yan, R. H. Gonçalves, D. A. Salvatore, C. P. Berlinguette, and T. E. Mallouk, *Electrolysis of CO2 to Syngas in Bipolar Membrane-Based Electrochemical Cells,* ACS Energy Letters **1**, 1149 (2016).

[10] M. Unlu, J. Zhou, and P. A. Kohl, *Hybrid Polymer Electrolyte Fuel Cells: Alkaline Electrodes with Proton Conducting Membrane,* Angewandte Chemie **122**, 1321 (2010).

[11] FCH JU, *Development of Water Electrolysis in the European Union*, Tech. Rep. (2014).

[12] J.-W. Schüttauf, M. A. Modestino, E. Chinello, D. Lambelet, A. Delfino, D. Dominé, A. Faes, M. Despeisse, J. Bailat, D. Psaltis, C. Moser, and C. Ballif, *Solar-to-Hydrogen Production at 14.2% Efficiency with Silicon Photovoltaics and Earth-Abundant Electrocatalysts,* Journal of The Electrochemical Society **163**, F1177 (2016).

[13] N. M. Vargas-Barbosa, G. M. Geise, M. A. Hickner, and T. E. Mallouk, *Assessing the utility of bipolar membranes for use in photoelectrochemical water-splitting cells,* ChemSusChem **7**, 3017 (2014).

[14] J. Xia, G. Eigenberger, H. Strathmann, and U. Nieken, *Flow battery based on reverse electrodialysis with bipolar membranes: Single cell experiments,* Journal of Membrane Science **565**, 157 (2018).

[15] N. van Linden, G. L. Bandinu, D. A. Vermaas, H. Spanjers, and J. B. van Lier, *Bipolar membrane electrodialysis for energetically competitive ammonium removal and dissolved ammonia production,* Journal of Cleaner Production **259**, 120788 (2020).

[16] R. Sharifian, M. Wagterveld, I. A. Digdaya, C. Xiang, and D. A. Vermaas, *Electrochemical carbon dioxide capture to close the carbon cycle,* Energy & Environmental Science **14**, 781 (2021).

[17] M. E. Leonard, L. E. Clarke, A. Forner-Cuenca, S. M. Brown, and F. R. Brushett, *Investigating Electrode Flooding in a Flowing Electrolyte, Gas-Fed Carbon Dioxide Electrolyzer,* ChemSusChem **13**, 400 (2020).

[18] M. A. Blommaert, J. A. H. Verdonk, H. C. B. Blommaert, W. A. Smith, and D. A. Vermaas, *Reduced Ion Crossover in Bipolar Membrane Electrolysis via Increased Current Density, Molecular Size, and Valence,* ACS Applied Energy Materials **3**, 5804 (2020).

[19] R. Pärnamäe, S. Mareev, V. Nikonenko, S. Melnikov, N. Sheldeshov, V. Zabolotskii, H. V. Hamelers, and M. Tedesco, *Bipolar membranes: A review on principles, latest developments, and applications,* Journal of Membrane Science **617**, 118538 (2021).

[20] P. K. Giesbrecht and M. S. Freund, *Recent Advances in Bipolar Membrane Design and Applications,* Chemistry of Materials **32**, 8060 (2020).

[21] M. A. Blommaert, R. Sharifian, N. Shah, N. T. Nesbitt, W. A. Smith, and D. A. Vermaas, *Orientation of bipolar membrane determines the dominant ion and carbonic species transport in membrane electrode assemblies for CO2 reduction,* Journal of Materials Chemistry A **9**, 11179 (2021).

[22] J. C. Bui, I. Digdaya, C. Xiang, A. T. Bell, and A. Z. Weber, *Understanding Multi-Ion Transport Mechanisms in Bipolar Membranes,* ACS Applied Materials & Interfaces **12**, 52509 (2020).

[23] D. A. Vermaas, S. Wiegman, T. Nagaki, and W. A. Smith, *Ion transport mechanisms in bipolar membranes for (photo)electrochemical water splitting,* Sustainable Energy and Fuels **2**, 2006 (2018).

[24] S. Oener, S. Ardo, and S. W. Boettcher, *Ionic Processes in Water Electrolysis: The Role of Ion-selective Membranes,* ACS Energy Letters **2**, 2625 (2017).

[25] M. Ünlü, J. Zhou, and P. A. Kohl, *Hybrid anion and proton exchange membrane fuel cells,* Journal of Physical Chemistry C **113**, 11416 (2009).

[26] M. Rodrigues, T. T. De Mattos, T. Sleutels, A. Ter Heijne, H. V. Hamelers, C. J. Buisman, and P. Kuntke, *Minimal Bipolar Membrane Cell Configuration for Scaling up Ammonium Recovery,* ACS Sustainable Chemistry and Engineering **8**, 17359 (2020).

[27] R. S. Reiter, W. White, and S. Ardo, *Communication—Electrochemical Characterization of Commercial Bipolar Membranes under Electrolyte Conditions Relevant to Solar Fuels Technologies,* Journal of The Electrochemical Society **163**, H3132 (2016).

[28] S. S. Daud, M. A. Norrdin, J. Jaafar, and R. Sudirman, *The effect of material on bipolar membrane fuel cell performance: A review,* IOP Conference Series: Materials Science and Engineering **736**, 032003 (2020).

[29] W. J. van Egmond, M. Saakes, I. Noor, S. Porada, C. J. Buisman, and H. V. Hamelers, *Performance of an environmentally benign acid base flow battery at high energy density,* International Journal of Energy Research **42**, 1524 (2018).

[30] A. Pătru, T. Binninger, B. Pribyl, and T. J. Schmidt, *Design Principles of Bipolar Electrochemical Co-Electrolysis Cells for Efficient Reduction of Carbon Dioxide from Gas Phase at Low Temperature,* Journal of The Electrochemical Society **166**, F34 (2019).

[31] M. A. Yandrasits, M. J. Lindell, and S. J. Hamrock, *New directions in perfluoroalkyl sulfonic acid–based proton-exchange membranes,* Current Opinion in Electrochemistry **18**, 90 (2019).

[32] A. Zhegur-Khais, F. Kubannek, U. Krewer, and D. R. Dekel, *Measuring the true hydroxide conductivity of anion exchange membranes,* Journal of Membrane Science **612**, 118461 (2020).

[33] M. A. Blommaert, D. A. Vermaas, B. Izelaar, B. in 't Veen, and W. A. Smith, *Electrochemical impedance spectroscopy as a performance indicator of water*

*dissociation in bipolar membranes,* Journal of Materials Chemistry A **7**, 19060 (2019).

[34] H. D. Hurwitz and R. Dibiani, *Experimental and theoretical investigations of steady and transient states in systems of ion exchange bipolar membranes,* Journal of Membrane Science **228**, 17 (2004).

[35] L. Onsager and S. K. Kim, *Wien effect in simple strong electrolytes,* Journal of Physical Chemistry **61**, 198 (1957).

[36] S. Z. Oener, M. J. Foster, and S. W. Boettcher, *Accelarating water dissociation in bipolar membranes and for electrocatalysis,* Science **369**, 1099 (2020).

[37] C. Shen, R. Wycisk, and P. N. Pintauro, *High performance electrospun bipolar membrane with a 3D junction,* Energy Environ. Sci. **10**, 1435 (2017).

[38] M. G. Marino and K. D. Kreuer, *Alkaline Stability of Quaternary Ammonium Cations for Alkaline Fuel Cell Membranes and Ionic Liquids,* ChemSusChem **8**, 513 (2015).

[39] J. Fan, A. G. Wright, B. Britton, T. Weissbach, T. J. G. Skalski, J. Ward, T. J. Peckham, and S. Holdcroft, *Cationic Polyelectrolytes, Stable in 10 M KOHaq at 100 °C,* ACS Macro Letters **6**, 1089 (2017).

[40] H. S. Dang and P. Jannasch, *A comparative study of anion-exchange membranes tethered with different hetero-cycloaliphatic quaternary ammonium hydroxides,* Journal of Materials Chemistry A **5**, 21965 (2017).

[41] J. S. Olsson, T. H. Pham, and P. Jannasch, *Poly(arylene piperidinium) Hydroxide Ion Exchange Membranes: Synthesis, Alkaline Stability, and Conductivity,* Advanced Functional Materials **28**, 1702758 (2018).

[42] A. D. Mohanty, S. E. Tignor, J. A. Krause, Y.-K. Choe, and C. Bae, *Systematic Alkaline Stability Study of Polymer Backbones for Anion Exchange Membrane Applications,* Macromolecules **49**, 3361 (2016).

[43] E. J. Park, S. Maurya, M. R. Hibbs, C. H. Fujimoto, K.-D. Kreuer, and Y. S. Kim, *Alkaline Stability of Quaternized Diels–Alder Polyphenylenes,* Macromolecules **52**, 5419 (2019).

[44] M. S. Cha, J. E. Park, S. Kim, S.-H. Han, S.-H. Shin, S. H. Yang, T.-H. Kim, D. M. Yu, S. So, Y. T. Hong, S. J. Yoon, S.-G. Oh, S. Y. Kang, O.-H. Kim, H. S. Park, B. Bae, Y.-E. Sung, Y.-H. Cho, and J. Y. Lee, *Poly(carbazole)-based anion-conducting materials with high performance and durability for energy conversion devices,* Energy & Environmental Science **13**, 3633 (2020).

[45] T. H. Pham, A. Allushi, J. S. Olsson, and P. Jannasch, *Rational molecular design of anion exchange membranes functionalized with alicyclic quaternary ammonium cations,* Polymer Chemistry **11**, 6953 (2020).

[46] L. Wang, X. Peng, W. E. Mustain, and J. R. Varcoe, *Radiation-grafted anion-exchange membranes: The switch from low- to high-density polyethylene leads to remarkably enhanced fuel cell performance,* Energy and Environmental Science **12**, 1575 (2019).

[47] Y. Chen, J. A. Wrubel, W. E. Klein, S. Kabir, W. A. Smith, K. C. Neyerlin, and T. G. Deutsch, *High-Performance Bipolar Membrane Development for Improved Water Dissociation,* ACS Applied Polymer Materials **2**, 4559 (2020).

[48] A. Münchinger and K.-D. Kreuer, *Selective ion transport through hydrated cation and anion exchange membranes I. The effect of specific interactions,* Journal of Membrane Science **592**, 117372 (2019).

[49] M. Tedesco, H. Hamelers, and P. Biesheuvel, *Nernst-Planck transport theory for (reverse) electrodialysis: III. Optimal membrane thickness for enhanced process performance,* Journal of Membrane Science **565**, 480 (2018).

[50] R. E. Moussaoui, G. Pourcelly, M. Maeck, H. D. Hurwitz, and C. Gavach, *Co-ion leakage through bipolar membranes. Influence of I-V responses and water-splitting efficiency,* Journal of Membrane Science **90**, 283 (1994).

[51] B. Mayerhöfer, D. McLaughlin, T. Böhm, M. Hegelheimer, D. Seeberger, and S. Thiele, *Bipolar membrane electrode assemblies for water electrolysis,* ACS Applied Energy Materials **3**, 9635 (2020).

[52] F. G. Wilhelm, I. Pünt, N. F. Van der Vegt, H. Strathmann, and M. Wessling, *Asymmetric bipolar membranes in acid-base electrodialysis,* Industrial and Engineering Chemistry Research **41**, 579 (2002).

[53] H. Sun, S. Liu, G. Zhou, H. M. Ang, M. O. Tadé, and S. Wang, *Reduced graphene oxide for catalytic oxidation of aqueous organic pollutants,* ACS Applied Materials and Interfaces **4**, 5466 (2012).

[54] Q. Wang, B. Wu, C. Jiang, Y. Wang, and T. Xu, *Improving the water dissociation efficiency in a bipolar membrane with amino-functionalized MIL-101,* Journal of Membrane Science **524**, 370 (2017).

[55] T. Sleutels, I. Kaniakidis, O. Oladimeji, H. van der Kooi, A. Ter Heijne, and M. Saakes, *An acid-doped ice membrane for selective proton transport,* International Journal of Energy Research **45**, 8041 (2020).

[56] S. Z. Oener, L. P. Twight, G. A. Lindquist, and S. W. Boettcher, *Thin Cation-Exchange Layers Enable High-Current-Density Bipolar Membrane Electrolyzers via Improved Water Transport,* ACS Energy Letters **6**, 1 (2021).

[57] D. A. Vermaas, M. Sassenburg, and W. A. Smith, *Photo-assisted water splitting with bipolar membrane induced pH gradients for practical solar fuel devices,* The Royal Society of Chemistry **3**, 19556 (2015).

[58] Z. Ge, B. Fu, J. Zhao, X. Li, B. Ma, and Y. Chen, *A review of the electrocatalysts on hydrogen evolution reaction with an emphasis on Fe, Co and Ni-based phosphides,* Journal of Materials Science **55**, 14081 (2020).

[59] S. Chabi, A. G. Wright, S. Holdcroft, and M. S. Freund, *Transparent Bipolar Membrane for Water Splitting Applications,* ACS Applied Materials and Interfaces **9**, 26749 (2017).

[60] R. A. Tufa, D. Chanda, M. Ma, D. Aili, T. B. Demissie, J. Vaes, Q. Li, S. Liu, and D. Pant, *Towards highly efficient electrochemical CO2 reduction: Cell designs, membranes and electrocatalysts,* Applied Energy **277**, 115557 (2020).

[61] Z. Yan, J. L. Hitt, Z. Zeng, M. A. Hickner, and T. E. Mallouk, *Improving the efficiency of CO2 electrolysis by using a bipolar membrane with a weak-acid cation exchange layer,* Nature Chemistry **13**, 33 (2021).

[62] D. A. Salvatore, D. M. Weekes, J. He, K. E. Dettelbach, Y. C. Li, T. E. Mallouk, and C. P. Berlinguette, *Electrolysis of Gaseous CO 2 to CO in a Flow Cell with a Bipolar Membrane,* ACS Energy Letters **3**, 149 (2017).

[63] Y. Chen, A. Vise, W. E. Klein, F. C. Cetinbas, D. J. Myers, W. A. Smith, W. A. Smith, W. A. Smith, T. G. Deutsch, and K. C. Neyerlin, *A Robust, Scalable Platform for the Electrochemical Conversion of CO2 to Formate: Identifying Pathways to Higher Energy Efficiencies,* ACS Energy Letters **5**, 1825 (2020).

[64] I. A. Digdaya, I. Sullivan, M. Lin, L. Han, W. H. Cheng, H. A. Atwater, and C. Xiang, *A direct coupled electrochemical system for capture and conversion of CO2 from oceanwater,* Nature Communications **11**, 4412 (2020).

[65] W. Pronk, M. Biebow, and M. Boller, *Treatment of source-separated urine by a combination of bipolar electrodialysis and a gas transfer membrane,* Water Science and Technology **53**, 139 (2006).

[66] W. A. Tarpeh, J. M. Barazesh, T. Y. Cath, and K. L. Nelson, *Electrochemical Stripping to Recover Nitrogen from Source-Separated Urine,* Environmental Science and Technology **52**, 1453 (2018).

[67] T. Li, E. W. Lees, M. Goldman, D. A. Salvatore, D. M. Weekes, and C. P. Berlinguette, *Electrolytic Conversion of Bicarbonate into CO in a Flow Cell,* Joule **3**, 1487 (2019).

[68] S. Peng, X. Xu, S. Lu, P. C. Sui, N. Djilali, and Y. Xiang, *A self-humidifying acidic-alkaline bipolar membrane fuel cell,* Journal of Power Sources **299**, 273 (2015).

[69] G.-M. Weng, C.-Y. V. Li, and K.-Y. Chan, *High Voltage Vanadium-Metal Hydride Rechargeable Semi-Flow Battery,* Journal of The Electrochemical Society **160**, A1384 (2013).

[70] C. Liu, X. Chi, Q. Han, and Y. Liu, *A High Energy Density Aqueous Battery Achieved by Dual Dissolution/Deposition Reactions Separated in Acid-Alkaline Electrolyte,* Advanced Energy Materials **10**, 1903589 (2020).

[71] R. Pärnamäe, L. Gurreri, J. Post, W. J. van Egmond, A. Culcasi, M. Saakes, J. Cen, E. Goosen, A. Tamburini, D. A. Vermaas, and M. Tedesco, *The acid–base flow battery: Sustainable energy storage via reversible water dissociation with bipolar membranes,* Membranes **10**, 409 (2020).

[72] M. A. Morales-Mora, J. J. Pijpers, A. C. Antonio, J. d. l. C. Soto, and A. M. A. Calderón, *Life cycle assessment of a novel bipolar electrodialysis-based flow battery concept and its potential use to mitigate the intermittency of renewable energy generation,* Journal of Energy Storage **35**, 102339 (2021).

# 3

# ELECTROCHEMICAL IMPEDANCE SPECTROSCOPY AS A PERFORMANCE INDICATOR OF WATER DISSOCIATION IN BPMS

*A bipolar membrane (BPM) can be used to maintain a pH difference in an electrolysis cell, which provides freedom to independently optimize the environments and catalysts used for paired redox reactions. A BPM consists of two physical layers, of which one is selective for the exchange of cations and the other for anions. The water dissociation reaction (WDR) splits water into protons and hydroxide ions under an electric field that concentrates at the interface of the two membrane layers. However, salt ions in commonly used electrolytes influence this WDR when they are present at the interface. Using electrochemical impedance spectroscopy (EIS), we observed the rate of water dissociation decrease in the presence of salt ions while also observing the diffusion and migration of these salt ions, showing a clear link between the peaks observed in EIS and ion crossover. In addition, we show how EIS can be used to in-situ monitor the stability and ageing of a BPM, revealing that degradation of the BPM is more prominent in extreme pH electrolyte pairs compared to non-extreme electrolyte pairs. The in-situ monitoring of the WDR and stability of a BPM are vital methods for adequate and consistent comparison of novel designs of BPM-based systems, where EIS allows for discriminating BPM characteristics from other components even during operation.*

This chapter has been published in *Journal of Materials Chemistry A*, 2019, **7**, 19060-19069 [1].

## 3.1. INTRODUCTION

The increasing concentration of greenhouse gases such as $CO_2$ in our atmosphere has destabilized Earth's climate, as confirmed by the most recent report from the Intergovernmental Panel on Climate Change (IPCC). [2] The consequences of a 1 °C increase of the global mean temperature compared to pre-industrial levels are already evident, requiring immediate actions to reduce our global $CO_2$ emissions and mitigate further dire consequences. With rapidly decreasing prices of renewable energy and an increasing electrification of the energy sector, a promising approach to close the carbon cycle with the production of valuable products is needed. This can be achieved by synthesizing chemicals and fuels using renewable energy via water electrolysis or the electrocatalytic reduction of carbon dioxide ($CO_2$ER).



When considering either of these electrochemical routes at an industrially relevant scale, it is important to have a system run at a high energy efficiency. In other words, the applied potential should be as close as possible to the thermo-neutral cell potential for the combined oxidation and reduction reactions. The importance of high energy efficiency arises from the relatively high contribution of electricity costs in electrochemical systems [3], which makes achieving a high efficiency a necessity to compete with current chemical production means, where nearly all the fuels and commodity chemicals originate from fossil-based resources. However, the state-of-the-art electrolysis of water or $CO_2$ still has a low energy efficiency at high current densities due to large overpotentials for the relevant reduction-oxidation reactions, ohmic losses across the electrolyte and potential drops across an ion exchange membrane that separates the anode and cathode compartments. [4–6] Making matters more difficult, catalysts for the reduction and oxidation reactions perform better—i.e., have a higher stability and lower overpotential—in different electrolytes with different pHs, thereby making a total system difficult to optimize with a single electrolyte. [7, 8]

To integrate different electrolytes into a single electrochemical cell, a bipolar membrane (BPM) can be implemented. Recently, several studies have successfully observed stable operation and lower cell potentials using independent electrolyte pairs for water oxidation coupled to water reduction or $CO_2$ER using a BPM. [8–11] A BPM consists of two physical layers, one which is selective for the exchange of cations (cation exchange layer, CEL) and the other for anions (anion exchange layer, AEL). Under an applied potential or pH gradient across the BPM, the interface between these layers enhances the dissociation of water into protons and hydroxide ions, described by the water dissociation reaction (WDR). [12–14] At this membrane-membrane interface, a catalyst can be deposited to further improve the kinetics of the WDR. A great deal of research on understanding and improving the characteristics of a BPM focuses on the interface between the anion-cation exchange layers. [15–17]

The ion-exclusivity of a BPM, with two different layers and their fixed charges, should in theory be impermeable for any charged species transported through both layers. Since the ion-exclusivity is imposed by finite fixed charges of the membrane layers, a (limited) co-ion exchange will occur between the two different solutions. In monopolar membranes, co-ions are described as ions with the same charge as the fixed charges in the membrane layer. However, for the BPM, co-ions have a more ambiguous definition because of the different polarity in the two membrane layers. Here, we define co-ions as ionic salt species that do not participate in the WDR, i.e., all ions except for $H^+$ and $OH^-$. It is important to note that a CEL and an AEL in contact with electrolytes with very high or very low pH such as KOH and $H_2SO_4$, respectively, theoretically do not contain co-ions in the membrane layers. The contribution to the ionic current, equal to the electrical current through the cell, of each individual ion species is described by the transport number. [18] As this ionic current in the BPM is composed of a movement of co-ions and charge transport due to water dissociation, migration of co-ions lowers the efficiency of the water dissociation reaction [19] and thus negatively affects the overall cell efficiency.



Recent studies have shown the dependency of electrolyte pH and composition surrounding the BPM on the voltage response across the BPM in the presence of an applied current. [14] Depending on the electrolytes used, the i-V curve typically contains a sharp increase of the voltage at a certain current density. After this initial increase, a plateau at a relatively constant current density, $j_{plateau}$, is observed until reaching the membrane voltage of water dissociation (0.829 V), where the current increases sharply with applied potential (see Figure 3.1). However, in contrast to monopolar membranes, which also show activity towards the WDR above a limiting current density, [20] bipolar membranes have shown that charge transport can be dominated by the WDR below the plateau current density under certain conditions. [21] At higher current densities, the water dissociation efficiency increases further. [13, 19, 22, 23] It is necessary to probe the electronic behavior of the interfacial layer to better understand the conditions that determine the WDR, and the relation with the i-V curve and the plateau region.

One way to probe the WDR is via electrochemical impedance spectroscopy (EIS), which differentiates the various components of the BPM as electrical features that can be derived from impedance responses upon a varying frequency. [18] In this way, factors such as the finite conductivity of the membrane layers and electrolyte solutions are measured as an ohmic resistor, the diffusion boundary layer is shown as a constant phase element, and the sudden changes in charge density at the BPM interfaces are shown as electrical double layers. [24–29] In this work, EIS is used to examine the equivalent circuit elements that represent a BPM separating two different pairs of electrolytes at various current densities, as schematically shown in Figure 3.2. The results show that EIS is a useful tool to monitor ion transport in BPMs, which is composed of products of the WDR and crossover of co-ions through the

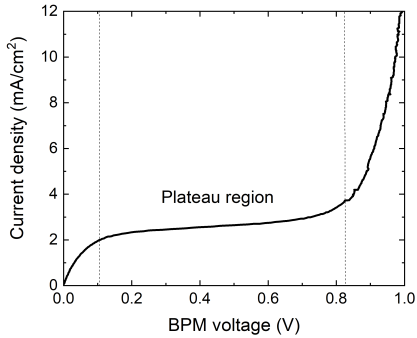


Figure 3.1: Typical i-V curve of a bipolar membrane in a salt electrolyte, with the plateau region between a BPM voltage of 0.1 to 0.8 V. A galvanodynamic scan was applied at a scan rate -0.01 mA $cm^{-2}$ $s^{-1}$ with 5 M NaCl in both compartments.

BPM. Furthermore, a decrease of impedance features linked to decreased co-ion transport through the BPM was observed when the current exceeded $j_{plateau}$. These findings are important to understand the role of co-ions in supporting and inhibiting the WDR at currents below the plateau current density. In addition, EIS was able to monitor the stability of the BPM and its individual components during operation in an electrochemical cell by performing EIS before and after galvanostatic experiments. These experiments showed a degradation in the membrane layers as well as the WDR performance for a case with a pH difference of 14, but relatively stable conditions for a case with less extreme electrolytes.

## 3.2. THEORY

### 3.2.1. WATER DISSOCIATION REACTION

A bipolar membrane has three electrochemical interfaces: two membrane-solution interfaces (CEL/catholyte and AEL/anolyte) and one internal interface (CEL/AEL). The latter is the membrane-membrane interface where the water dissociation reaction occurs when a reverse bias is applied to the system, with the negatively charged layer opposing the negative charged cathode.

The reaction rate of the WDR is $5x10^7$ times faster in a BPM than in aqueous electrolyte, which is enhanced by the electrochemical properties of a BPM. [15] There are multiple theories describing the WDR [15]: some focus on the Donnan equilibrium, [30] some on the second Wien effect, [31] and others on proton transfer reactions with fixed charges. [32, 33] In the latter theory, which has the most realistic simulated reaction rates, weak acids and bases catalyze the WDR, shown in the

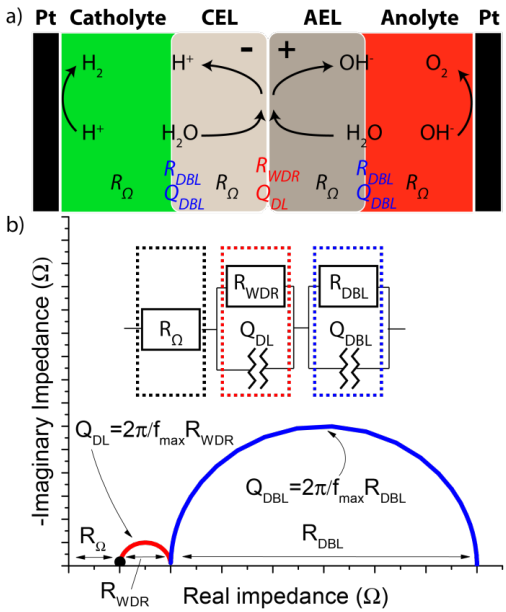


Figure 3.2: (a) Schematic representation of individual components of the impedance response of a BPM in an electrochemical cell, with (black) Ohmic losses of membrane and solution, (red) membrane-membrane interface where WDR occurs, and (blue) diffusion boundary region with a constant phase element. (b) The equivalent circuit used to describe the impedance results is shown with the corresponding Nyquist plot.

following reaction schemes:

$$A^- + H_2O \rightleftharpoons AH + OH^- \rightleftharpoons A^- + H^+ + OH^- \tag{3.1}$$

$$B + H_2O \rightleftharpoons BH^+ + OH^- \rightleftharpoons B + H^+ + OH^- \tag{3.2}$$

Here AH and B are a weak acid and base, respectively. Both membrane layers perform one reaction dominantly, e.g. the cation exchange layer with negatively charged species would preferentially perform reaction (3.1), while the anion exchange layer with positively charged species preferentially performs reaction (3.2). To avoid the reverse reaction, separation of both $H^+$ and $OH^-$ via membrane charges with opposite charge is required, which implies that the WDR is most effective near the CEL/AEL interface. [34] A catalyst present at the interface between the AEL and CEL improves the kinetics of these reactions as well by lowering the activation energy—in this case, the reaction of (3.1) or (3.2), producing protons and hydroxide ions. [15]



### 3.2.2. ELECTROCHEMICAL IMPEDANCE SPECTROSCOPY

Electrochemical impedance spectroscopy can be used to examine the electronic responses of individual components of a membrane by varying the applied frequency. [18] An introduction of the theory behind the EIS data and interpretations is provided in the supporting information. Figure 3.2(b) shows the proposed equivalent circuit describing the three components of a BPM. The first component is $R_\Omega$, related to the conductivity of the combined membrane layers. This component follows Ohm's law ($V = IR$), and since there is no capacitive effect in $R_\Omega$, it is independent of frequency. The resistance can be determined from a Nyquist plot by measuring the distance between the origin and the start of the first semicircle. This value also includes the Ohmic losses of the electrolytes from the membrane to the reference electrodes.

The second component of the equivalent circuit describes the WDR, and the kinetics of this reaction are in the form of a resistance ($R_{WDR}$). In parallel with the resistor is the electric double layer of the internal interface, represented as a non-ideal capacitor ($Q_{DL}$). This RQ-network shows the typical semicircle of a charge transfer reaction, [18] in this case to produce protons and hydroxide ions. $R_{WDR}$ is equal to the width of the semicircle, and $Q_{DL}$ is the inverse of the angular velocity ($\omega = 2\pi f$) of the peak height and $R_{WDR}$. Since a BPM typically has a non-uniform current distribution, the system cannot be described with an ideal capacitor. Instead, a constant phase element is used, including a non-ideality factor $n$, lying between 0 and 1, with $n = 0$ being a resistor and $n = 1$ an ideal capacitor. [24] Hurwitz and Dibiani (2003) described the water dissociation component of their equivalent circuit in combination with a component related to the proton gradient near the membrane-membrane interface. [28] However, in our and their experiments, there is no indication that this gradient component is required for successful fitting of the

results, and it is therefore considered to be a part of the water dissociation component.

The third component relates to the diffusion boundary layer between the membrane layers and electrolytes. When ions are transported out of the membrane layer and surrounded by mobile charges with the same charge, they enter an electroneutral solution with which they differ in concentration. This effect happens due to the Donnan exclusion in the membrane layer, which is the source of the Donnan potential between the diffusion layer of the electrolyte solution and the membrane layer. [35, 36] This is especially true when the concentration of the protons or hydroxide ions is low in the electrolyte (e.g. in a bicarbonate electrolyte). Similar to the second component, the resistance that the transported ions encounter ($R_{DBL}$) is in parallel with a non-ideal capacitor, represented by a constant phase element ($Q_{DBL}$). These two elements both show non-linear behavior upon a variation of current. First, the resistance is created by concentration polarization at the membrane-electrolyte interface. Since impedance is the ratio of the voltage, which is described by the Donnan potential $\Delta\Phi_{Donnan} = ln(C_i/\bar{C}_i)$ with $\bar{C}_i$ the concentration of species $i$ in the membrane and the current, the resistance is non-linear dependent upon a varying current. This is because of the logarithmic behavior as well as the non-linear behavior of $C_i/\bar{C}_i$ in non-steady state. [37] Second, the non-ideal capacitor, which is created by the change in charges at these interfaces, is also a function of concentration. Since the change in charge of all species in this region is not linear, the DBL is not linear [38], as shown in Figure 3.3 which gives a schematic representation of the concentration profile of three electrolytes of the membrane-solution interface. For example, for a CEL the concentration of the cations is equal to the sum of the concentrations of the fixed charges and the anions, which are present due to non-ideality of the membrane layer. Once a current is applied, cations migrate out of the CEL towards the cathode, and protons replenish the membrane layer to maintain electroneutrality. This is visible when $KHCO_3$ is used as catholyte (left in Figure 3.3). Due to the different diffusion coefficients in the membrane layer and electrolyte, a diffusion boundary layer is formed once a current is applied, which is dominated by the main carrier of the current, e.g. $OH^-$ in the case of the AEL.

Most literature has focused on the first two components, since the third component is typically found at lower frequencies (<1 Hz) and requires a stable setup to perform long term measurements to reduce noise. [25, 26, 28] In addition to the experimental data present in the literature, also modelling has been performed of the electrochemical impedance response by Alcaraz et al. based on the Nernst-Planck and Poisson equations, describing the membrane-membrane interface as a pn-junction. [39] The model does not include the diffusion boundary layers at the electrolyte-membrane interface, which is a limitation for comparing the results with this work. Yan et al. studied a BPM at lower frequency in their supple-

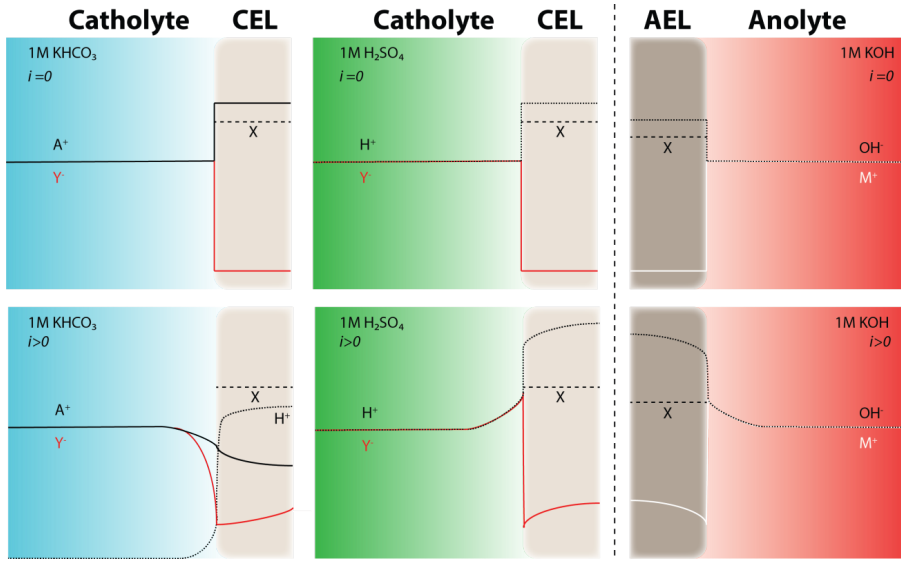


Figure 3.3: Concentration profiles of electrolytes near ion exchange layer, in the diffusion boundary layer. Assuming that no ion exchange occurs when no current is applied, there is no DBL when $i = 0$. If $i > 0$, migration component results in an increased concentrations of present ions. At the membrane-solution interface, there is the double layer where no electroneutrality occurs, with $X$ concentration of fixed charges, $A^+$ and $M^+$ concentration of cations and $Y^-$ concentration of anions.

mentary information; however, they described the third component as a Gerischer impedance coupling the diffusion boundary layer to a chemical reaction. [40] In our work, the EIS results from two different electrolyte pairs across a BPM are shown, indicating that the co-ion plays a role in the diffusion boundary layer as well as in the WDR component of the equivalent circuit.

## 3.3. METHODS

In this work, we compare two different electrolyte combinations across a BPM during electrolysis to determine the effect of co-ions on the water dissociation reaction. One electrolyte pair theoretically contains no co-ions in the membrane layer ($H_2SO_4$ as the catholyte and KOH as the anolyte), because $SO_4^{2-}$ and $K^+$ will be excluded from the CEL and AEL, respectively, based on ion-selectivity of the membrane layers. For simplicity, this case will be designated as the 'no co-ions$_{mem}$' case, where the 'mem' indicates that this is only the case in ideal membrane layers. Another electrolyte pair, $KHCO_3$ and KOH, does contain a co-ion in the CEL in the form of $K^+$, and is designated as the 'co-ions' case. Bicarbonate is often used as an electrolyte for the $CO_2$ reduction reaction due to its buffer capacities and optimal pH to partially suppress the hydrogen evolution reaction. [41] Therefore this electrolyte was chosen to assess its compatibility with a BPM for use in a $CO_2$ER system.

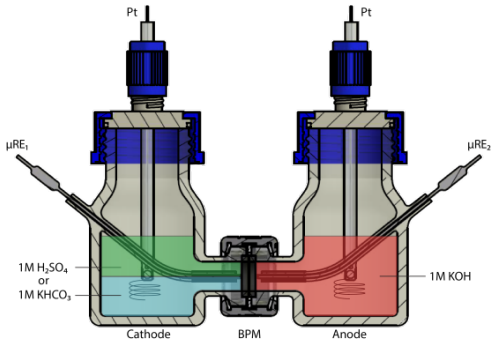


Figure 3.4: Schematic illustration of impedance setup in H-cell configuration with the two used electrolytes ($H_2SO_4$ and $KHCO_3$) in the catholyte, separated from the anolyte (KOH) by a BPM.



Specifications of the chemicals and materials used are described in the supporting information (see Section 3.7).

A commercially available Fumatech BPM was used in all experiments, which were performed with a SOLARTRON potentiostat (EnergyLab XM) in galvanostatic mode and three cycles of frequency to reduce noise. The frequency was varied from 10 kHz to 1 mHz. Bode plots shown here are smoothed with a Lowess method. EIS measurements were performed in a 4-electrode setup (Figure 3.4) with two Ag/AgCl reference electrodes placed on both sides of the BPM, and the effective distance is therefore approximately 0.5 mm from the bipolar membrane in an aqueous H-cell configuration. The membrane has a surface area of 1.33 $cm^2$. Working and counter electrodes are made of Pt-wires and each have a surface area of 2.83 $cm^2$. Ageing experiments were performed in a flow cell (see Figure S3.1), with a membrane and electrode surface area of 10 $cm^2$. Analysis of the impedance data was performed with ZView 2 (Scribner), and the fitting was performed with the equivalent circuit shown in Figure 3.2, which will be used to indicate the performance of the individual components of the BPM discussed in the results.

## 3.4. RESULTS & DISCUSSION

Nyquist plots for the case of co-ions ($KHCO_3$ vs. KOH) were obtained as a function of current density, shown in Figure 3.5(a). As the current density increased, the diameter of the semicircle decreased, showing a lower resistance across the membrane. The variation of the origin of the semicircle is due to the changing of the position of the reference electrode in each experiment, and does not affect the resistive features associated with the semicircle itself. Bode plots were also obtained as a function of current density, as shown in Figure 3.5(b) where two major features can be seen in the form a phase shift. A peak in the phase shift indicates an increase of the imaginary impedance, indicative for a capacitive effect. At low current den-

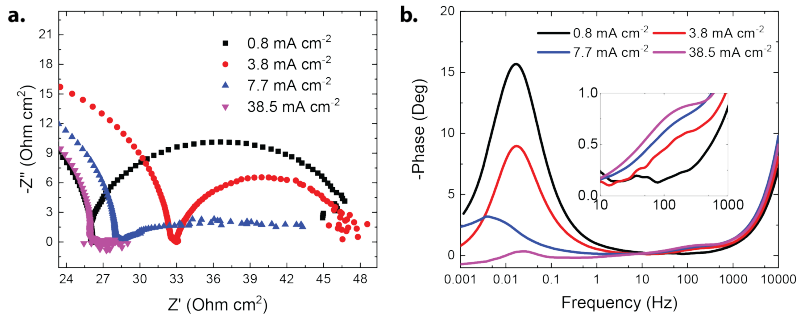


Figure 3.5: Presence of co-ions (1 M $KHCO_3$ vs. KOH) in function of DC current with an amplitude of 50% of the direct current. (a) Nyquist plot and (b) Bode plot with varying frequency.

sities, a large peak is present below 1 Hz, and a minimum in the phase shift can be seen around 100 Hz. As the current density is increased, the peak below 1 Hz decreases significantly, while a subtle peak emerges between 10 and 500 Hz, shown in the inset of Figure 3.5(b). In addition, another increase of the phase shift is visible at frequencies above 1000 Hz; however, this increase is independent of the applied current. Furthermore, it is a high frequency dispersion or stray capacitance of the reference electrodes, which is caused by the limited exchange capacity of the glass frit at high frequencies and appears as a capacitance effect in the Bode plot. Additionally, 1M $Na_2SO_4$ vs. $Na_2SO_4$ was tested, similar to the case of the co-ions does this electrolyte combination also contain co-ions at the membrane-membrane interface and showed similar behavior as for 1M $KHCO_3$ vs. KOH (see Figure S3.5).

EIS experiments were also performed at different current densities in the no co-ions$_{mem}$ case ($H_2SO_4$ vs. KOH) and reveal a completely different behavior compared to the prior case. Nyquist plots similarly show a changing origin of the semicircle, but no variation in the radius of the semicircle with increasing current density, shown in Figure 3.6(a). The Bode plot shows no peak in phase shift below 1 Hz and only a peak between 10 and 1000 Hz is observed, which does not change significantly with different current densities, as shown in Figure 3.6(b). At higher frequencies, a stray capacitance is visible, similar to the case with no co-ions$_{mem}$.

When the data from Figures 3.5 and 3.6 is compared, the previously described equivalent circuit can be matched to specific frequency ranges and physical phenomena. The first component of the equivalent circuit, related to the Ohmic resistance ($R_\Omega$), depends primarily on the conductivity of the membrane, relating to the mobility of ions in the membrane layers as shown schematically in Figure 3.7(a). It is important to note that EIS does not allow the ability to determine $R_\Omega$ without including the conductivity of the electrolyte, which should be limited due to the relatively short distance between the reference electrodes and the membrane. The second com-

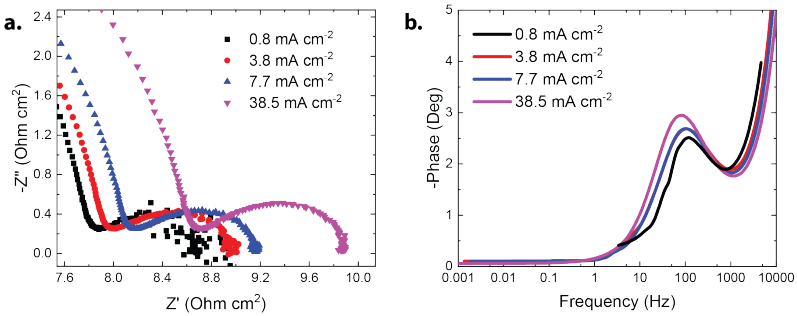


Figure 3.6: Impedance results of the no co-ions$_{mem}$ case (1 M $H_2SO_4$ vs. KOH) in function of DC current with an amplitude of 50% of the direct current. (a) Nyquist plot and (b) Bode plot with varying frequency.

ponent of the equivalent circuit is related to the water dissociation reaction, shown schematically in Figure 3.7(b). Based on the presence of two peaks in the co-ions case (1 M $KHCO_3$ vs. KOH), and only one peak in the no co-ion case (1 M $H_2SO_4$ vs. KOH), it is likely that the shared peak in the frequency range between 10 and 1000 Hz (for this specific membrane) is related to the water dissociation reaction that occurs in both cases above $j_{plateau}$. This peak is represented in the equivalent circuit with a resistor ($R_{WDR}$) and a constant phase element ($Q_{DL}$) in parallel. The peaks are fitted with ZView2, and an example of the fitting curve is given in Figure S3.4. For the no co-ions$_{mem}$ case, Table 3.1 shows the fitted $R$ and $Q$ values, alongside the position of the phase shift peaks. The slight variation in the fitted values corresponds with the limited change in the kinetics of the WDR that may be related to ageing of the BPM, as will be discussed later. In the case of $H_2SO_4$ vs. KOH, the local environment at the catalytic active sites remains similar since the bulk electrolyte contains the same mobile species at these different currents, consisting mostly of fixed charges, water and protons or hydroxide ions, depending on the membrane layer. The role of the flux of ions produced at the membrane-membrane interface does not affect the WDR peak, since the flux has to match the consumption of ions at the electrode. The amount of crossover of co-ions at 50 mA $cm^{-2}$ is 1.5% (see Table S3.1), while the rest of the current transported towards the electrodes comes from the WDR.

Table 3.2 and 3.3 show the fitted RC-values for the co-ions case (1 M $KHCO_3$ vs. KOH) for the WDR and DBL peak, respectively. In this case, both peaks are dependent on the applied current. The lower $n$-value of the WDR capacitor indicates that the capacitor is less ideal than the no co-ions$_{mem}$ case. Furthermore, when a current is applied below the plateau current density, $j_{plateau}$, e.g. in the case of 0.8 mA $cm^{-2}$, no WDR peak is visible. Indeed, analysis from an ion-coupled plasma optical emission spectrometer (ICP-OES) showed a 100% co-ion crossover (see Table S3.2), implying that below $j_{plateau}$ no net WDR occurs. At higher currents, a

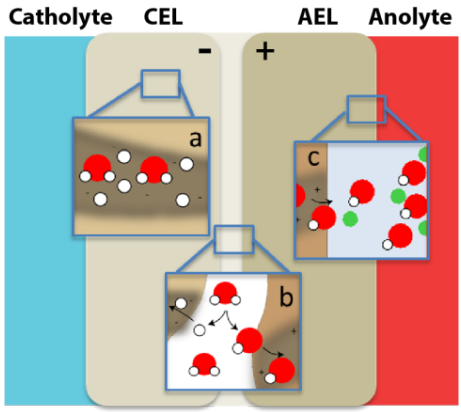


Figure 3.7: Schematic representation of (a) Ohmic losses, (b) water dissociation reaction, and (c) diffusion boundary layer.

Table 3.1: Impedance data of the no co-ion case (1 M $H_2SO_4$-KOH), with the WDR semicircle fitted via an equivalent circuit. $f_{WDR}$ is the frequency at which the phase shift ($\theta_{WDR}$) is maximised. $R_{WDR}$, $Q_{DL}$ and $n_{WDR}$ are resistance, constant phase element and fitting parameter of the WDR semicircle.

| **j** $mA\,cm^{-2}$ | **-$\vartheta_{WDR}$** $Deg$ | **$f_{WDR}$** $Hz$ | **$R_{WDR}$** $\Omega\,cm^2$ | **$Q_{DL}$** $mF\,cm^2$ | **$n_{WDR}$** - |
|---|---|---|---|---|---|
| 0.8 | 2.51 | 116.5 | 0.91 | 7.80 | 0.85 |
| 3.8 | 2.68 | 107.8 | 1.07 | 6.50 | 0.85 |
| 7.7 | 2.69 | 100.0 | 1.08 | 7.15 | 0.85 |
| 38.5 | 2.95 | 79.6 | 1.29 | 7.41 | 0.85 |

Table 3.2: Impedance data of the no co-ion case (1 M $KHCO_3$-KOH), with the WDR semicircle fitted via an equivalent circuit. $f_{WDR}$ is the frequency at which the phase shift ($\theta_{WDR}$) is maximised. $R_{WDR}$, $Q_{DL}$ and $n_{WDR}$ are resistance, constant phase element and fitting parameter of the WDR semicircle.

| **j** $mA\,cm^{-2}$ | **-$\vartheta_{WDR}$** $Deg$ | **$f_{WDR}$** $Hz$ | **$R_{WDR}$** $\Omega\,cm^2$ | **$Q_{DL}$** $mF\,cm^2$ | **$n_{WDR}$** - |
|---|---|---|---|---|---|
| 0.8 | - | - | - | - | - |
| 3.8 | 0.55 | 146.8 | 1.95 | 3.64 | 0.60 |
| 7.7 | 0.64 | 108.0 | 1.69 | 6.50 | 0.60 |
| 38.5 | 0.80 | 125.9 | 1.30 | 9.10 | 0.70 |

Table 3.3: Impedance data of the co-ions case (1 M $KHCO_3$ vs. KOH), with DBL semicircle fitted via equivalent circuit. $f_{DBL}$ is the frequency at which the phase shift ($\theta_{DBL}$) is maximised. $R_{DBL}$, $Q_{DBL}$ and $n_{DBL}$ are resistance, constant phase element and fitting parameter of the DBL semicircle.

| **j** $mA\,cm^{-2}$ | **-$\vartheta_{DBL}$** $Deg$ | **$f_{DBL}$** $Hz$ | **$R_{DBL}$** $\Omega\,cm^2$ | **$Q_{DBL}$** $mF\,cm^2$ | **$n_{DBL}$** - |
|---|---|---|---|---|---|
| 0.8 | 15.68 | 0.017 | 22.35 | 0.91 | 0.95 |
| 3.8 | 8.97 | 0.017 | 13.00 | 1.39 | 1.00 |
| 7.7 | 3.19 | 0.004 | - | - | - |
| 38.5 | 0.34 | 0.025 | 0.52 | ~19.5 | 0.70 |

lower capacitance in the electrical double layer is observed, trending towards similar values as in the case with no co-ions$_{mem}$. In addition, the resistance of the WDR converges towards similar values for both electrolyte pairs as the current densities increases, indicating that the conditions near the membrane-membrane interface are the same at those conditions. At these higher currents, fewer co-ions—in this case $K^+$—are present at the interface, which corresponds more to the situation of the case of no co-ions$_{mem}$. The increase in $R_{WDR}$ compared to the no co-ions$_{mem}$ case is clarified via Figure 3.8, which shows the i-V curve (red) of a BPM in the co-ion case (1 M $KHCO_3$ vs. KOH). In this figure, a plateau current density is observed between 0.4 and 0.8 V of the BPM potential.

The third component of the equivalent circuit is related to the diffusion boundary layer at the electrolyte-membrane interface, and is only visible at frequencies below 1 Hz, as shown in Figure 3.5 experimentally and Figure 3.7(c) schematically. The EIS data obtained from the fitted DBL semicircle for the co-ion case is shown in Table 3.3. Quantifying the resistance is useful to determine the energy loss of this component as it is noticeable during direct current operation, whereas the $Q_{DBL}$ is not noticeable during direct current operations. However, $Q_{DBL}$ is still a good measure for the build-up of charge caused by the change of transport numbers of the ions that move across in the membrane layer compared to the bulk solution. [24] At lower current densities, diffusion and migration are of the same order of magnitude, indicating that ion transport is not dominated by either of them, and co-ions

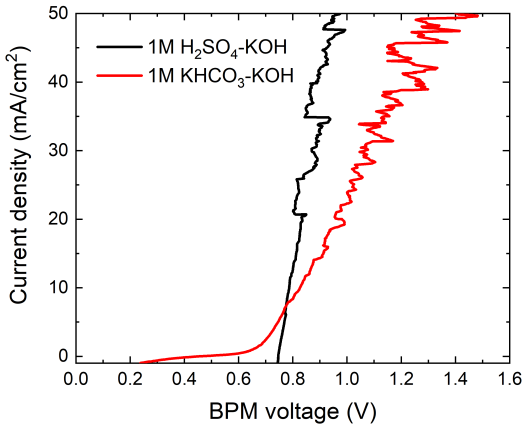


Figure 3.8: i-V curves of a BPM for the co-ion case (1 M $KHCO_3$ vs. KOH) in red and for the no-co-ion case (1 M $H_2SO_4$-KOH) in black. Both curves are obtained with a galvanodynamic scan at a scan rate -0.1 mA cm$^{-2}$ s$^{-1}$ with the flow cell.

with their respective charge are present at the interfaces. As a result of the presence of these co-ions, a lower capacitance is noticed at lower current densities (see Table 3.2).

Both for the WDR and the DBL peak, the decrease in the capacitance at higher current densities for the co-ions case (1 M $KHCO_3$ vs. KOH) can possibly be explained by changes in concentrations of species at the respective interfaces. One hypothesis to explain this is that the supporting electrolyte is more conducting at higher current densities, as $H^+$ and $OH^-$ are the most mobile ions. In addition, the buffer capacity of the electrolyte near the BPM may decrease due to the change in local pH, as simulated by Ke et al. [21] This decrease in buffer capacity results in a lower capacitance since the charge can no longer be stored near the BPM. [42] At higher current densities, there will be relatively less transport of co-ions at steady state because of the direction of the migration component, which transports the co-ions away from the BPM. Combined with the change of local pH, this reduces the difference in transport numbers of the ions ($H^+$ and $OH^-$ for these high currents) that are transported in the membrane layer compared to the bulk solution. In the no co-ions$_{mem}$ case (1 M $H_2SO_4$ vs. KOH), this difference in transport number at the membrane-electrolyte interface is rather small, since the concentration of protons is similar to the concentration in the bulk solution. Similar trends are observed when negative currents are applied for the case of no co-ions$_{mem}$ ($H_2SO_4$ vs. KOH), while a plateau also appears in the i-V curve around -35 mA cm$^{-2}$ along with a DBL component in the Bode plot (see Figure S3.2). Although this mechanism is not yet

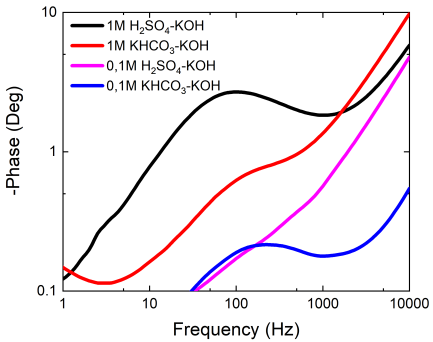


Figure 3.9: Bode plot of 1 M and 0.1 M electrolyte concentrations across the BPM. Curves were obtained at 7.7 mA $cm^{-2}$ with 50% amplitude.



fully understood, it does imply that the equivalent circuit shown in Figure 3.2(b) is generalizable for different combinations of pHs surrounding the BPM, as well as different concentrations that will be discussed in the following section.

### 3.4.1. CONCENTRATION EFFECT

In order to understand the effect of the concentrations of ions in and around the BPM, EIS data were obtained for electrolyte pairs as a function of electrolyte concentration. When the concentration of $H_2SO_4$-KOH was lowered from 1 M to 0.1 M, for the no co-$ions_{mem}$ case, the WDR peak is reduced in size, as shown in Figure 3.9 and Table S3.3 with the fitted results. However, no WDR peak is visible for 0.1 M $KHCO_3$ vs. KOH, as the peak might be hidden within the stray capacitance.

From the i-V curve of the 0.1 M $H_2SO_4$/KOH case (Figure S3.3), the kinetics of the WDR seems to be lowered compared to the higher concentration case. Also, the WDR capacitance has reduced (Table S3.3), indicating that fewer mobile charge species are present in the membrane-membrane interface. This is schematically shown in Figure 3.10, with the concentrations profile of three electrolytes with a concentration of 0.1 M when a current is applied to the system. The flux of ions will create a DBL at the membrane-solution interface, which is smaller than in the case of a 1 M concentration (Figure 3.3). Since there is a lower concentration of co-ions in the bulk, the concentration gradient is also lower, reducing the driving force for ions with a similar charge as the fixed charges to diffuse into the membrane layer. Because of electroneutrality, this then leads to a lower concentration of the ions of opposing charge, which reduces the charge at the membrane-membrane interface.

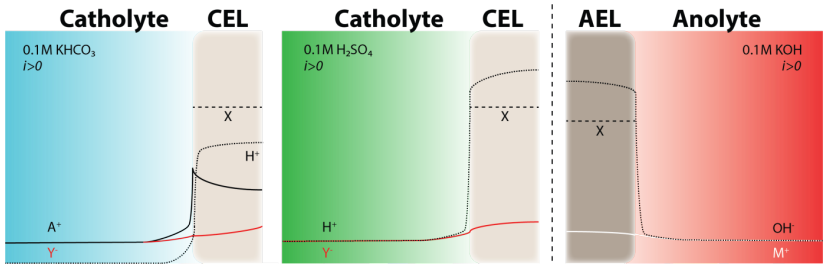


Figure 3.10: Qualitative estimation of concentration profiles for diluted salt concentrations in the electrolyte.

## 3.5. AGEING OF BPM

In this section, we introduce electrochemical impedance spectroscopy as a tool to in-situ observe the ageing of a BPM and membranes in general. When a BPM is used in industrial applications, high activity and durability are of high importance. The performance of the BPM should also be measurable in operation, which is possible by applying a small perturbation to the DC current or voltage, resulting in the typical EIS graphs presented above. Differentiating between the individual components, such as conductivity of the membrane or kinetics of the WDR, reveals which methods can be used to prolong the lifetime of the membrane, e.g. lowering the current or replacing the electrolyte(s), or, if that is no longer sufficient, renewing the BPM.

For this purpose, a BPM was tested in a flow cell (see Figure S3.1) of 10 $cm^2$ with a flow rate of 0.07 $cm^3\ s^{-1}$ in 1 M $H_2SO_4$ vs. 1.3 M KOH. An impedance measurement was performed at the beginning of the experiment with an applied direct current of 20 mA $cm^{-2}$ and an EIS amplitude of 5 mA $cm^{-2}$. After this, for 5 days a DC current of 0, 50, and 100 mA $cm^{-2}$ was applied, respectively. Immediately after this experiment, the same EIS measurement was repeated. Similarly, 0 and 50 mA $cm^{-2}$ were tested for 1M $KHCO_3$ vs. NaOH. Both experiments for all current densities are shown in Figure 3.11.

For the experiment with no current applied, only a slow exchange of co-ions via diffusion was observed, driven by the concentration gradient across the BPM. For the no co-$ions_{mem}$ case ($H_2SO_4$ vs. KOH), analysis from ICP-OES showed an exchange of 10% $K^+$ from the anolyte towards the catholyte after 5 days of open-circuit operation. Once a current was applied, the crossover increased to 20% and 32% for 50 and 100 mA $cm^{-2}$, which was 11% and 13.5% of the applied current, respectively. The crossover of $SO_4^{2-}$ was minor compared to $K^+$, as can be seen in Table S3.1. The increase of the crossover can be described by the extra migration component that is related to the electric field gradient on the system, which transports $K^+$ through the membrane towards the cathode that attracts positive charged ions. These high

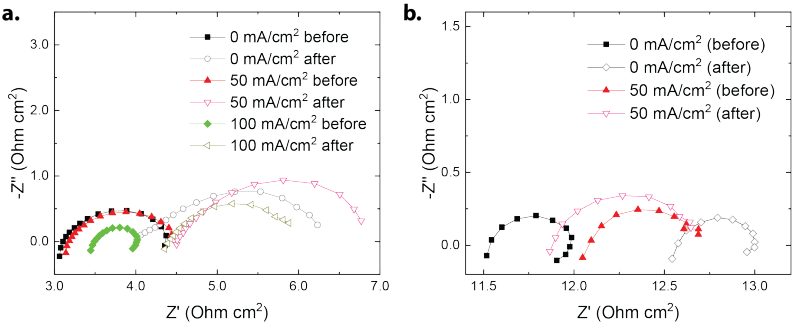


Figure 3.11: Ageing of a BPM over 5 days (a) at 0, 50, and 100 mA $cm^{-2}$ in 1 M $H_2SO_4$ and 1.3M KOH and (b) at 0 and 50 mA $cm^{-2}$ in 1 M $KHCO_3$ and 1 M NaOH in a flow cell with 60 rpm. EIS performed with a frequency range between 10 kHz and 0.4 Hz. Lower frequencies are not shown because of the noise limitations of the flow cell (e.g., due to gas bubbles) in that frequency range.

Table 3.4: Impedance data of WDR semicircles after stability measurements.

| **Electrolyte** | **Current density** $mA\,cm^{-2}$ | **State** | $\mathbf{R_{WDR}}$ $\Omega\,cm^2$ | $\mathbf{Q_{WDR}}$ $F\,cm^2$ | $\mathbf{n_{WDR}}$ - |
|---|---|---|---|---|---|
| 1M $H_2SO_4$-KOH | 0 | Before | 1.30 | 0.35 | 0.80 |
| | 0 | After | 2.10 | 0.30 | 0.80 |
| | 50 | Before | 1.30 | 0.55 | 0.75 |
| | 50 | After | 2.40 | 0.26 | 0.85 |
| | 100 | Before | 0.52 | 0.25 | 0.90 |
| | 100 | After | 1.70 | 0.52 | 0.75 |
| 1M $KHCO_3$-NaOH | 0 | Before | 0.50 | 0.40 | 0.85 |
| | 0 | After | 0.45 | 0.55 | 0.85 |
| | 50 | Before | 0.60 | 0.55 | 0.85 |
| | 50 | After | 0.85 | 0.55 | 0.85 |

crossover numbers indicate that this membrane is not ideal for systems that are sensitive to fouling from neighboring co-ions. This strong degradation is not visible in the co-ions case (Figure 3.11(b)). Alongside the strong degradation of the membrane in extreme conditions, there is a strong need for further membrane development using the discussed techniques in order to successful implement BPMs in current technologies and reduced energy costs.

When the system is subject to an applied current density of 50 mA $cm^{-2}$ for 5 days, the increase in the potential over the BPM is around 170 mV. EIS results (Figure 3.11(a), two measurements in red), show the individual increases of the membrane components can be determined. The Ohmic resistance increased from 3.2 $\Omega$ $cm^2$ to 4.2 $\Omega$ $cm^2$, which corresponds to a voltage loss of 50 mV. This extra Ohmic

resistance loss is associated to the bulk of the membrane layers, which is known from literature to occur via charge leaching at high pH. [43] The difference in the width of the two semicircles resulted in another 50 mV increase. The remaining extra potential of the 170 mV can be attributed to the finite membrane selectivity, which causes ion crossover, lowering the conductivity and resulting in an extra Ohmic loss. Other effects have a minimal impact on the ageing including the diffusion boundary component, which is neglected since this component is negligible for the no co-ions$_{mem}$ case ($H_2SO_4$ vs. KOH), and the pH remained nearly constant throughout the experiment.



The increase in the WDR resistance after ageing is noteworthy, especially since it is not accompanied by an increase in the capacitive component in the equivalent circuit. The capacitor is represented as a double layer in the internal interface because of the strong polarized environment. There are two possible explanations for the decrease in the kinetics. The first is the reduced activity of the catalyst at the interface, which performs reactions (3.1) and (3.2), due to lowered number of fixed charges via recombination—where positive and negative fixed charges recombine to form a neutral component. The importance of the catalyst loading has been studied earlier in relation with required voltage, and in general the lower the catalyst loading, the higher voltage is required. [12, 40] The second explanation is the widened interface thickness, which was proven in literature to have an import impact on the voltage. [16] Here, the integration of the layers at the membrane-membrane interface separated in time. Therefore, the interfacial catalyst and the electronic properties of the interface itself should be main focus points in the future developments and minimization of operational losses in BPMs.

## 3.6. CONCLUSIONS

In this work, a bipolar membrane was examined using electrochemical impedance spectroscopy, which makes it possible to differentiate electronic information among the different components of the membrane. In particular, the interface between the two membrane layers was of interest. At this interface, the water dissociation reaction occurs, which dissociates water into protons and hydroxide ions under an applied potential. However, depending on the electrolyte(s) surrounding the membrane, the i-V curves behaves differently. Therefore, two cases were studied, one without co-ions and the other with co-ions. It was demonstrated that the individual components, such as the kinetics of the water dissociation reaction and the capacitance of the diffusion boundary layer, can be identified using EIS, contributing to understanding of electrochemical elements within the BPM. EIS shows that at low current densities below the plateau current density, a different behavior exists, which is dominated by co-ion transport. The co-ions case showed a plateau at a low current density, where co-ions seem to be responsible for the charge transport (shown with ICP-OES analysis) and no WDR peak is visible in the impedance measurement. At higher current densities for $KHCO_3$/KOH, and at all (positive) current

densities for the $H_2SO_4$/KOH case, impedance spectra show a clear capacitive element that is ascribed to the WDR. Finally, EIS has proven to be a useful tool to monitor the ageing of a BPM and to determine which component is affected most by the ageing, which is important to design and implement BPMs in electrochemical cells for industrial applications.

## 3.7. SUPPLEMENTARY INFORMATION

### 3.7.1. MATERIALS

The H-cell used in the experiments was designed by Ben in 't Veen and produced by Shell. The Pt wires used as work and counter electrode were produced by Heraeus with a diameter of 300 µm, with a Pt electrode sputtered on a Ti substrate and a Ni electrode of analytical grade. The flow cell, MicroFlowCell, was purchased from Electrocell (Denmark). The micro reference electrodes of type LF-1-100 are manufactured by Innovative Instruments Inc. and have a polyetheretherketone (PEEK) body with a diameter of 1 mm. The commercial BPM, Fumasep FBM-PK, used in this study was produced by Fumatech GmbH (Germany). $H_2SO_4$ (95-97% purity), KOH (45 wt% in H2O) and $KHCO_3$ (99.7% purity) were purchased from Sigma Aldrich. NaOH (Baker analyzed, J.T. Baker) was purchased from Boom.

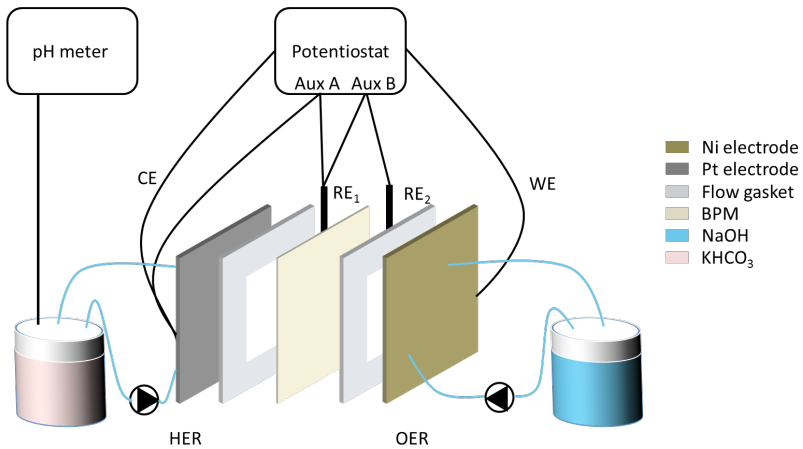


Supplementary Figure S3.1: Flow cell schematic for studying the aging of BPMs for a longer duration.

### 3.7.2. ELECTROCHEMICAL IMPEDANCE SPECTROSCOPY

By performing the impedance measurements in galvanostatic mode, i.e. applying a fixed direct current (DC), a positive potential difference across the BPM is measured. Upon the application of this current, an alternating current is applied around this direct current. This secondary current has the form of a sinusoidal wave ($I = I_0 sin(\omega t)$) with the applied current shown as the amplitude, $I_0$, of the wave and the angular frequency, $\omega = 2\pi f$, which depends on the applied frequency, $f$. The impedance is then determined by the ratio of the measured voltage versus the applied current. Hereby, it is important to minimize the ratio of noise versus data by increasing the amplitude $I_0$ without exceeding the local linear region, which is important to avoid distortion of the impedance data. This region can be assessed by performing galvanodynamic scans as shown in Figure 3.1. At lower current den-

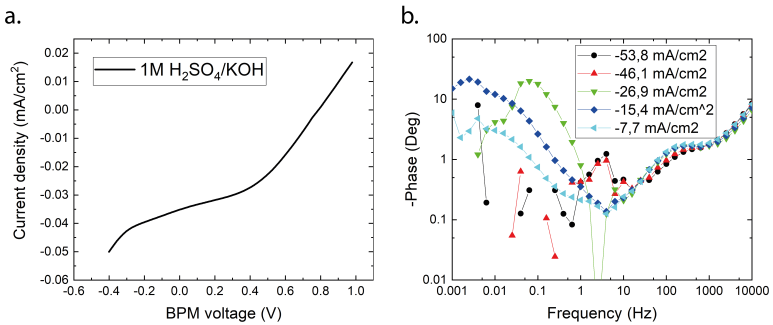


Supplementary Figure S3.2: (a) i-V curve of $H_2SO_4$-KOH in H-cell, and (b) impedance plots at negative currents of a BPM in $H_2SO_4$-KOH, lower current densities suffered from noise in the lower frequency region (<1 Hz).

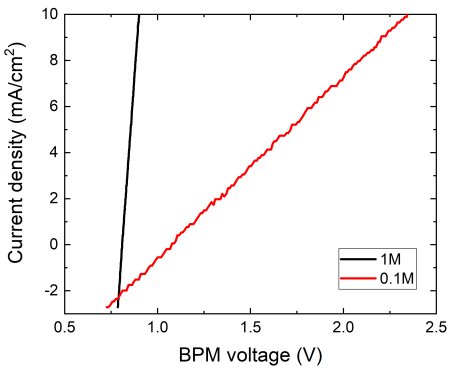


Supplementary Figure S3.3: i-V curves of 1M and 0.1M of $H_2SO_4$ vs. KOH.

sities, the amplitude is rather small to avoid ending up in the plateau region, resulting in a higher noise vs data ratio, explaining the scattering in for example in Figure 3.6. Data obtained from impedance measurements are often shown in a Nyquist plot, where the negative imaginary impedance is plotted as a function of the real impedance on the x-axis and in a Bode plot (examples shown in Figure 3.5), where the phase shift is plotted as a function of the applied frequency. An increase on the negative axis of the phase shift indicates a capacitive effect and is shown as a semi-circle on a Nyquist plot.

Supplementary Table S3.1: Co-ion crossover data, with values obtained after ageing measurements (5 day experiments). If one wants to know the relative crossover through the bipolar membrane (BPM), the crossover value, expressed in mol per liter, should be divided by the total amount of protons consumed. The total amount of protons can be calculated by dividing the total charge by the Faraday constant ($F = 96485 C/mol$). For example, for 50 mA $cm^{-2}$ in 5 days in the flow cell, the total consumption of protons is 2.23 mol protons. Using a 100 ml reservoir, the concentration is 22.3 M $H^+$. If the exchange of $K^+$ in those 5 days is 11 g/l, with an atomic mass of 39.09 g/mol, the concentration in the catholyte is 0.46 mol/l, which is 10% crossover of the exchanged current. If a similar calculation is performed for $SO_4^{2-}$, the reported value of 13% is found.

| **Current density** | **1M KHCO3** | | | **1M NaOH** | | |
|---|---|---|---|---|---|---|
| $mA\ cm^{-2}$ | **S [g/l]** | **K [g/l]** | **Na [g/l]** | **S [g/l]** | **K [g/l]** | **Na [g/l]** |
| 0 | <0.1 | 40.2 | 4.39 | <0.1 | 3.9 | 18.48 |
| 50 | <0.1 | 50.8 | 10 | <0.1 | 0.2 | 19 |
| **Current density** | **1M H2SO4** | | | **1.3M KOH** | | |
| $mA\ cm^{-2}$ | **S [g/l]** | **K [g/l]** | **Na [g/l]** | **S [g/l]** | **K [g/l]** | **Na [g/l]** |
| 0 | 35 | 4.9 | <0.1 | 0.5 | 50 | 0.34 |
| 50 | 39 | 11 | <0.1 | 0.7 | 55 | 0.35 |
| 100 | 46 | 18 | 0.13 | 0.9 | 62 | 0.42 |

Supplementary Table S3.2: Co-ion crossover of KHCO3 and NaOH at currents below plateau current density (1 mA/cm2) applied for 45 min.

| | **1M KHCO3** | | | **1M NaOH** | | |
|---|---|---|---|---|---|---|
| | **S [g/l]** | **K [g/l]** | **Na [g/l]** | **S [g/l]** | **K [g/l]** | **Na [g/l]** |
| 1 mA/cm2 | <0.1 | 41.8 | 0.71 | <0.1 | 0.4 | 21.52 |
| REF | <0.1 | 37.1 | 0.12 | <0.1 | <0.1 | 21.96 |

Supplementary Table S3.3: Impedance data to observe concentration effect of the two investigated cases. All measurements are performed at 7.7 mA $cm^{-2}$.

| **Electrolyte** | **-$\vartheta_{WDR}$** *Deg* | **$f_{WDR}$** *Hz* | **$R_{WDR}$** $\Omega\ cm^2$ | **$Q_{DL}$** $mF\ cm^2$ | **$n_{WDR}$** – |
|---|---|---|---|---|---|
| 1M H2SO4-KOH | 2.69 | 100.0 | 1.08 | 7.15 | 0.85 |
| 0.1M H2SO4-KOH | 0.23 | 184.8 | 1.30 | 3.90 | 0.82 |
| 1M KHCO3-KOH | 0.64 | 108.0 | 1.69 | 6.50 | 0.60 |
| 0.1M KHCO3-KOH | - | - | - | - | - |

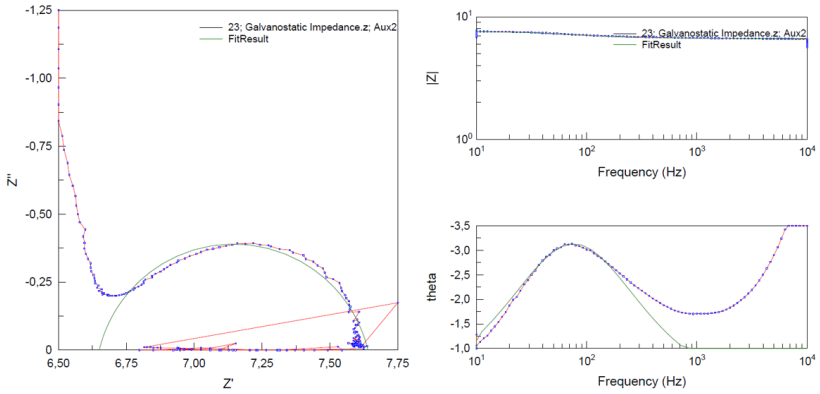


Supplementary Figure S3.4: Example of fitting curve of impedance measurement (1M $H_2SO_4$ vs. KOH at 38.5 mA $cm^{-2}$), which resulted in $R_{WDR} = 1.29\ \Omega\ cm^2$, $Q_{DL} = 7.41 mF\ cm^2$ and $n = 0.85$. Values of Nyquist plot (a) should be multiplied by membrane surface area ($1.3 cm^2$). The fitting occurs according the equivalent circuit (see Figure 3.2 of the manuscript), where n is a fitting parameter, to compensate for non-idealities. The n-value can vary slightly (+-0.1) in order to optimize the R and Q values.

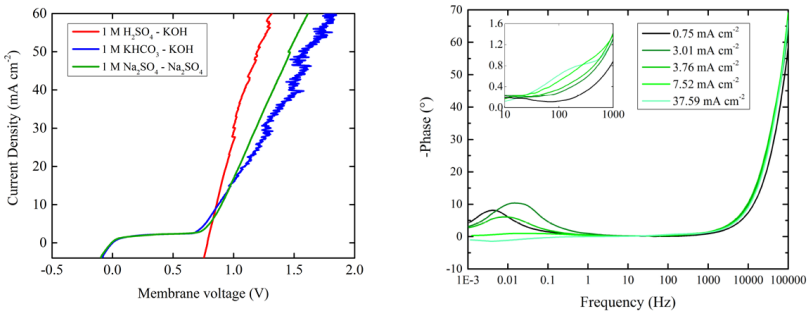


Supplementary Figure S3.5: i-V curve of 1M $Na_2SO_4$ vs. $Na_2SO_4$ compared to previous tested electrolytes and bode plot of 1M $Na_2SO_4$ vs. $Na_2SO_4$ under various current densities, showing similar behavior as the case of co-ions (1M KHCO3 vs. KOH).

## REFERENCES


[1] M. A. Blommaert, D. A. Vermaas, B. Izelaar, B. in 't Veen, and W. A. Smith, *Electrochemical impedance spectroscopy as a performance indicator of water dissociation in bipolar membranes,* Journal of Materials Chemistry A **7**, 19060 (2019).

[2] IPCC, *Global Warming of 1.5 degC*, Tech. Rep. (2018).

[3] FCH JU, *Development of Water Electrolysis in the European Union*, Tech. Rep. (2014).

[4] T. Burdyny and W. A. Smith, *CO2 reduction on gas-diffusion electrodes and why catalytic performance must be assessed at commercially-relevant conditions,* Energy & Environmental Science **12**, 1442 (2019).

[5] M. Jouny, W. W. Luc, and F. Jiao, *A General Techno-Economic Analysis of CO2 Electrolysis Systems,* Industrial & Engineering Chemistry Research , acs.iecr.7b03514 (2018).

[6] S. Ma, R. Luo, S. Moniri, Y. Lan, and P. J. A. Kenis, *Efficient Electrochemical Flow System with Improved Anode for the Conversion of CO 2 to CO,* Journal of The Electrochemical Society **161**, F1124 (2014).

[7] J. Luo, D. A. Vermaas, D. Bi, A. Hagfeldt, W. A. Smith, and M. Grätzel, *Bipolar Membrane-Assisted Solar Water Splitting in Optimal pH,* Advanced Energy Materials **6**, 1 (2016).

[8] Y. C. Li, D. Zhou, Z. Yan, R. H. Gonçalves, D. A. Salvatore, C. P. Berlinguette, and T. E. Mallouk, *Electrolysis of CO2 to Syngas in Bipolar Membrane-Based Electrochemical Cells,* ACS Energy Letters **1**, 1149 (2016).

[9] D. A. Salvatore, D. M. Weekes, J. He, K. E. Dettelbach, Y. C. Li, T. E. Mallouk, and C. P. Berlinguette, *Electrolysis of Gaseous CO 2 to CO in a Flow Cell with a Bipolar Membrane,* ACS Energy Letters **3**, 149 (2017).

[10] D. A. Vermaas and W. A. Smith, *Synergistic Electrochemical CO2 Reduction and Water Oxidation with a Bipolar Membrane,* ACS Energy Letters , 1143 (2016).

[11] N. M. Vargas-Barbosa, G. M. Geise, M. A. Hickner, and T. E. Mallouk, *Assessing the utility of bipolar membranes for use in photoelectrochemical water-splitting cells,* ChemSusChem **7**, 3017 (2014).

[12] M. B. McDonald, S. Ardo, N. S. Lewis, and M. S. Freund, *Use of bipolar membranes for maintaining steady-state pH gradients in membrane-supported, solar-driven water splitting,* ChemSusChem **7**, 3021 (2014).

[13] H.Strathmann, J.J.Krol, H.J.Rapp, and G.Eigenberger, *Limiting current density and water dissociation in bipolar membranes,* Journal of Membrane Science **125**, 123 (1997).

[14] D. A. Vermaas, S. Wiegman, T. Nagaki, and W. A. Smith, *Ion transport mechanisms in bipolar membranes for (photo)electrochemical water splitting,* Sustainable Energy and Fuels **2**, 2006 (2018).

[15] J. Balster, S. Srinkantharajah, R. Sumbharaju, I. Pünt, R. G. H. Lammertink, D. F. Stamatialis, and M. Wessling, *Tailoring the interface layer of the bipolar membrane,* Journal of Membrane Science **365**, 389 (2010).

[16] C. Shen, R. Wycisk, and P. N. Pintauro, *High performance electrospun bipolar membrane with a 3D junction,* Energy Environ. Sci. **10**, 1435 (2017).

[17] J. Pan, L. Hou, Q. Wang, Y. He, L. Wu, A. N. Mondal, and T. Xu, *Preparation of bipolar membranes by electrospinning,* Materials Chemistry and Physics **186**, 484 (2017).

[18] A. J. Bard and L. R. Faulkner, *Electrochemistry* (Wiley, 1944) p. 850, arXiv:1011.1669v3 .

[19] R. E. Moussaoui, G. Pourcelly, M. Maeck, H. D. Hurwitz, and C. Gavach, *Co-ion leakage through bipolar membranes. Influence of I-V responses and water-splitting efficiency,* Journal of Membrane Science **90**, 283 (1994).

[20] H. W. Rösler, F. Maletzki, and E. Staude, *Ion transfer across electrodialysis membranes in the overlimiting current range: chronopotentiometric studies,* Journal of Membrane Science **72**, 171 (1992).

[21] K. Sun, R. Liu, Y. Chen, E. Verlage, N. S. Lewis, and C. Xiang, *Solar-Driven Water Splitting: A Stabilized, Intrinsically Safe, 10% Efficient, Solar-Driven Water-Splitting Cell Incorporating Earth-Abundant Electrocatalysts with Steady-State pH Gradients and Product Separation Enabled by a Bipolar Membrane,* Advanced Energy Materials **6**, 1 (2016).

[22] F. G. Wilhelm, I. Pünt, N. F. Van der Vegt, H. Strathmann, and M. Wessling, *Asymmetric bipolar membranes in acid-base electrodialysis,* Industrial and Engineering Chemistry Research **41**, 579 (2002).

[23] H. Holdik, A. Alcaraz, and S. Mafe, *Electric field enhanced water dissociation at the bipolar membrane junction from ac impedance spectra measurements,* Journal of Electroanalytical Chemistry **442**, 13 (1998).

[24] P. Długołecki, P. Ogonowski, S. J. Metz, M. Saakes, K. Nijmeijer, and M. Wessling, *On the resistances of membrane, diffusion boundary layer and double layer in ion exchange membrane transport,* Journal of Membrane Science **349**, 369 (2010).

[25] V. Zabolotskii, N. Sheldeshov, and S. Melnikov, *Heterogeneous bipolar membranes and their application in electrodialysis,* Desalination **342**, 183 (2014).

[26] S. Mafe, A. Alcaraz, H. Holdik, T. Ruf, and P. Ramõ, *AC impedance spectra of bipolar membranes : an experimental study,* Journal of Membrane Science **150**, 43 (1998).

[27] A. Alcaraz, P. Ramirez, J. A. Manzanares, and S. Mafe, *Conductive and Capacitive Properties of the Bipolar Membrane Junction Studied by AC Impedance Spectroscopy,* J. Phys. Chem. B **105**, 11669 (2001).

[28] H. D. Hurwitz and R. Dibiani, *Experimental and theoretical investigations of steady and transient states in systems of ion exchange bipolar membranes,* Journal of Membrane Science **228**, 17 (2004).

[29] M. S. Park, W. Joo, and J. K. Kim, *Porous structures of polymer films prepared by spin coating with mixed solvents under humid condition,* Langmuir **22**, 4594 (2006).

[30] P. Ramirez, J. A. Manzanares, and S. Mafe, *Water Dissociation Effects in Ion Transport Through Anion Exchange Membranes with Thin Cation Exchange Surface Films,* Ber. Bunsenges. Phys. Chem **95**, 499 (1991).

[31] M. Wien, *Uber die Gultigkeit des Ohmschen Gesetzes fur Elektrolyte bei sehr hohen Feldstarken,* Annalen der Physik **3**, 161 (1924).

[32] R. Simons, *Strong electric field effects on proton transfer between membrane-bound amines and water,* Nature **280**, 824 (1979).

[33] R. Simons, *Water splitting in ion exchange membranes,* Electrochimica Acta **30**, 275 (1985).

[34] R. Simons and G. Khanarian, *Water dissociation in bipolar membranes: Experiments and theory,* The Journal of Membrane Biology **38**, 11 (1978).

[35] A. H. Galama, J. W. Post, M. A. Cohen Stuart, and P. M. Biesheuvel, *Validity of the Boltzmann equation to describe Donnan equilibrium at the membrane-solution interface,* Journal of Membrane Science **442**, 131 (2013).

[36] F. Donnan, *The theory of membrane equilibrium in oresence of a non-dialyzable electrolyte,* Z. Electrochem **17**, 572 (1911).

[37] P. Sistat and G. Pourcelly, *Chronopotentiometric response of an ion-exchange membrane in the underlimiting current-range. Transport phenomena within the diffusion layers,* Journal of Membrane Science **123**, 121 (1997).

[38] J. Bisquert, G. Garcia-Belmonte, F. Fabregat-Santiago, and P. R. Bueno, *Theoretical models for ac impedance of finite diffusion layers exhibiting low frequency dispersion,* Journal of Electroanalytical Chemistry **475**, 152 (1999).

[39] A. Alcaraz, P. Ramırez, S. Mafe, and H. Holdik, *A Simple Model for Ac Impedance Spectra in Bipolar Membranes,* J. Phys. Chem. **3654**, 15555 (1996).

[40] Z. Yan, L. Zhu, Y. C. Li, R. J. Wycisk, P. N. Pintauro, M. A. Hickner, and T. E. Mallouk, *The balance of electric field and interfacial catalysis in promoting water dissociation in bipolar membranes,* Energy & Environmental Science **11**, 2235 (2018).

[41] A. Wuttig, Y. Yoon, J. Ryu, and Y. Surendranath, *Bicarbonate Is Not a General Acid in Au-Catalyzed CO2 Electroreduction,* Journal of the American Chemical Society **139**, 17109 (2017).

[42] R. E. G. V. Hal, J. C. T. Eijkel, and P. Bergveld, *A novel description of ISFET sensitivity with the buffer capacity and double-layer capacitance as key parameters,* Sensors and Actuators B **25**, 201 (1995).

[43] J. R. Varcoe, P. Atanassov, D. R. Dekel, A. M. Herring, M. A. Hickner, P. A. Kohl, A. R. Kucernak, W. E. Mustain, K. Nijmeijer, K. Scott, and L. Zhuang, *Anion-exchange membranes in electrochemical energy systems,* Energy & Environmental Science **7**, 3135 (2014).

# 4

# Reduced Ion Crossover in BPM Electrolysis via Increased Current Density, Molecular Size, and Valence

*A bipolar membrane (BPM) can be used to accelerate water dissociation to maintain a pH gradient in electrochemical cells, providing freedom to independently optimize the environments and catalysts used for paired reduction and oxidation reactions. The two physical layers in a BPM, respectively, selective for the exchange of cations and anions, should ideally reject ion crossover and facilitate ionic current via water dissociation in an interfacial layer. However, ions from the electrolyte do cross over in actual BPMs, competing with the water dissociation reaction and negatively affecting the stability of the electrolytes. Here, we explore the mechanisms of ion crossover as a function of pH and current density across a commercial BPM. Our unique series of experiments quantifies the ion crossover for more than 10 electrolyte combinations that cover 10 orders of magnitude in acid dissociation constant ($K_a$) and current densities spanning over more than 2 orders of magnitude. It was found that the ion crossover is dominated by diffusion for current densities up to a maximum of 10–40 mA cm$^{-2}$ depending on the electrolyte, while migration is of higher importance at high current densities. The influence of the electrolyte p$K_a$ or pH on the ion crossover is not straightforward. However, ions with a higher valence or ion size show significantly lower crossover. Moreover, high current densities are the most favorable for high water dissociation efficiencies for all electrolyte combinations. This operational*

This chapter has been published in *ACS Applied Energy Materials*, 2020, **3**, 6, 5804-5812 [1].

*mode aligns well with practical applications of BPMs in electrolysis at industrial relevant current densities.*

## 4.1. INTRODUCTION

Research and adoption of new renewable energy technologies is accelerated by the combined rapidly decreasing costs of solar and wind-derived electricity and increasing governmental requirements to limit $CO_2$ emissions. The renewable energy capacity is expected to reach 5 TW by 2030, [2] which exceeds the average electricity consumption of 3.5 TW. [3] However, renewables deal with a strongly fluctuating production, expressed by the utilization factor of approximately 20%. [4] Thus, long-term energy storage in the form of synthetic fuels is indispensable to cope with the intermittency (daily and seasonally) of the renewable electricity sources. [5] Such fuels can be produced via electrochemical technologies, which have the potential to directly convert (renewable) electrical energy to chemical bonds. Examples include the water-splitting reaction and electrocatalytic reduction of carbon dioxide ($CO_2$RR), producing hydrogen and various carbon products, respectively. [6] To make these systems perform efficiently at scales relevant for the global energy supply, [7] these reactions should be performed at high current density, high energy efficiency, and with Earth-abundant materials. These constraints require minimizing the applied potential for the entire electrochemical cell, including losses associated with overpotentials for the combined oxidation and reduction reactions, the electrolyte resistance, and membrane functionality.



Considering that the optimal conditions of electrolytes for given redox reactions often differ from each other, a bipolar membrane (BPM) can be implemented to maintain optimized conditions for both half-reactions. [8–13] A BPM consists of a cation and anion exchange layer (CEL and AEL), which are connected by an interfacial layer (IL). This configuration efficiently impedes charged species in the surrounding electrolytes from being transported through the BPM. [14] To maintain the ionic transport within the overall electrochemical cell, the water dissociation reaction (WDR) occurs at the interfacial layer between the CEL and AEL. [15, 16] The WDR, which can be enhanced by the deposition of catalysts [17–20] at the interfacial layer, generates protons and hydroxide ions in the IL at an accelerated rate compared to the water dissociation rate in water. When a reverse bias is applied (i.e., when the CEL faces the cathode), the protons and hydroxide ions are removed from the IL through the cation and anion exchange layer, respectively, which keeps the WDR to proceed. [21–23]

In reality, products of the WDR ($H^+$and $OH^-$) are not the only ions present in the interfacial layer. First, electrolyte salt ions with a charge opposite of the fixed charge of the adjacent membrane layer (i.e., counter ions) can enter the first membrane layer through diffusion. Second, a minority of salt ions with the same charge (i.e., co-ions) can enter the membrane layer because of the finite charge density of the polymer structure, as described in the Teorell-Meyer-Sievers theory, [24, 25] and subsequently reach the interfacial layer. Dependent on the concentration and potential gradient across the membrane, these species can slowly diffuse and/or mi-

grate in a process called ion crossover. When this ion is migrating, the WDR efficiency is reduced because the charge carried by ion crossover cannot be used to release protons and hydroxide ions from the IL. For a water electrolysis cell, where protons are being consumed at the cathode and hydroxides at the anode, ion crossover gradually destabilizes the electrolyte pH values and causes mixing of the two electrolytes. [26] Hence, ion crossover should be minimized in order to maintain optimal and stable conditions at the electrodes and avoid electrolyte regeneration or catalyst degradation.

Very little literature discusses the impact of ion crossover through a BPM. Experimental work is limited to a small set of electrolytes and current densities, which is insufficient to understand how ion crossover can be effectively minimized in practical applications because of the wide variety of experimental conditions and materials. Moussaoui *et al.* showed that higher current densities and lower salt concentrations generally decrease the relative ion crossover. [26] The effect of current density was confirmed by Sun *et al.*, [27] while Vermaas *et al.* showed that some common ions with larger hydrated radii demonstrate a lower ion crossover. [21] The latter also established a link between the pH and current-voltage (i-V) curves of a BPM. However, each previous crossover work was performed at a single pH all different from each other and using different electrolytes and a different range in current density. At the same time, it is likely that the pH is of major importance for ion crossover, as the molar fractions of ions, protons, and hydroxides in the membrane determine the ion migration and WDR. Also,the ion valence and $pK_a$ of the electrolyte ions are expected to impact the concentration in the membrane moiety and thus its crossover. A good understanding of the electrolyte properties onion crossover is additionally motivated by the significant effect of electrolytes on the efficiency and selectivity of the reduction and oxidation reactions at the anode and cathode. [28] For example, it is established that bigger cations suppress the hydrogen evolution reaction (HER) and promote $CO_2$RR. [29] Hence, the choice of the electrolytes is crucial for the performance of the entire electrochemical cell, and therefore, the electrolyte-dependent ion crossover is needed to be further understood to enable highly efficient electrochemical systems. However, none of the previous work systematically investigated the impact of $pK_a$ and pH on ion crossover, let alone in combination with current density, concentration, and ionic radius. In this work, we focus on ion crossover through a BPM, using 10 different catholytes in four distinct $pK_a$ regimes and tested at various current densities. The different catholyte properties allow the ability to experimentally observe the effect of pH and ion size on ion crossover, providing a useful guide for a proper electrolyte choice.

## 4.2. THEORY

Mass transport of ions in a BPM exists because of a gradient in electrochemical potential $\bar{\mu}$. [30] This electrochemical potential gradient arises from two components: a concentration gradient driving diffusion and an electric field gradient driving ion

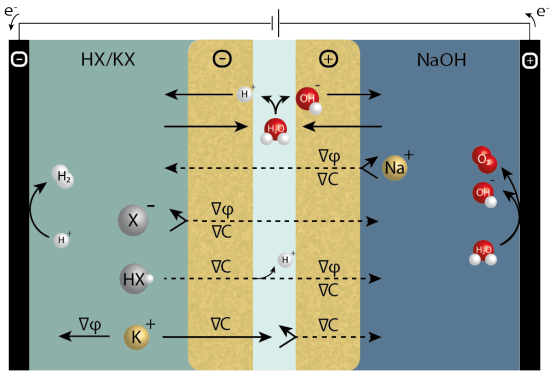


Figure 4.1: Schematic representation of an electrochemical cell with the WDR and different ion transport mechanisms described in a BPM. Ion transport that is not impeded by fixed charges (such as the WDR on top) is described by a solid line; ion crossover is represented by a dotted line.



migration. Convective transport in the membrane is neglected because of the non-porous structure of a membrane. [31] The mass transport, described by the flux $J_k$ of ions $k$, is given by the Nernst-Planck (NP) equation [30]

$$J_k = -\frac{C_k D_k}{RT}\frac{\delta\bar{\mu}}{\delta x} = -D_k\frac{\delta C_k}{\delta x} - \frac{z_k F}{RT}C_k D_k\frac{\delta\varphi}{\delta x} \tag{4.1}$$

where $C_k$ is the concentration of species $k$ with a valence $z_k$, $D_k$ is the diffusion coefficient, $F$ is the Faraday constant, $R$ is the gas constant, and $T$ is the temperature. The directions of diffusion and migration for several ionic species in an electrochemical cell are schematically represented in Figure 4.1. It is important to note that diffusion of an ion can never occur alone to comply with electroneutrality. To maintain electroneutrality, it should be either neutralized by an ion of the opposing charge travelling in the same direction, or from the same charge in the opposite direction, or maintained by consumed ions in the reaction. In the latter case, the anolyte will turn more acidic and the catholyte will turn more alkaline. Hence, the chemical potential difference between the two compartments is reduced, requiring a higher electrical potential to compensate. Also, assuming initial conditions with a more alkaline anolyte compared to the catholyte, the ionic strength is reduced when ion crossover is balanced by redox reactions that create $H^+$ neutralizing the alkaline anolyte or $OH^-$ neutralizing the acidic catholyte. Altogether, ion crossover should be minimized to sustain a favorable environment for the electrolysis reactions.

Equation 4.1 suggests that the electrolyte properties, such as ion charge ($z_k$) and diffusion coefficient ($D_k$), influence the ion crossover. However, as the diffusion coefficient and local concentration inside the two membrane layers are unknown, [32, 33] there is insufficient data to accurately simulate the ion crossover in this region.

Moreover, the membrane fixed charge density and degree of cross-linking affect the selectivity toward ions of different valences or sizes. [14, 34] The multitude of electrolytes and membrane parameters that impact the ion concentration and potential in the membrane (Equation 4.1) requires more experimental exploration to understand and control ion crossover in BPMs.

## 4.3. METHODS

**Membrane Cell.** A commercially available BPM (Fumatech Fumasep BPM) was used to perform electrochemical experiments. Membrane characteristics are given in Table S4.1. A MicroFlowCell (ElectroCell) flow cell was used (see Figure S4.2), with a surface area of 10 $cm^2$ and with a Pt-coated cathode and anode. A constant current density was applied for 45 min. The applied current densities were varied from 0 to 150 mA $cm^{-2}$. The current densities were applied in a random order to avoid a misleading relation between ion crossover and aging. By keeping the duration of the experiment fixed, the ion crossover by diffusion should remain equal for all experiments. The voltage across the BPM was measured with two microreference electrodes at a distance of 2.14 mm from the membrane surfaces and was iR-corrected based on the measured conductivities of the electrolytes used. The electrolyte was pumped through the respective cathode and anode compartments with a constant flow rate of 0.07 mL $s^{-1}$.

**Electrolytes.** Four $pK_a$ groups were selected to determine the pH dependency. Each $pK_a$ group contains different electrolytes with a similar $pK_a$, [35] which excludes the pH effect in the group itself. Within a $pK_a$ group, electrolytes were selected with a significant difference in ion size, represented by the molecular weight, as the Stokes radius used in previous work [21] was not available for many organic catholytes used here. These organic electrolytes also require an addition of either an acid (HBr) or base (KOH) to reach the pH of their respective $pK_a$. All electrolytes had an equimolar concentration of 0.5 M of an acid/base and conjugate base/acid, according to the following reaction $HX \rightleftharpoons H^+ + X^-$, where $X$ is the respective buffer species.

Between every experiment, the cell was thoroughly cleaned and a new membrane was used. After every experiment, a sample was taken of the electrolytes, and ion crossover was analyzed with an ion-coupled plasma optical emission spectrometer. Because glycine and tricine have no elements detectable by ion-coupled plasma optical emission spectrometry (ICP-OES), their ion crossover was analyzed with nuclear magnetic resonance (NMR). More specifications on the cell and chemicals used can be found in the Supporting Information. All electrolytes were considered to have an average valence of one for determining the relative ion crossover. Because the conditions at the anolyte were the same for each experiment, a statistical analysis was performed on the $Na^+$ crossover.

Table 4.1: Summary of tested catholytes and anolyte with their chemical formula, $pK_a$, molecular weight (MW), pH at the start of the measurement, products (HBr or KOH) added to achieve a pH equivalent to its acid dissociation constant ($pK_a$), and conductivity of solution ($\sigma$). All catholytes had a concentration of 0.5 M total of acid and base species.

| **Catholyte** | **Chemical formula** | **$pK_a$** | **MW** ($g\ mol^{-1}$) | **$pH_{solution}$** | **Addition** | $\sigma$ ($mS\ cm^{-1}$) |
|---|---|---|---|---|---|---|
| **Tricine** | $C_6H_{13}NO_5$ | 2.023 | 179.17 | 1.99 | 0.28 M HBr | 20.7 |
| **Phosphate** | $H_3PO_4$ / $KH_2PO_4$ | 2.148 | 98.00 | 2.03 | - | 26.0 |
| **Glycine** | $C_2H_5NO_2$ | 2.351 | 75.07 | 2.35 | 0.16 M HBr | 25.3 |
| **MOPS** | $C_7H_{15}NO_4S$ | 7.184 | 209.26 | 7.18 | 0.18 M KOH | 11.5 |
| **BES** | $C_6H_{15}NO_5S$ | 7.187 | 213.25 | 7.12 | 0.21 M KOH | 14.7 |
| **Phosphate** | $KH_2PO_4$ / $K_2HPO_4$ | 7.198 | 96.99 | 6.74 | - | 51.0 |
| **AMPSO** | $C_7H_{15}NO_5S$ | 9.138 | 227.28 | 9.14 | 0.34 M KOH | 13.0 |
| **Boric acid** | $H_3BO_3$ | 9.237 | 61.83 | 9.19 | 0.21 M KOH | 16.5 |
| **Potassium bicarbonate** | $KHCO_3$ | 10.329 | 61.02 | 10.33 | 0.34 M KOH | 70.8 |
| **CAPS** | $C_9H_{19}NO_3S$ | 10.499 | 221.32 | 10.44 | 0.37 M KOH | 10.8 |
| **Anolyte** | **Chemical formula** | **$pK_a$** | **MW** ($g\ mol^{-1}$) | **$pH_{solution}$** | **Addition** | $\sigma$ ($mS\ cm^{-1}$) |
| **Sodium hydroxide** | NaOH | - | 40.00 | 13.30 | - | 100.0 |



## 4.4. RESULTS

Ten different catholytes were paired with 0.5 M NaOH as the anolyte across the BPM. To assess the pH dependency, four groups of catholyte buffers were chosen with a distinctive $pK_a$ (2, 7, 9, and 10). All tested catholytes and anolytes, with their respective parameters, are summarized in Table 4.1. As a reference case, we first discuss the crossover of phosphate buffer ($H_3PO_4/KH_2PO_4$) versus NaOH across a BPM at various current densities.

**Reference Case: the Phosphate Buffer (pH 2).** Figure 4.2a illustrates the possible transport mechanisms for the ionic species in these electrolytes across a BPM when a current is applied to the phosphate buffer (pH 2) versus NaOH electrolyte case. The *i-V* curve for the BPM is plotted in Figure 4.2b. The absolute ion crossover of species from the phosphate buffer ($H_3PO_4$, $H_2PO_4^-$, and $K^+$) and $Na^+$ from the anolyte is given in Figure 4.2c. When this ion crossover flux is compared as a function of the total molar charge flux ($J = i/F$) with $i$ (mA $cm^{-2}$) the current density that is applied, a relative ion crossover is obtained, which is shown in Figure 4.2d. The sum of all exchanged ions can be added up to estimate the total ion crossover as a function of applied current density. The remaining part of the charge is attributed to the WDR and is therefore a measure for the efficiency of the WDR.

The linear relation between crossover and current density also provides information on the phosphate crossover mechanism. At pH 2, phosphate can either cross over as $H_2PO_4^-$ or as $H_3PO_4$. In the latter, the uncharged $H_3PO_4$ species diffuses

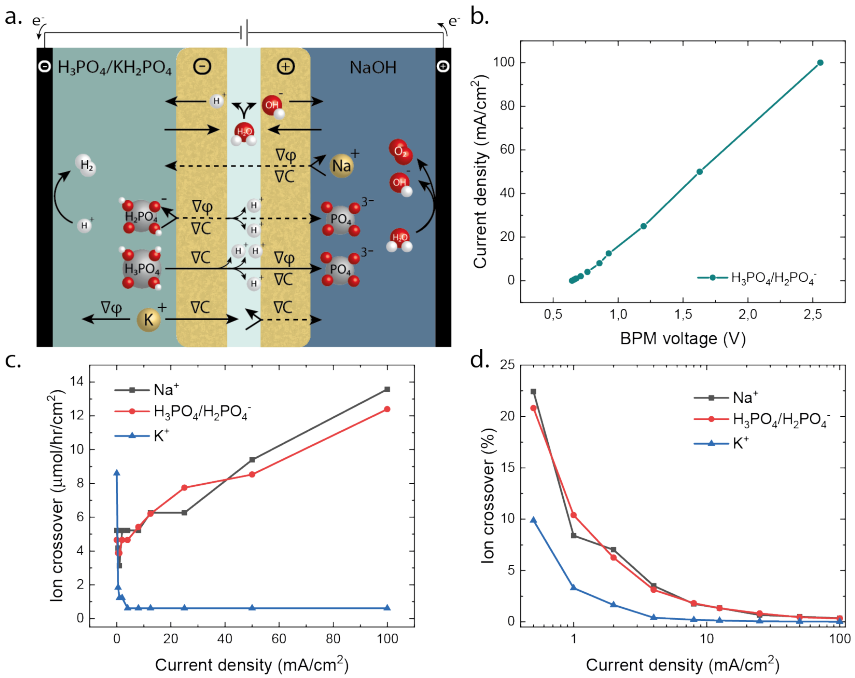


Figure 4.2: (a) Schematic illustration of ion-transport mechanisms for a phosphate buffer (0.25 M $H_3PO_4$ + 0.25 M $KH_2PO_4$) as a catholyte and 0.5 M NaOH as an anolyte, with (b) iR-corrected *i-V* curve of the membrane response among these electrolytes. The ion crossover of the ions present in these electrolytes is shown in (c) absolute numbers and (d) relative crossover of the total charge as a function of current density in a linear and logarithmic scale, respectively. For improved readability, a representative data set is selected.

through the CEL. When $H_2PO_4^-$ or $H_3PO_4$ reach the membrane interface layer, the conditions change rapidly from acidic to alkaline. It is hypothesized that protons are liberated from $H_3PO_4$ and $H_2PO_4^-$ and will be consumed in the interaction with the WDR or surrounding $OH^-$ (Figure 4.2a). The net effect of this crossover is a deficit of $OH^-$ in the anolyte compared to the unaffected WDR, while this mechanism does not change the catholyte pH. Because the phosphate crossover shows a linear dependency on current density and because $H_3PO_4$ diffusion is not dependent on the current density, the crossover mechanism at high current goes either via $H_2PO_4^-$, or the diffusion of $H_3PO_4$ in the CEL is not rate-limiting. This will be further assessed when comparing it to other species (see effect of ion valence).

For all species, the relative crossover decreases with increased current density (Figure 4.2d). Based on the Faraday constant, a total (monovalent) charge equivalent of 37 µmol $h^{-1}$ $cm^{-2}$ $mA^{-1}$ is transported. That means, for high current densities, when diffusion is negligible, $H_2PO_4^-$ and $Na^+$ crossovers are both responsible for 0.3% of the charge transport. Hence, the relative crossover decreases asymptotically to this value for $H_2PO_4^-$ and $Na^+$, as shown in Figure 4.2d, when increasing the current densities. This demonstrates that the WDR becomes the main driver of ion transport at medium to high current densities. Current densities of 5 mA $cm^{-2}$ and higher imply that more than 95% of the charges are being carried by protons and hydroxide ions from the WDR.

Given the absolute ion crossover of $K^+$ of 9 µmol $h^{-1}$ $cm^{-2}$ at 0 mA $cm^{-2}$, the diffusion of $K^+$ is larger than that of $Na^+$ and phosphate (Figure 4.2c). As the conditions at 0 mA $cm^{-2}$ do not allow net charge transport over the BPM, the flux of $K^+$ is compensated by $Na^+$ crossover in the opposite direction or cotransport with $H_2PO_4^-$. This is in agreement with the $K^+$ crossover at zero current being approximately equal to the sum of $Na^+$ and phosphate crossover. When a small current (0.5 mA $cm^{-2}$) is applied, the $K^+$ crossover already drops to 2 µmol $h^{-1}$ $cm^{-2}$. The downward trend at higher current densities continues in both absolute and relative terms, indicating that migration indeed reverts the potassium transport instead of driving it through the BPM, as hypothesized in Figure 4.2a. As a result, also the relative potassium crossover reduces asymptotically to near 0% for high current densities (Figure 4.2d).

**Probing the effect of p$K_a$ on Ion Crossover.** To compare the ion crossover of different electrolytes with the same pH and buffering strength, the relative ion crossover of all 10 catholytes is presented in Figure 4.3b,d,f,h, grouped by p$K_a$. In addition, the respective *i-V* curves across the BPMs are shown in Figure 4.3a,c,e,g. The majority of the *i-V* curves demonstrate a plateau at current densities <0.5 mA $cm^{-2}$, while for the p$K_a$ 2 group, a plateau at positive currents is absent as expected from the significant pH difference ($\Delta$pH > 11). [21] These results differ from the earlier reported plateau current densities, which were measured with galvanodynamic scans

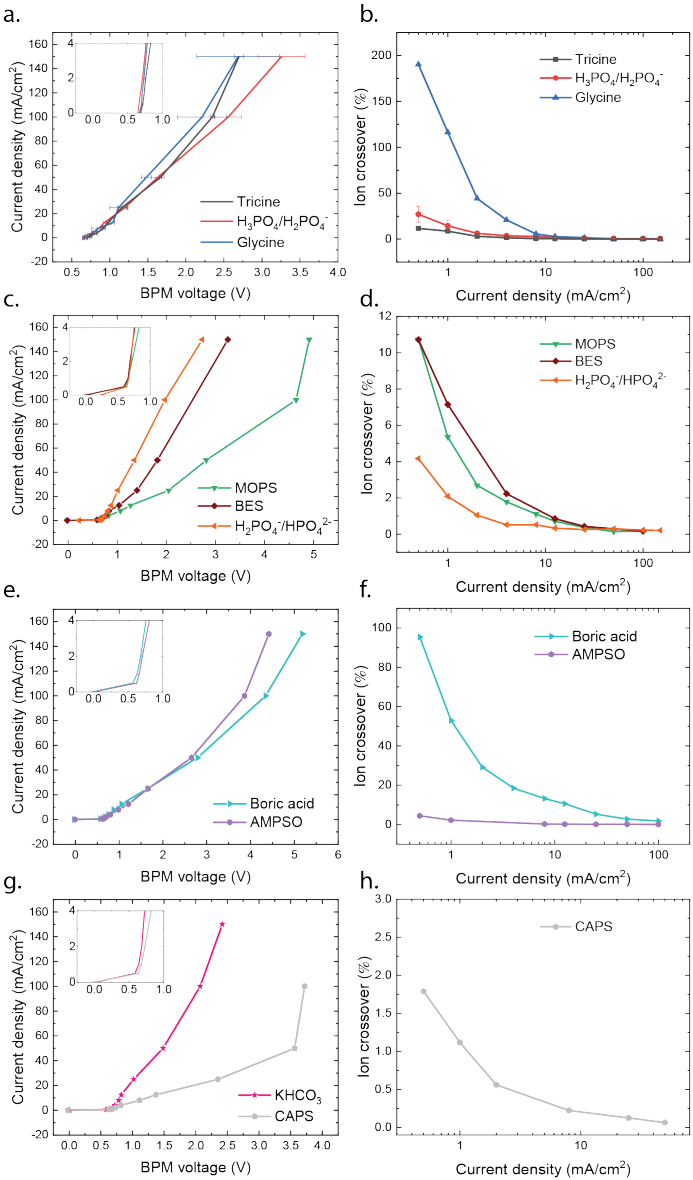


Figure 4.3: *i-V* curve and relative ion crossover of the catholyte ions, for (a,b) p$K_a$ 2 group with data from an average of three measurement runs for reproducibility purposes where the error bars indicate the calculated mean square error, (c,d) p$K_a$ 7 group, (e,f) p$K_a$ 9 group, and (g,h) p$K_a$ 10 group. For the $KHCO_3$ buffer, no ion crossover data of (bi)carbonate were obtained. Absolute ion crossover data are presented in Figure S4.3.

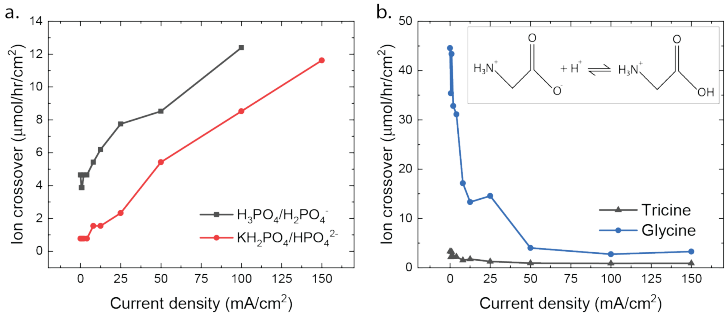


Figure 4.4: Absolute ion crossover of the (a) phosphate buffers at pK$_a$ 2 (black) and pK$_a$ 7 (red), which illustrate the dependence of valence for ion crossover and (b) glycine and tricine buffers with cationic species, with the equilibrium reaction of glycine under acidic conditions in the inset. The tricine structure has the same backbone as glycine, with a tris(hydroxymethyl)methyl group attached.

4

and in a flow cell with a larger shear velocity. [17] The crossover in all pK$_a$ groups shows a decrease in relative ion transport when the current density is increased, in agreement with previous findings. [26, 27] This extensive dataset shows a linear regression for absolute ion crossover in nearly all electrolytes ($y_{ioncrossover} = \alpha_{diff} + \beta_{migr} j$), as shown in Table S4.2. Diffusion is responsible for the majority of the ion crossover under a current density that varies from 10 to 40 mA cm$^{-2}$ depending on the electrolyte (Figure S4.3). When a neutral conjugate is present (e.g., $H_3PO_4$), transport by diffusion increases.

Nevertheless, Figure 4.3 also demonstrates large differences in crossover magnitude between the ions, with extremely high crossover for boric acid and glycine. Because the crossover of these ions deviates from other electrolytes with similar pK$_a$ and pH, we have further studied possible differentiating factors in ionic properties.

**Effect of Ion Valence.** The effect of ion valence on their crossover rate across a BPM can be demonstrated using a phosphate buffer at pH 2 and pH 7. However, the ion crossover of the phosphate buffer at pH 7 also has barely any crossover at 0 mA cm$^{-2}$, while the equimolar phosphate buffer at pH 2 has a crossover rate of 4 µmol h$^{-1}$ cm$^{-2}$ at 0 mA cm$^{-2}$ (Figure 4.4a). This can be explained by the neutral species, $H_3PO_4$, which is only diffusion-driven and adds a constant amount of crossover compared to the buffer at pH 7 throughout all current densities. The absence of uncharged species and a higher (average) ion charge at pH 7 causes stronger repelling of ions by the fixed charges of the CEL. From a practical point of view, there are multiple advantages of using a higher valence phosphate, as multivalent species provide higher concentration of $K^+$ and therefore result in a higher conductivity (Table 4.1), lowering the resistance losses of the electrolytes. As the current density

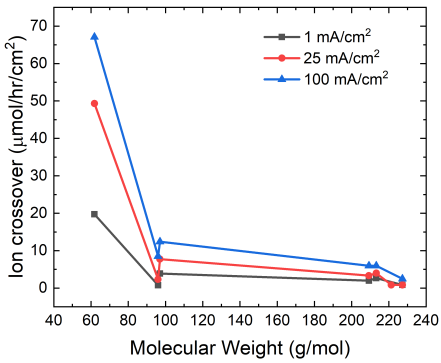




Figure 4.5: Ion crossover of catholytic anions as a function of molecular weight. Glycine and tricine are excluded because of their zwitter-ionic form, and no anion crossover of $KHCO_3$ is measured. Figure S4.4b represents the same data without boric acid (MW 61.8 g $mol^{-1}$), which still shows a decreasing trend.

increases, the phosphate crossover due to migration increases linearly, with similar slopes at both pH 2 and pH 7. This suggests that $H_2PO_4^-$ is responsible for the crossover at high current densities rather than the earlier mentioned mechanism via $H_3PO_4$ and its deprotonation at the BPM interface (Figure 4.2). Similarly, glycine and boric acid, which have neutral species, show a high ion crossover because of diffusion at 0 mA $cm^{-2}$ (Figure 4.3). In specific, glycine has a zwitter-ionic nature: $H_2A^+ \rightleftharpoons HA$, without a negatively charged component, as schematically shown in the inset of Figure 4.4b. The tricine buffer is comparable to glycine in the $pK_a$ 2 group, also having neutral and cationic species but has a larger molecular weight. For both glycine and tricine ions, migration transports the cations away from the BPM, which is visible in the downward trend of the absolute ion crossover, see Figure 4.4b. However, the ion crossover of tricine is an order of magnitude lower than that of glycine. As tricine has a much larger ionic radius, the effect of the ionic radius for all ions is being further assessed.

**Effect of Ionic Size.** The dependency of ion size, expressed in molecular weight, on the ion crossover is illustrated in Figure 4.5 for all sets of electrolyte pairs. It can be seen that the ion crossover decreases with increasing molecular weight. Especially boric acid has a low ionic radius, explaining the high ion crossover. As membranes have limited interstitial spaces, ions with a molecular weight of 100 g $mol^{-1}$ and higher are subject to strong steric hindrance and show minimal crossover.

Although these results imply that larger molecules may be advantageous for use in stable electrochemical systems, the higher molecular weights typically also feature a lower conductivity and solubility than smaller ionic species. This effect may

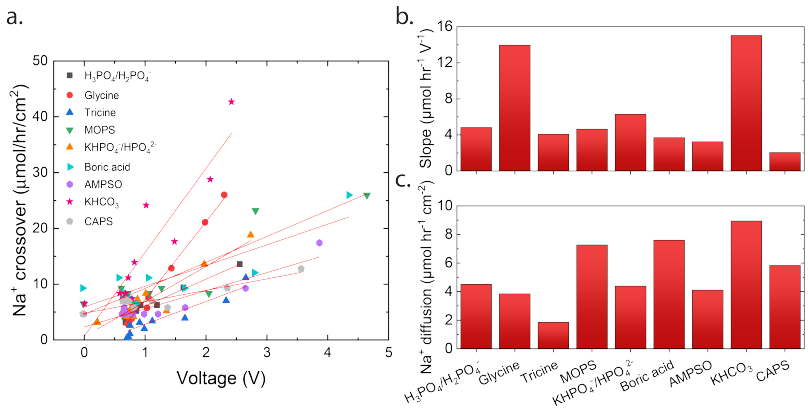


Figure 4.6: (a) Ion crossover of $Na^+$ through a BPM opposing different buffers as a function of the BPM voltage, (b) slope of the $Na^+$ crossover in function of membrane voltage for each opposing electrolyte, and (c) $Na^+$ diffusion rates for each opposing electrolyte. The corresponding linear regression equations and $R^2$ values are provided in Supporting Information (Table S4.2).

lead to extra resistive losses in the electrolyte as well as in the membrane layer itself. The latter is visible in Figure 4.3c,e,g where the larger molecules show an increased membrane voltage, similar to monopolar membranes. [36]

**$Na^+$ Crossover.** Although anions are transported by migration from the catholyte to anolyte, the electric field forces cations from the anolyte to the catholyte when a reverse bias is applied. Because the NaOH anolyte is used as a constant factor in all experiments in this study, the effect of the opposing electrolyte on the $Na^+$ ion crossover can be isolated. According to the NP equation (see Equation 4.1), the electric potential gradient and $Na^+$ properties should determine the migration of $Na^+$, suggesting a linear relation with the membrane voltage independent of the opposing electrolyte. Indeed, a linear trend for all electrolyte pairs as predicted from Equation 4.1 is shown in Figure 4.6a. The gap of data between 0 and 0.8 V reflects the plateau current density and explains the large collection of data points just above 0.8 V because of an intensification of measurements at low current densities. For each electrolyte combination, a simple linear regression is calculated to predict the ion crossover of $Na^+$ through a BPM based on the membrane voltage (Figure 4.6a, Table S4.2). All fits have an intercept reasonably close to the origin, which indicates that the $Na^+$ crossover is mainly driven by migration. Most slopes are similar, while the *i-V* curves show much more variation, which justifies the use of voltage as the determining factor for ion crossover. However, when bicarbonate and glycine are used as the catholyte, the crossover of $Na^+$ increases more dramatically with increasing voltage (Figure 4.6b). It is important to note that the crossover of glycine reduces with increasing current density (Figure 4.3b), while that of $Na^+$

crossover increases steeply with increasing voltage and current.

The dependency of the opposing electrolyte composition on the $Na^+$ crossover is surprising, as the anion exchange membrane is the first and only electronically repelling layer for $Na^+$. Although the membrane-membrane interface should in theory be of no influence for the crossover of the sodium ions, Figure 4.6a demonstrates that the crossover of the separated electrolytes is still dependent on one another. More specifically, the diffusion rate for $Na^+$ can be found via the y-intercept of the corresponding linear regression equations based on the current density and show a similar dependence on the opposing electrolyte (Figure 4.6c). One could speculate that glycine and (bi)carbonate shield off fixed charges in the AEL, which would facilitate the $Na^+$ crossover. However, the ion valence of glycine and (bi)carbonate is not uniquely compared to the other tested electrolytes, which cannot justify this hypothesis directly. Also, this dependency does not relate to the MW of the opposing electrolyte (Figure S4.4a). Although the absolute $Na^+$ crossover may vary with membrane production batches, demonstrated by a 4 times higher crossover when membranes from different batches are used (see Supporting Information, Figure S4.1), the same dependency on the opposing electrolytes is consistent throughout membrane batches. A similar trend is visible for a given electrolyte, as well as the trend among different electrolytes, showing the significance of our results independent of the batch used. The pH (or $pK_a$) and ion size of the opposing electrolytes do neither provide an explanation. Thus, a clear justification is not readily available from the investigated parameters, and further investigation is required to understand the difference in crossover of the $Na^+$ as a function of the opposing electrolyte across a BPM.

## 4.5. CONCLUSIONS

Ion crossover negatively affects the stability of both electrolytes in energy technologies and is affected by voltage, ion size, valence, $pK_a$, and charge density. The ion crossover in BPMs does follow the NP equation, reflected in a diffusion-driven crossover flux at zero current and a linearly increasing crossover rate because of migration. For all the studied cases, no limiting co-ion fluxes are reached, in contrast to earlier reported work. [26] At low current densities, depending on the electrolyte up to 10—40 mA $cm^{-2}$, diffusion accounts for the majority of the ion crossover, while at high current densities, migration is of higher importance. When relative ion crossover is considered, which is a measure for the stability of the electrolytes, the lowest relative crossover is obtained at high current density independent of any electrolyte combination, which favors the use of a BPM at high current density rates as in industrial applications. The selection of electrolytes involves a trade-off between low crossover (for larger ions) which usually comes at the expense of lower conductivity. The influence of the $pK_a$ or pH of the catholyte does not have a straightforward influence on the ion crossover. However, the distinct difference in ion crossover of phosphate depending on the pH (pH 2 and 7) shows that a BPM

is clearly better repelling ions with a higher average valence. The demonstrated effects of pH, ion size, current density, and membrane properties on the ion crossover can further guide the practical application of electrolytes and BPM development for electrochemical conversion.

## 4.6. SUPPLEMENTARY INFORMATION

### 4.6.1. MEMBRANE CHARACTERISTICS

Another important parameter of ion crossover across a membrane is the physical characteristics of the membrane itself. Different membrane production batches may result in a different average charge density (i.e., the amount of fixed charges per water molecule in the membrane), porosity and water uptake, which influences the interaction with mobile ionic species. To test this, the $pK_a$ 2 group was examined with two different batches of the Fumasep BPM with a distinct water uptake and charge density. In Figure S4.1, the ion crossover of $Na^+$ from the anolyte is compared for three different opposing catholytes (phosphate, glycine and tricine). The trend among the different electrolyte combinations is still maintained between the different batches (tricine < glycine < phosphate). However, the ion crossover is up to five times higher for the batch 2 compared to batch 1. The investigated membrane properties (thickness, ion exchange capacity, swelling degree & charge density) do not provide a valuable explanation for this major difference (Table S4.1). A possible explanation lies in the production process, where either ageing or cracking of a membrane layer can occur. Therefore, assessing trends for ionic crossover through BPMs can be generalized, but quantitative crossover parameters are specific to the membrane characteristics.

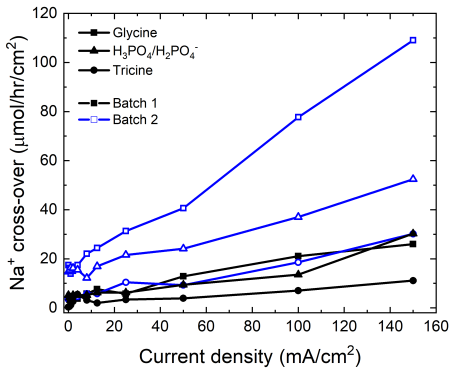


Supplementary Figure S4.1: Ion crossover of $Na^+$ when opposing phosphate, glycine or tricine with two different batches of the BPM.

### 4.6.2. MATERIALS

The flow cell, MicroFlowCell, was purchased from Electrocell (Denmark). The micro reference electrodes of type LF-1-100 are manufactured by Innovative Instruments Inc. and have a polyetheretherketone (PEEK) body with a diameter of 1 mm. The commercial BPM, Fumasep FBM-PK, used in this study was produced

Supplementary Table S4.1: Thickness, ion exchange capacity (IEC), swelling degree (SD) and charge density of different BPM production batches.

| Production batch | Thickness (µm) | IEC (meq/g dry) | SD (g/g dry) | Charge density (meq/g ≈ M) |
|---|---|---|---|---|
| **Batch 1** | 175 | 1.81 | 0.299 | 6.06 |
| **Batch 2** | 181 | 1.81 | 0.288 | 6.27 |

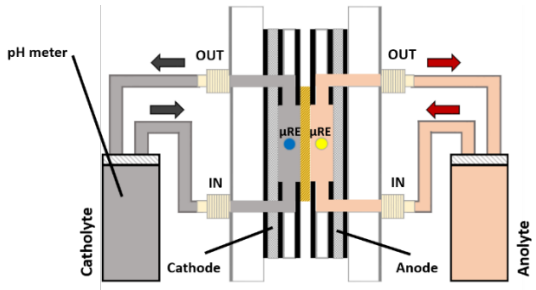


Supplementary Figure S4.2: Schematic of the flowcell used in this work, with two micro reference electrodes (µRE) positioned close to the BPM to determine the voltage drop across the BPM during electrolysis.

by Fumatech GmbH (Germany). Following chemicals were used: Tricine (Sigma-Aldrich, >99%), Phosphoric acid (Sigma-Aldrich, >99%), Glycine (Sigma-Aldrich, >99%), MOPS (Sigma-Aldrich, >99.5%), BES (Sigma-Aldrich, >99%), Potassium phosphate monobasic (Sigma-Aldrich, >99%), Potassium phosphate dibasic (Sigma-Aldrich, >98%), AMPSO (Sigma-Aldrich, >99%), Boric acid (Sigma-Aldrich, >99.5%), Potassium bicarbonate (Sigma Aldrich, 99.7% purity), CAPS (Sigma-Aldrich, >99%), Sodium hydroxide (J.T.Baker, >99%), Hydrobromic acid (Sigma-Aldrich, 48 wt.% in H2O), Potassium hydroxide (Sigma-Aldrich, 45 wt.% in H2O), Potassium sulphate (Sigma-Aldrich, >99%).

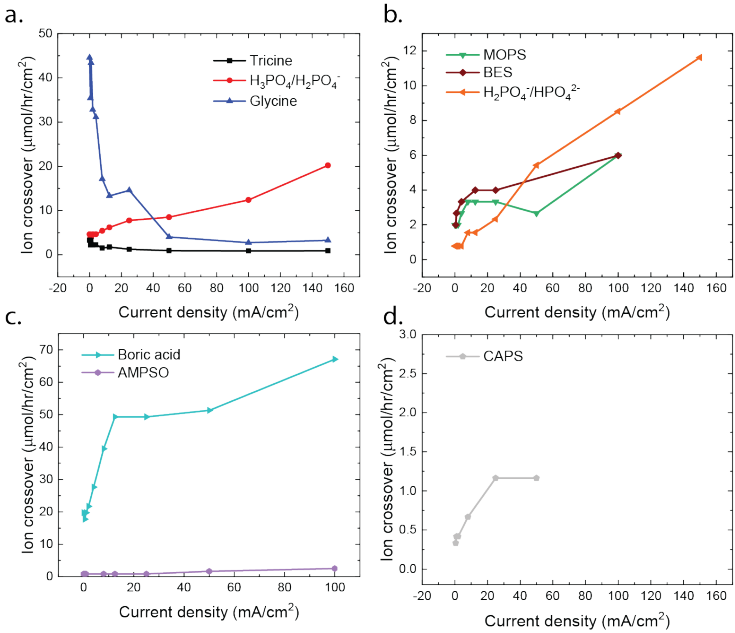


Supplementary Figure S4.3: Absolute ion crossover of the catholyte ions, for (a) p$K_a$ 2 group, (b) p$K_a$ 7 group, (c) p$K_a$ 9 group, and (d) p$K_a$ 10 group. For the $KHCO_3$ buffer no ion crossover data of (bi)carbonate was obtained.

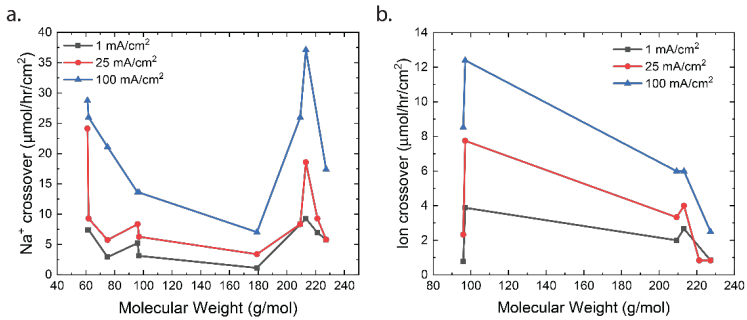


Supplementary Figure S4.4: (a) $Na^+$ crossover as a function of molecular weight of catholytic anions and (b) Figure 4.5 without the data point of Boric acid.

Supplementary Table S4.2: Linear regression analysis on co-ion crossover data in function of either the current density or the membrane voltage. $R^2$ indicates the variance on the linear fit for each variable (current density or membrane voltage).

| | **Current density** | | | **Voltage** | | |
|---|---|---|---|---|---|---|
| | **Y1=a.J+b [µmol hr-1 mA-1]** | | | **Y2=c.V+d [µmol hr-1 V-1]** | | |
| | $R^2$ | a (std) | b (std) | $R^2$ | c | d |
| **Na AMPSO** | 0.95 | 0.12 (0.01) | 4.11 (0.38) | 0.84 | 3.25 (0.50) | 2.34* (0.85) |
| **AMPSO** | 0.78 | 0.02 (0.003) | 0.506 (0.14) | 0.70 | 0.53 (0.12) | 0.21* (0.12) |
| **Na Boric acid** | 0.83 | 0.16 (0.02) | 7.60 (0.92) | 0.74 | 3.71 (0.78) | 5.91 (1.41) |
| **Boric acid** | 0.72 | 0.46 (0.10) | 26.98 (3.68) | 0.75 | 11.55 (2.33) | 20.92(4.23) |
| **Na CAPS** | 0.83 | 0.13 (0.02) | 5.83 (0.43) | 0.87 | 2.06 (0.30) | 4.77 (0.49) |
| **CAPS** | 0.58 | 0.02* (0.007) | 0.22* (0.13) | 0.66 | 0.34 (0.09) | 0.03* (0.15) |
| **Na Glycine** | 0.97 | 0.16 (0.01) | 3.85 (0.57) | 0.98 | 13.97 (0.65) | - 6.74 (0.83) |
| **Glycine** | - | - | - | - | - | - |
| **Na KHCO3** | 0.9 | 0.22 (0.02) | 8.95 (1.40) | 0.84 | 15.04 (2.18) | 0.66* (2.66) |
| **KHCO3** | - | - | - | - | - | - |
| **Na MOPS** | 0.86 | 0.20 (0.03) | 7.27 (1.04) | 0.82 | 4.65 (0.76) | 4.60* (1.49) |
| **MOPS** | 0.75 | 0.033 (0.007) | 2.25 (0.24) | 0.76 | 0.77 (0.16) | 1.79 (0.30) |
| **Na Phos7** | 0.89 | 0.091 (0.01) | 4.39 (0.60) | 0.89 | 6.30 (0.73) | 0.58* (0.93) |
| **Phos7** | 0.99 | 0.075 (0.002) | 0.76 (0.14) | 0.95 | 5.11 (0.38) | -2.29 (0.49) |
| **Na Phos2** | 0.95 | 0.09 (0.007) | 4.51 (0.27) | 0.95 | 4.83 (0.39) | 1.23* (0.47) |
| **Phos2** | 0.95 | 0.08 (0.006) | 4.54 (0.23) | 0.96 | 4.34 (0.29) | 1.59 (0.36) |
| **Na Tricine** | 0.81 | 0.06 (0.009) | 1.85 (0.53) | 0.78 | 4.09 (0.72) | -1.28* (1.01) |
| **Tricine** | - | - | - | - | - | - |

* non-significant values (p>0.05)

## REFERENCES


[1] M. A. Blommaert, J. A. Verdonk, H. C. Blommaert, W. A. Smith, and D. A. Vermaas, *Reduced Ion Crossover in Bipolar Membrane Electrolysis via Increased Current Density, Molecular Size, and Valence,* ACS Applied Energy Materials **3**, 5804 (2020).

[2] International Energy Agency, *Renewables 2018*, Tech. Rep. (2018).

[3] U.S. Energy Information Administration, *International Energy Outlook 2019*, Tech. Rep. (2020).

[4] H. W. Sinn, *Buffering volatility: A study on the limits of Germany's energy revolution,* European Economic Review **99**, 130 (2017).

[5] W. A. Smith, T. Burdyny, D. A. Vermaas, and H. Geerlings, *Pathways to Industrial-Scale Fuel Out of Thin Air from CO2 Electrolysis,* Joule **3**, 1822 (2019).

[6] J. Durst, A. Rudnev, A. Dutta, Y. Fu, J. Herranz, V. Kaliginedi, A. Kuzume, A. A. Permyakova, Y. Paratcha, P. Broekmann, and T. J. Schmidt, *Electrochemical CO2 Reduction – A Critical View on Fundamentals, Materials and Applications,* CHIMIA International Journal for Chemistry **69**, 769 (2015).

[7] T. Burdyny and W. A. Smith, *CO2 reduction on gas-diffusion electrodes and why catalytic performance must be assessed at commercially-relevant conditions,* Energy & Environmental Science **12**, 1442 (2019).

[8] J. Luo, D. A. Vermaas, D. Bi, A. Hagfeldt, W. A. Smith, and M. Grätzel, *Bipolar Membrane-Assisted Solar Water Splitting in Optimal pH,* Advanced Energy Materials **6**, 1 (2016).

[9] Y. C. Li, D. Zhou, Z. Yan, R. H. Gonçalves, D. A. Salvatore, C. P. Berlinguette, and T. E. Mallouk, *Electrolysis of CO2 to Syngas in Bipolar Membrane-Based Electrochemical Cells,* ACS Energy Letters **1**, 1149 (2016).

[10] D. A. Vermaas, M. Sassenburg, and W. A. Smith, *Photo-assisted water splitting with bipolar membrane induced pH gradients for practical solar fuel devices,* The Royal Society of Chemistry **3**, 19556 (2015).

[11] M. B. McDonald, S. Ardo, N. S. Lewis, and M. S. Freund, *Use of bipolar membranes for maintaining steady-state pH gradients in membrane-supported, solar-driven water splitting,* ChemSusChem **7**, 3021 (2014).

[12] S. Oener, S. Ardo, and S. W. Boettcher, *Ionic Processes in Water Electrolysis: The Role of Ion-selective Membranes,* ACS Energy Letters **2**, 2625 (2017).

[13] M. Lin, L. Han, M. R. Singh, and C. Xiang, *An Experimental- And Simulation-Based Evaluation of the CO2 Utilization Efficiency of Aqueous-Based Electrochemical CO2 Reduction Reactors with Ion-Selective Membranes,* ACS Applied Energy Materials **2**, 5843 (2019).

[14] T. Sata, *Ion exchange membranes : preparation, characterization, modification and application* (Royal Society of Chemistry, Cambridge, 2004).

[15] R. Simons and G. Khanarian, *Water dissociation in bipolar membranes: Experiments and theory,* The Journal of Membrane Biology **38**, 11 (1978).

[16] H.Strathmann, J.J.Krol, H.J.Rapp, and G.Eigenberger, *Limiting current density and water dissociation in bipolar membranes,* Journal of Membrane Science **125**, 123 (1997).

[17] M. B. McDonald and M. S. Freund, *Graphene oxide as a water dissociation catalyst in the bipolar membrane interfacial layer,* ACS Applied Materials and Interfaces **6**, 13790 (2014).

[18] S. S. Mel'nikov, O. V. Shapovalova, N. V. Shel'deshov, and V. I. Zabolotskii, *Effect of d-metal hydroxides on water dissociation in bipolar membranes,* Petroleum Chemistry **51**, 577 (2011).

[19] R. Q. Fu, T. W. Xu, G. Wang, W. H. Yang, and Z. X. Pan, *PEG-catalytic water splitting in the interface of a bipolar membrane,* Journal of Colloid and Interface Science **263**, 386 (2003).

[20] J. Li, S. Thage Morthensen, J. Zhu, S. Yuan, J. Wang, A. Volodine, J. Lin, J. Shen, and B. V. D. Bruggen, *Exfoliated MoS 2 nanosheets loaded on bipolar exchange membranes interfaces as advanced catalysts for water dissociation,* Sparation and Purification Technology **194**, 416 (2018).

[21] D. A. Vermaas, S. Wiegman, T. Nagaki, and W. A. Smith, *Ion transport mechanisms in bipolar membranes for (photo)electrochemical water splitting,* Sustainable Energy and Fuels **2**, 2006 (2018).

[22] M. A. Blommaert, D. A. Vermaas, B. Izelaar, B. in 't Veen, and W. A. Smith, *Electrochemical impedance spectroscopy as a performance indicator of water dissociation in bipolar membranes,* Journal of Materials Chemistry A **7**, 19060 (2019).

[23] A. M. Ashrafi, N. Gupta, and D. Neděla, *An investigation through the validation of the electrochemical methods used for bipolar membranes characterization,* Journal of Membrane Science **544**, 195 (2017).

[24] T. Teorell, *An Attempt to Formulate a Quantitative Theory of Membrane Permeability,* Proc Soc Exp Biol Med **33**, 282 (1935).

[25] J. S. K.H. Meyer, *La perméabilité des membranes I. Théorie de la perméabilité ionique,* Helv Chim Acta **19**, 649 (1936).

[26] R. E. Moussaoui, G. Pourcelly, M. Maeck, H. D. Hurwitz, and C. Gavach, *Co-ion leakage through bipolar membranes. Influence of I-V responses and water-splitting efficiency,* Journal of Membrane Science **90**, 283 (1994).

[27] K. Sun, R. Liu, Y. Chen, E. Verlage, N. S. Lewis, and C. Xiang, *Solar-Driven Water Splitting: A Stabilized, Intrinsically Safe, 10% Efficient, Solar-Driven Water-Splitting Cell Incorporating Earth-Abundant Electrocatalysts with Steady-State pH Gradients and Product Separation Enabled by a Bipolar Membrane,* Advanced Energy Materials **6**, 1 (2016).

[28] J. Resasco, L. D. Chen, E. Clark, C. Tsai, C. Hahn, T. F. Jaramillo, K. Chan, and A. T. Bell, *Promoter Effects of Alkali Metal Cations on the Electrochemical Reduction of Carbon Dioxide,* Journal of the American Chemical Society **139**, 11277 (2017).

[29] J. Resasco, Y. Lum, E. Clark, and Z. Zeledon, *Effects of Anion Identity and Concentration on Electrochemical Reduction of CO2,* ChemElectroChem **5**, 1064 (2018).



[30] A. J. Bard and L. R. Faulkner, *Electrochemistry* (Wiley, 1944) p. 850, arXiv:1011.1669v3 .

[31] J. J. Krol, *Membrane Technology Group* (1997) p. 165.

[32] L. C. Weng, A. T. Bell, and A. Z. Weber, *Towards membrane-electrode assembly systems for CO2 reduction: A modeling study,* Energy and Environmental Science **12**, 1950 (2019).

[33] M. P. Mier, R. Ibañez, and I. Ortiz, *Influence of ion concentration on the kinetics of electrodialysis with bipolar membranes,* Separation and Purification Technology **59**, 197 (2008).

[34] B. Van der Bruggen, *Membrane Technology,* in *Kirk-Othmer Encyclopedia of Chemical Technology*, Major Reference Works (2017).

[35] R. N. Goldberg, N. Kishore, and R. M. Lennen, *Thermodynamic quantities for the ionization reaction of buffers.* Journal of Physical and Chemical Reference Data **31**, 231 (2002).

[36] T. Luo, S. Abdu, and M. Wessling, *Selectivity of ion exchange membranes: A review,* Journal of Membrane Science **555**, 429 (2018).

# 5

# ORIENTATION OF BIPOLAR MEMBRANE DETERMINES THE DOMINANT ION AND CARBONIC SPECIES TRANSPORT IN MEMBRANE ELECTRODE ASSEMBLIES FOR $CO_2$ REDUCTION

*A bipolar membrane (BPM), consisting of a cation and an anion exchange layer (CEL and AEL), can be used in an electrochemical cell in two orientations: reverse bias and forward bias. A reverse bias is traditionally used to facilitate water dissociation and control the pH at either side. A forward bias has been proposed for several applications, but insight into the ion transport mechanism is lacking. At the same time, when implementing a BPM in a membrane electrode assembly (MEA) for $CO_2$ reduction, the BPM orientation determines the environment of the $CO_2$ reduction catalyst, the anolyte interaction and the direction of the electric field at the interface layer. In order to understand the transport mechanisms of ions and carbonic species within a bipolar membrane electrode assembly (BPMEA), these two orientations were compared by performing $CO_2$ reduction. Here, we present a novel BPMEA using a Ag cat-*

This chapter has been published in *Journal of Materials Chemistry A*, 2021, **9**, 11179-11186 [1].

*alyst layer directly deposited on the membrane layer at the vapour-liquid interface. In the case of reverse bias, the main ion transport mechanism is water dissociation. $CO_2$ can easily crossover through the CEL as neutral carbonic acid due to the low pH in the reverse bias. Once it enters the AEL, it will be transported to the anolyte as (bi)carbonate because of the presence of hydroxide ions. When the BPM is in the forward bias mode, with the AEL facing the cathode, no net water dissociation occurs. This not only leads to a 3 V lower cathodic potential but also reduces the flux of carbonic species through the BPM. As the pH in the AEL is higher, (bi)carbonate is transported towards the CEL, which then blocks the majority of those species. However, this forward bias mode showed a lower selectivity towards CO production and a higher salt concentration was observed at the cathode surface. The high overpotential and $CO_2$ crossover in reverse bias can be mitigated via engineering BPMs, providing higher potential for future application than that of a BPM in forward bias owing to the intrinsic disadvantages of salt recombination and poor faradaic efficiency for $CO_2$ reduction.*

## 5.1. INTRODUCTION

Electrochemical $CO_2$ reduction using renewable energy sources is a key element in closing the carbon cycle while still providing carbon-based fuels and chemicals. [2] The products from this reaction are chemical building blocks, which can be used in a wide variety of fuels and plastics. In order to be competitive with current industrial technologies, a high selectivity and throughput need to be achieved. In recent years, the technique of combining an electrode with a membrane, creating a membrane electrode assembly (MEA), has led to great improvements in the $CO_2$ reduction field by achieving high selectivity and current densities relevant for industrial application. [3–6] MEAs have intrinsic advantages to upscale $CO_2$ reduction electrolysers, as they allow operation in a gas–liquid configuration (improving the $CO_2$ concentration and mass transport towards the catalyst) while ensuring product separation. Different types of ion exchange membranes can be used in such MEA configurations, among which a cation exchange membrane (CEM) [7, 8] or an anion exchange membrane (AEM) are the most used in $CO_2$ electrolysers [3–6]. A third type of membrane used in an MEA is a bipolar membrane (BPM), consisting of a cation and an anion exchange layer (CEL and AEL, respectively) with an internal interface between the two layers where a catalyst is deposited to enhance the possible water dissociation. [9–11] In addition to the catalyst at the internal interface, electrolyte composition, [12] and pH gradient, [13] the two-layer configuration of the BPM allows us to choose the orientation of the membrane in an electrochemical cell.



For a monopolar membrane (e.g., AEM or CEM), the orientation of the membrane has no impact on its function. For a BPM, the orientation of the membrane, determining which membrane layer faces the cathode, has great implications for its ion transport mechanism. Two modes of operation are possible with a BPM: reverse and forward bias (Figure 5.1).

The first mode of operation is reverse bias with the CEL facing the cathode, where ions are depleted at the internal bipolar membrane interface upon applying a current. To fulfil the requirement of a current throughout the cell, ions need to be formed via the water dissociation reaction (WDR) into $H^+$ and $OH^-$ ions. [14] This configuration using a BPM provides ample possibilities in the cell design, since an electrolyte with a different pH can be used at either side; e.g. a near-neutral pH environment at the cathode against a high pH at the anode. [15] The reverse bias mode is traditionally used in bipolar membrane electrodialysis (BPMED) [16, 17] and commonly used for energy applications (including $CO_2$ reduction and water splitting) [15, 18] and resource recovery. [19] Li *et al.* demonstrated better stability when sandwiching a BPM between gas diffusion electrodes (GDEs), compared to monopolar membranes, at various current densities. [9] Salvatore *et al.* reached a faradaic efficiency (FE) of 50% at 200 mA $cm^{-2}$ with a liquid support layer of$NaHCO_3$ between the BPM and GDE. [10] However, in neutral pH, the over-

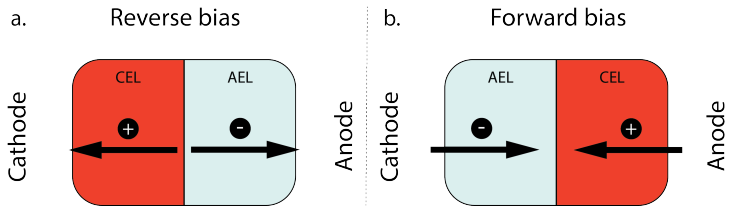


Figure 5.1: Modes of operation of BPM, consisting of a cation exchange layer (CEL) and an anion exchange layer (AEL): (a) reverse bias and (b) forward bias.

potential of the WDR increases significantly. On the other hand, when the cathodic catalyst layer is attached to the CEL of the BPM directly in an MEA configuration, an acidic environment surrounds the catalyst, possibly favouring the unwanted hydrogen evolution reaction.

The second operating mode is forward bias with the AEL facing the cathode, where ions are transported towards the interface where recombination or precipitation can occur. [20] In the forward bias mode, water is being formed at the interface layer, which can cause blistering. [21, 22] This configuration was proposed for $CO_2$ reduction [11] to leverage the recent achievements in AEM-based MEAs. [23, 24] Although ions may accumulate at the BPM interface layer, [25, 26] the cathode–AEL environment could be combined with a low membrane overpotential in the forward bias mode. Pătru *et al.* demonstrated a forward bias system (vapour-vapour) reaching a FE towards CO of 13% at 50 mA $cm^{-2}$ while inhibiting $CO_2$ crossover to the anode. [11] This unwanted crossover of $CO_2$ (and its negatively charged dissolved species, $CO_3^{2-}$ and $HCO_3^-$, or carbonic acid, $H_2CO_3$, which are all grouped under the term dissolved inorganic carbon, DIC) compromises the efficiency of $CO_2$ electrolysers and is a well-known problem, especially in AEM-based MEA configurations. [27]

In general, both biases of a BPM showed stability in the order of a few hours. For developing BPM-based $CO_2$ electrolysers, long term stability and therefore low ion and product crossover through the membrane are essential. In order to achieve long term stability for both BPM orientations in an MEA-based $CO_2$ electrolyser, knowledge of the ion transport is needed, which is currently lacking in a vapour-liquid environment. In particular,little is published on the transport mechanisms in the forward bias mode. In this study, we reveal the ion transport mechanisms and practical feasibility of a BPM in reverse bias and forward bias embedded in an MEA for $CO_2$ electrolysis.

## 5.2. RESULTS & DISCUSSION

To study the different transport mechanisms of ions and carbonic species within a BPM-based MEA (BPMEA), we examine two cases for $CO_2$ electrolysis, one case using a BPM in reverse bias and another case in forward bias. In order to preferentially make gaseous products, Ag was used as a catalyst that was directly sputtered onto the membrane. Ag has shown the ability to reduce $CO_2$ to CO and $H_2$ with different product ratios depending on the applied potential, electrolyte, and pH. [2] The use of a catalytic layer deposited directly on the membrane, in the absence of a carbon based porous diffusion layer, allows the ability to observe the possible salt formation (i.e., occurring due to transportation of the electrolyte ions through the BPM towards the catalyst). To achieve a direct deposition on the membrane via sputtering in a vacuum, and to avoid structural changes in the membrane moiety, which would occur if absorbed water vaporizes, a heterogeneous Ralex™ bipolar membrane was used in its dry state as the catalyst support. During the sputtering process, the BPM was de-aerated, creating micro-cracks that facilitate the crossover of $CO_2$ (see later). A description of the fabrication process can be found in the Supplementary Information.



A diagram of the BPMEA in reverse bias mode is illustrated in Figure 5.2a. Upon applying a current, water is dissociated into protons ($H^+$) and hydroxide ions ($OH^-$) in between the CEL and AEL. $OH^-$ will then transport through the AEL into the electrolyte to replenish the consumed hydroxide ions at the Pt anode (resulting in the oxygen evolution reaction). For the forward bias mode (Figure 5.2b), the Ag catalyst was deposited on the AEL, where anions (e.g., (bi)carbonate) migrate towards the interface with the CEL. Similarly, cations migrate in the CEL in the opposite direction. Hence, the hypothesis for the forward bias is that no ion depletion occurs at the internal BPM interface and therefore no net WDR is expected, but salt accumulation occurs instead. The implications of each of these two different charge transport mechanisms will be discussed in the following sections.

The selectivity of the cathodic reaction in our MEA vapour-liquid configuration depends on the orientation of the bipolar membrane. The reverse bias demonstrates a stable CO production (60% FE) for one hour of operation as shown in Figure 5.2c, after an initial stabilisation period where more $H_2$ was produced. With an opposite membrane orientation (forward bias mode), a significantly lower selectivity was obtained: initially some CO was produced (maximum FE of 20%), whereas CO could no longer be detected after 20 minutes and only $H_2$ was observed (Figure 5.2d). As we will explain further on, the ion transport mechanism changes around 20 minutes of operation, and this also influences the selectivity at the cathode. The experiments were performed in triplicate to observe possible sample-to-sample variation, and similar maximum FEs were obtained in each case with the exception that one sample in the forward bias mode, with little $CO_2$ crossover, showed a continuous CO production of 10% (see Figure S5.2).

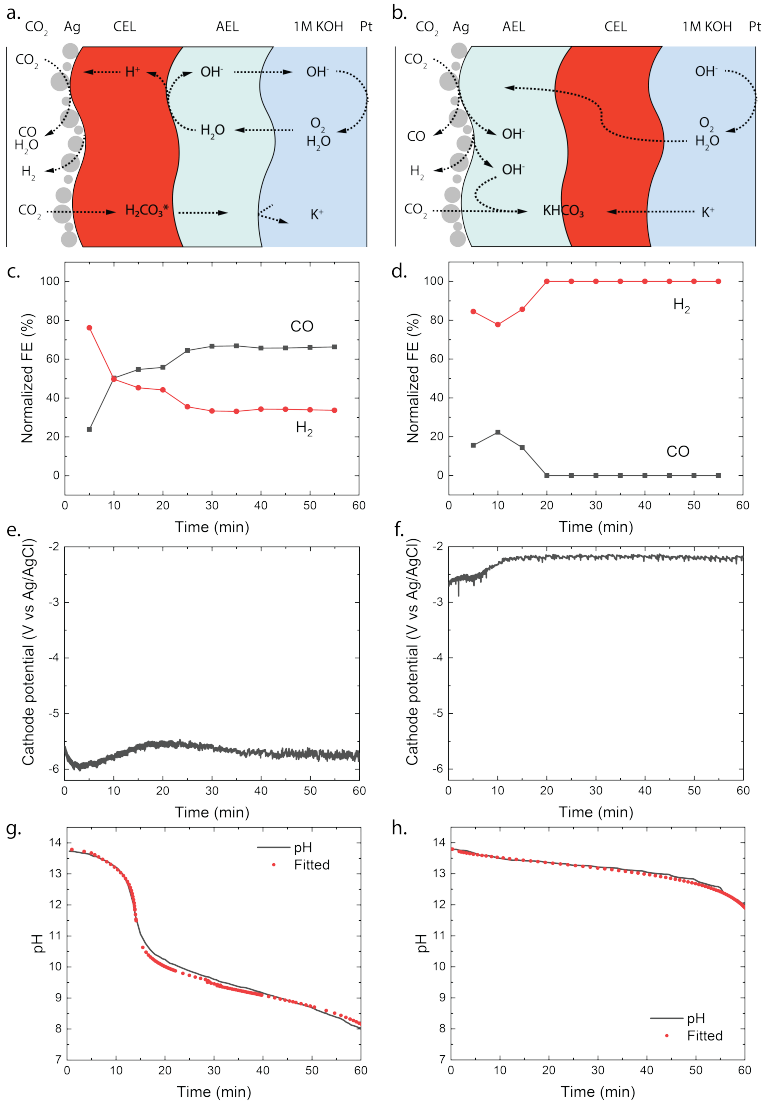


Figure 5.2: Schematic illustration for transport of water, $CO_2$ and ionic species transport for (a) the reverse, (b) the forward bias mode. The catalyst at the cathode is Ag, at the anode it is Pt. The normalized Faradaic efficiencies are shown for c) reverse, and d) forward bias mode. Normalization to the total evolved product is needed to compensate for the varying gas flow rate. Graphs e and f show cathodic potentials at current density of 25 mA $cm^{-2}$ (1.56 $cm^2$ surface area, 0.036 $cm^3$ $s^{-1}$ flow rate with 4 mm electrolyte spacing and reference electrode (3.4 M KCl, 240 mV vs SHE) in anolyte) for each mode and the graphs g and h show measured pH in the anolyte with a fitted pH based on molar flux of dissolved inorganic carbon species. The anolyte is initially 1 M KOH.

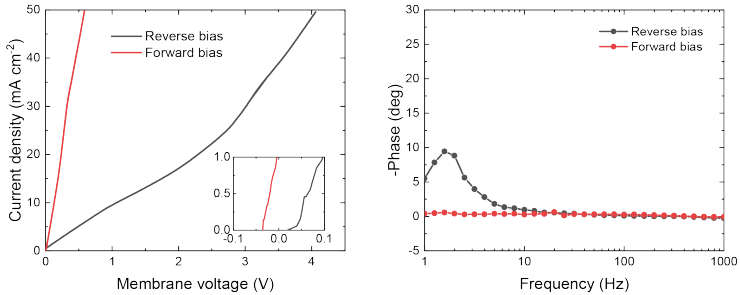


Figure 5.3: (a) linear sweep potentiometry at 0.5 mA $s^{-1}$ in 1M NaCl (corrected for electrolyte losses) with positive membrane potential indicating reverse bias and negative forward bias; values at 25 mA $cm^{-2}$ are 2.74 V (reverse) and 0.41 V (forward), (b) galvanostatic impedance at 25 mA $cm^{-2}$ with 6.4 mA $cm^{-2}$ amplitude.

5

The potential required to reach the applied 25 mA $cm^{-2}$ strongly differs depending on the membrane orientation. For the reverse bias mode, with the cathodic potential shown in Figure 5.2e, a highly negative potential (up to -5.5 V vs. Ag/AgCl in the anolyte) was needed to perform the cathodic reactions, while for the forward bias mode a cathodic potential of around -2.0 V vs. Ag/AgCl was required to achieve the same current density (Figure 5.2f). The major difference can be explained from the processes in the interfacial layer between the CEL and AEL. The main energy loss in the reverse bias mode appears to be associated with the WDR, shown by the membrane voltage difference of 2.3 V at 25 mA $cm^{-2}$, when reverse bias is applied compared to forward bias (see Figure 5.3a). In addition, the impedance of the BPM measured in each orientation supports the hypothesis that the WDR is (almost completely) absent in forward bias: the peak related to the WDR disappears in comparison to reverse bias (see Figure 5.3b). [14] The voltage required to drive the WDR indicates that the catalyst at the internal interface is kinetically slow. Because our membrane was chosen to allow synthesis in a dry state, this particular commercial BPM is not optimized for $CO_2$ reduction in this configuration. Recent literature has shown via experimental work [28–30] and simulations [31, 32] that the catalyst overpotential can be easily reduced by two orders of magnitude at these current densities compared to the one that was used for these studies. Hence, the cathode potentials in Figure 5.2e and f are expected much closer to their thermodynamic equivalent in an optimized BPMEA system.

As no net WDR occurs in the forward bias mode and ion transport is directed towards the internal interface, ions can neutralize in the BPM. The type of neutralization differs depending on the type of ion, e.g.protons and hydroxide ions will perform water association and allow harvesting a significant membrane voltage due to

the high gradients in the $H^+/OH^-$ concentration over the CEL/AEL interface, leveraged in BPM-based batteries. [17, 33] However, only limited protons are present in the CEL in the forward bias mode, and $K^+$ is present in abundance instead (as the anolyte is chosen to be KOH). In the case of such alkaline $CO_2$ electrolysis, $K^+$ will neutralize the anions (i.e., the carbonate ions entering the AEL from the gas side) at the internal interface, which will in theory generate a relatively small potential drop of 59.1 mV for every order of magnitude difference in the concentration across the interface. Based on the work of Strathmann and co-workers, the concentration in the membrane layers was found to be a function of the charge density of the BPM (which is experimentally determined to be 3.2 M, see the Supplementary Information) and the concentration of ions in the electrolyte. [34] The potential drop can then be calculated based on the concentration of $K^+$ in the CEL (3.5 M) and in the AEL (0.3 M), resulting in a potential drop of 64 mV. This salt neutralisation would imply a reduced cell voltage, also indicated by the negative membrane voltage at low current density in forward bias (Figure 5.3a).



Although carbonate species may be the dominant charge carriers through the BPM layers, the crossover of $CO_2$ seems to be lower in the forward bias than in the reverse bias, derived from the pH of the anolyte, as illustrated in Figure 5.2g and h. Initially, the $OH^-$ is consumed to turn $CO_2$ into $CO_3{}^{2-}$ (via $HCO_3{}^-$) as shown in Equation 5.1 and 5.2.

$$CO_2 + OH^- \rightarrow HCO_3^-, \qquad pK_a = 6.3 \tag{5.1}$$

$$HCO_3^- + OH^- \rightarrow CO_3^{2-} + H_2O, \quad pK_a = 10.3 \tag{5.2}$$

Once the pH of the anolyte decreases below the pKa shown in Equation 5.2, after approximately 15 minutes, only the reaction shown in Equation 5.1 will proceed in the right hand direction, while the reaction shown in Equation 5.2 is reversed since the equilibrium conditions change.

Equation 5.1 and 5.2 allow estimation of the $CO_2$ crossover from the experimentally observed change in pH for each mode. Chemical equilibrium software, Visual MINTEQ, was used to fit the molar flux of carbonic species through the entire BPM. A constant flux did not give a good fit with the experimental measurements, which seems reasonable since the conditions in the cell change over time as the carbonic species get absorbed by the KOH anolyte. The gradual build-up of DIC in the anolyte leads to a lower concentration gradient over the BPM, which lowers the DIC flux over time (see Figure S5.3).

For the reverse bias mode, a rapid pH change is observed during the experiment as a pH of 8.0 is reached after 60 minutes. The forward bias mode reaches a pH of 12.0 after only 60 minutes, indicating that the $OH^-$ is consumed at a rate approximately 5x slower than that in the reverse bias. It is important to note that in the forward bias mode no net WDR occurs and therefore no replenishment of consumed $OH^-$

ions at the anode takes place. The consumption of $OH^-$ at the anode accounts for 15% of the $OH^-$ loss.

To explain the stark difference in $CO_2$ crossover depending on the BPM orientation, we need to realise via which species the $CO_2$ dissolves and migrates through the BPM membrane layers. For the reverse bias mode, where the CEL is adjacent to the catalyst, the majority of the mobile species in the CEL have a positive charge. There is a flux of protons coming from the internal membrane interface, resulting in a pH below 7 in the CEL. Therefore, the $CO_2$(g) will dissolve and transport as carbonic acid ($H_2CO_3$(aq) or $CO_2$(aq)) through the CEL, as illustrated in Figure 5.2a. Once the carbonic species cross the internal membrane interface due to diffusion, the environment becomes more alkaline due to the high concentration of hydroxide ions either from the anolyte or from the WDR. Here, the carbonic acid will be converted into (bi)carbonate species. These (bi)carbonate species will move further into the anolyte and consume $OH^-$ ions.

The forward bias mode causes the pH to be higher than 7 at the catalyst-membrane interface, since the AEL prevents high concentrations of protons and the $CO_2$RR produces a significant amount of $OH^-$. The carbonic species will enter the AEL layer, depending on the actual pH, as carbonic acid, bicarbonate and/or carbonate. If the pH is higher than 8.5, then the formation of bicarbonate is dominant compared to that of the carbonic acid as the $CO_2$(g) will react directly with $OH^-$. [35] These carbonic species will then move towards the internal membrane interface. At the internal interface, the bicarbonate ions will be rejected by the negative fixed charges of the CEL. Unlike in the case of the reverse bias mode, where the CEL is being fed with protons (produced from the WDR at the interface layer), no source for $H^+$ is present in the forward bias. Therefore, we hypothesise that the (bi)carbonate species cannot easily cross the CEL in an electrolysis cell with an alkaline anolyte. Carbonic acid will not be formed due to the high pH in the AEL, and the (bi)carbonate species are rejected by the positive fixed charges in the AEL. This behaviour explains the mild pH change in forward bias shown in Figure 5.2g.

The differences in concentration profiles between reverse and forward bias are summarized in Figure 5.4, along with the potential and pH of the electrolyte layer, AEL and CEL. For the reverse bias case, a jump in pH and potential (due to the WDR) occurs at the membrane-membrane interface (Figure 5.4a) when a current is applied, which is qualitatively based on recent simulations. [32] As the pH in the AEL and anolyte decreases, the required potential across the membrane-membrane interface reduces, but is compensated at the anode. Over time, the flux will decrease as the DIC concentration gradient over the CEL decreases. The distribution of $K^+$ remains approximately constant over time, and the concentration at the CEL is similar to the ion exchange capacity. For the forward bias case (Figure 5.4b), there is no increase in potential at the AEL-CEL interface when going from the AEL to CEL;

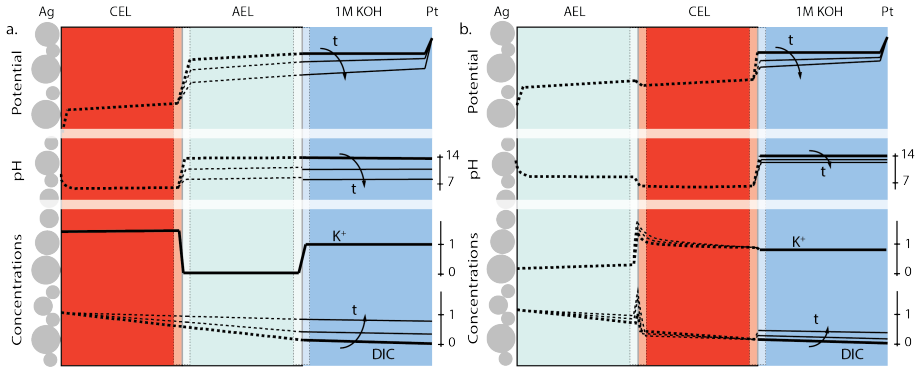


Figure 5.4: Potential gradient, pH and concentration profiles of $K^+$ and dissolved inorganic carbon (DIC) species at a fixed current density with $CO_2$ leakage through the BPM for (a) reverse bias and (b) forward bias orientation. For graphical clarity, the membrane-membrane and membrane-electrolyte interface are shown at increased scale. Solid lines are experimentally obtained values, while the dotted ones are illustrative approximations.

5

instead, a small decrease in potential exists due to the recombination of salt and potentially water in the membrane. This is also reflected in the concentration polarisation of $K^+$ in the CEL near the membrane-membrane interface, and the concentration polarisation of (bi)carbonate in the AEL (Figure 5.4b). Due to the water association and salt accumulation in forward bias, a substantial pH difference between the AEL and CEL is absent, which limits the concentration of DIC in the CEL. Hence, the change of the pH, DIC and potential of the anolyte is slower over time in the case of forward bias (Figure 5.4b) than that in reverse bias (Figure 5.4a).

Due to the high concentrations of $K^+$ and (bi)carbonate at the AEL-CEL interface in the forward bias mode, ion interaction could occur, possibly leading to salt formation at the membrane interface. This hypothesis is formed based on fuel cells with a BPM, where transport of $H^+$ and $OH^-$ ions to the interface is reported and thus water recombination occurs at the interface. [21] However, in the case of $CO_2$ electrolysis, few protons are available and water recombination will not occur; therefore, it is suggested that other reactions, such as the formation of potassium salts, occur. Although this AEL-CEL voltage brings a slight negative contribution to the total cell voltage, it will compromise the chemical potential difference over time, as the electrolyte loses its ionic strength. The increase of $K^+$ in the membrane layers is confirmed for the forward bias mode via inductively coupled plasma-optical emission spectroscopy (ICP-OES) measurements before and after the experiment, as shown in the mass balance in Figure 5.5. In the forward bias mode, the $K^+$ ions migrate at a rate of 130 µmol $cm^{-2}$ per hour, of which 80 µmol $cm^{-2}$ is transported to the catalyst surface. The remaining 50 µmol $cm^{-2}$ after one hour implies that the total $K^+$ concentration is doubled (to twice the ion exchange capacity), while the

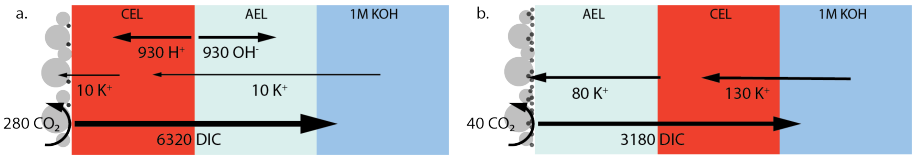


Figure 5.5: Mass balance of WDR products, $K^+$ ions, $CO_2$ conversion and DIC crossover for (a) reverse bias and (b) forward bias orientation. The values are in µmol $cm^{-2}$ and is the total number exchanged after the duration of the experiment (1 hr). Calculations of the ionic mol balances are described in SI.

amount of mobile charges in the membrane remains constant in the reverse bias mode.

In this study we also focus on the crossover of $K^+$ from the anolyte to the catalyst at the cathode where it can form salts, which is a common issue in MEAs for $CO_2$ electrolysis. [36] Figure 5.5a and b show the mass balance for each configuration of the BPM. The crossover in the reverse bias mode does follow the same crossover rate as when the bipolar membrane is placed in a liquid-liquid interface (at 25 mA $cm^{-2}$,7 µmol $h^{-1}$ $cm^{-2}$). [12] As mentioned earlier, the flux of $K^+$ through the CEL is significantly higher in the forward bias mode due to the neutralization of the carbonic species. In addition, the $K^+$ deposits almost 8 times faster at the Ag catalyst layer in the forward bias than in the reverse bias, while the $K^+$ needs to pass the exact same membrane layers (only in a different order). The strongly enhanced $K^+$ crossover could be due to the higher concentration of $K^+$ in the CEL near the CEL-AEL interface, leading to a higher concentration gradient over the AEL. Another hypothesis is the diffusion of dissolved salt ($KHCO_3$ or $K_2CO_3$), formed at the internal interface, towards the cathode.

A parameter that would influence the ion crossover — in addition to the orientation, current density and electrolyte composition — is the thickness of the membrane layers. As we prepared our membrane electrode assemblies based on a commercial bipolar membrane (heterogeneous Ralex™ bipolar membrane), it was not possible to change the thickness. However, based on the literature we can already estimate what the consequences would be if the thickness is altered. Recent simulations by Bui *et al.* (2020) and experimental work by Mayerhöfer *et al.* (2020) showed that the thickness of the anion exchange layer (AEL) is of main influence on the ion crossover. [36, 37] Although the influence of membrane thickness on the crossover of (uncharged) $CO_2$ is not studied previously, we can hypothesize that in reverse bias the $CO_2$ crossover is insensitive to the AEL thickness as the CEL determines the speciation of $CO_2$ and forms the main barrier for carbon transport. However, the $K^+$ transport would increase if the AEL thickness were reduced. [32] Similarly, for the forward bias case, we would expect that both carbon transport and more $K^+$ crossover would increase as the AEL thickness reduces. At the same time, a thinner membrane could strongly enhance the conductance of the membrane,

lowering the energy losses. To break this trade-off, a more active interlayer catalyst (enhancing the WDR) is required. Given that the much thinner FumaSep™ bipolar membranes (<200 µm) feature much lower resistance and similar relative cation crossover [12] compared to the Ralex™ membrane, thinner membranes with a more active WDR catalyst seem a realistic approach to improve the system. The effort to test this hypothesis, via reproducing BPMs at different thicknesses, is out of the scope of the study.

Figure 5.5 also reveals that the earlier discussed $CO_2$ crossover is at least one order of magnitude larger than the flux of potassium. For the reverse bias mode, the amount of $CO_2$ crossing over is 36% of the $CO_2$ feed (10 mL $min^{-1}$), while only 1.6% is consumed at the cathode. For the forward bias mode, these values are 18% and 0.3% at maximum FE, respectively. A physical description for the high crossover in both cases is the deposition method of the Ag, via vacuum sputtering, which de-aerates the BPM, creating micro-cracks that facilitate the crossover of the $CO_2$. These micro-cracks did not penetrate both layers, but most likely reduced the physical barrier for $CO_2$ of one membrane layer, increasing the diffusion coefficient of the carbonic species through these layers.

The combination of observed micro-cracks and high cell voltages in the reverse bias mode (Figure 5.2e), low faradaic efficiency in the forward bias mode (Figure 5.2d), and the literature results from Pătru *et al.* [11] could be associated with water management in the membrane layers. The water dissociation in the reverse bias mode may dehydrate the membrane layer, which provides a suitable faradaic efficiency (Figure 5.2c), but increases the membrane voltage (Figure 5.2e) and $CO_2$ crossover due to micro-cracks. At the same time, the forward bias mode, without water dissociation or even water recombination at the membrane interface, may suffer from a too high water content that compromises the faradaic efficiency. The latter effect has been observed as well by Pătru *et al.* [11] To test this hypothesis, a BPMEA was pre-treated by soaking it in demi water for 24 hours, which resulted in a 100% FE for $H_2$ in the reverse bias mode (see Figure S5.5).

The high overpotentials and $CO_2$ crossover, and water management of membrane layers, show that a different BPM is required to optimize the absolute performance for $CO_2$R in this catalyst integrated MEA. In this work, the architecture was chosen to understand the ion transport mechanisms with the different orientations of the BPM, allowing the ability to assess the ion accumulation at the surface(s). However, a BPM for an MEA in practical $CO_2$ electrolysis should possess a higher catalytic energy efficiency and ionic conductance. Also for the deposition method, spray deposition could be used as a less destructive technique than the vacuum sputtering used in this study. The spray deposition often requires a conductive support, such as a gas diffusion electrode. Considering such a practical architecture, the salt formation that was observed in the forward bias mode can facilitate flooding when

used in combination with a gas diffusion electrode, impacting the performance of the system. [36] In general, forward bias operation has intrinsic instability issues in terms of salt accumulation, which limits the operational lifetime of the BPM from hours to days. [11] Reverse bias operation suffers from significant $CO_2$ crossover and requires a very high membrane voltage (see Figure S5.4), but these aspects can be tuned by engineering more robust, thin membrane layers and better WDR catalysts for optimised $CO_2$ electrolysers. Furthermore, despite the acidic conditions of the cathode in reverse bias, the faradaic efficiency for CO is still considerably higher than that in the forward bias mode, even when the catalyst is sputtered directly on the (acidic) CEL.

## 5.3. CONCLUSIONS

We have studied the transport mechanisms of ions and (both charged and neutral) carbonic species as a function of the orientation of a bipolar membrane within a MEA performing electrochemical $CO_2$ reduction. A BPM-based MEA with the reverse bias orientation was compared to the opposite orientation, forward bias. Both orientations had a vapour-liquid cell configuration where a $CO_2$R catalyst (Ag) was directly deposited on the membrane interface. For the reverse bias mode, where the cation exchange layer of the BPM is in contact with the catalyst, the dominant ion transport mechanism is water dissociation that occurs at the internal membrane interface. At the same time, $CO_2$ crosses over through the BPM, starting by entering the CEL as carbonic acid (due to the low pH in the CEL) and being transported through the AEL towards the Pt anode as (bi)carbonate. The molar flux of $CO_2$ that crosses over through the BPM decreases over time due to the reduction in the dissolved inorganic carbon (DIC) concentration gradient.

For the case where the BPM is placed in the forward bias orientation (i.e., the CEL facing the anode), no water dissociation reaction occurs, saving 3 V in the cathodic potential at 25 mA $cm^{-2}$ compared to the reverse bias mode. The molar flux of carbonic species is half of that in the reverse bias mode and has a similar decreasing trend over time. After 10 minutes of operation, a reduction in the absolute cathodic potential is observed which coincided with a decreased selectivity towards CO evolution. We hypothesize that these observations indicate salt accumulation and higher water content due to the absence of water dissociation in the internal membrane interface, which are intrinsic to the forward bias operation. Because of the salt build-up and high concentration of $K^+$ and (bi)carbonates at the CEL-AEL interface, more $K^+$ can cross over through the AEL, depositing on the catalyst surface. Our study shows that there are performance trade-offs for each BPM orientation with regard to potential, selectivity, and stability: the forward bias lowers the overall cell potential by reducing the chemical potential, while the reverse bias gives a stable product formation of $CO_2$ conversion products.

## 5.4. SUPPLEMENTARY INFORMATION

### 5.4.1. FABRICATION OF BPMEA

A heterogeneous dry bipolar membrane (Ralex™ BM, MemBrain s.r.o.), with a thickness of 460 µm, was used to fabricate the bipolar membrane electrode assembly (BPMEA). We opted for the Ralex membrane as it is produced dry, allowing to be vacuum sputtered on the surface. On the membrane, a 100 nm layer of Ag was deposited (50 Watt DC power, 20 sccm argon and 3 microbar pressure; sputter deposition time was 306 seconds). The same method was used for the reverse bias case and the forward bias case. The rough structure of the membrane layers leads to holes in the Ag layer (see SEM figure, Fig). Once the membrane starts to swell and is electrochemically active, the Ag layer is no longer conformal and has small ruptures. These gaps in the Ag layer are actually required to facilitate the transport of ions and $CO_2$ to the active sites.



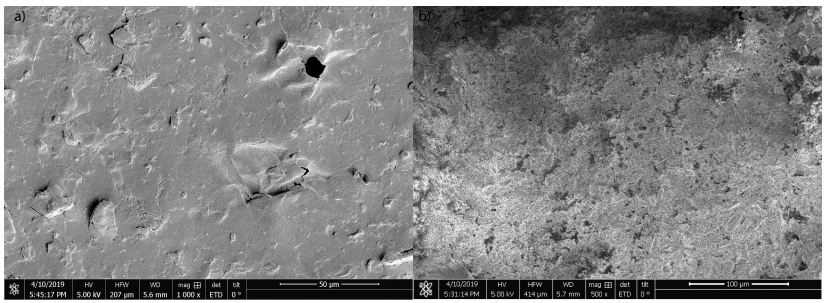


Supplementary Figure S5.1: SEM-image of the sputtered Ag-layer on the BPM in (a) dry state and (b) after $CO_2$ reduction in reverse bias case.

### 5.4.2. ELECTROCHEMICAL EXPERIMENTS

The experiments were performed in a flow cell (MicroFlowCell, purchased from Electrocell, Denmark). The catalyst on the BPMEA was fixed at the flow cell with copper tape, which also served as current collector. The catalyst surface area was 1.56 $cm^2$, the catalyst at the anode (Ni) had a similar surface area. Between the BPMEA and the anode, an anolyte was flushed around (0.035 $cm^3\ s^{-1}$). A micro reference electrode of type LF-1-100 (manufactured by Innovative Instruments Inc. with a polyetheretherketone (PEEK) body and a diameter of 1 mm) was inserted in the anolyte to measure the cathode potential. Just before the experiment was started, $H_2O$ was flown in the anolyte, in order to wet the membrane. This wetting allowed the membrane to swell, reducing the resistance of the BPMEA.

### 5.4.3. CALCULATION CHARGE DENSITY AND MEMBRANE CONCENTRATION

The charge density of the Ralex membrane was determined via the procedure described by Galama *et al.* [38] Only the cations (Na, resp.) were measured via ICP-OES. The amount of Na present in the CEL was 84.06 µmol. With a water uptake of 0.84 g $H_2O$/g for the entire membrane (assuming that for the CEL this is half of the water uptake, 0.42 g $H_2O$/g), and an ion exchange capacity of 0.0013 mol/g, this leads to a charge density of 3.18 mol/kg $H_2O$.

The concentration in the membrane layers during operation were determined via Strathmann et al. [34] With the use of following formula, one can calculate (for the reverse bias mode) the concentrations in the CEL, knowing that $C_{K^+,bulk} = 1$:

$$C_{K^+,CEL} = \frac{X + \sqrt{X^2 + 4CK^+,bulk}}{2} = 3.48 \tag{5.3}$$

And in the AEL:

$$C_{K^+,AEL} = \frac{X - \sqrt{X^2 + 4CK^+,bulk}}{2} = 0.28 \tag{5.4}$$

5

### 5.4.4. MOLAR FLUX CALCULATION

Molar flux of DIC is calculated based on the consumption of the hydroxide ions and therefore its concentration.

$$[OH^-]_{consumed} = 10^{-(pK_W - pH_1)} - 10^{-(pK_W - pH_2)} \tag{5.5}$$

Where $pH_1$ and $pH_2$ are two values between a certain time, $t$, in which the molar flux should be calculated with $z_i$ the valence of the DIC species dominating at that time:

$$J_{DIC} = \frac{[OH^-]_{consumed}}{z_i t} \quad [M/min] \tag{5.6}$$

Due to the high salinity of the 1M KOH, the $pK_W$ is not exactly 14, but around 13.65.

### 5.4.5. CALCULATION MASS BALANCE

Based on the applied charge throughout the operation ($t = 1hr$, $i = 25mAcm^{-2}$, $A = 1.56cm^2$):

$$Q = i * t * A = 140.4C \tag{5.7}$$

One can calculate the amount of protons consumed at the cathode:

$$\#protons = Q/96485 = 0.00145mol \tag{5.8}$$

Divided by time and surface area one finds the flux, which should be the same at the cathode as at the internal BPM interface:

$$J_{protons} = \frac{0.00145mol}{1hr * 1.56cm^2} = 932.8\mu molhr^{-1}cm^{-2} \tag{5.9}$$

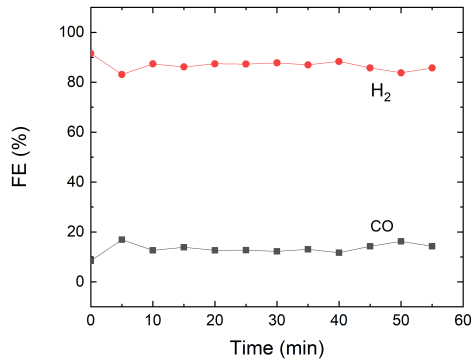


Supplementary Figure S5.2: Sample of forward bias mode with continued CO production.



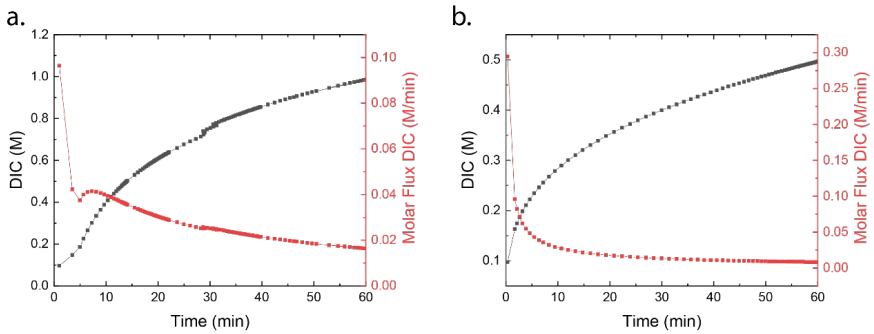


Supplementary Figure S5.3: DIC and molar flux of DIC in function of time of (a) reverse bias mode and (b) forward bias mode.

The crossover of $K^+$ is determined via ICP-OES in mol and via a similar method converted to a flux. To determine the amount of $CO_2$ converted by the cathode, the amount of charge is multiplied by the faradaic efficiency of each case and then converted into a flux. For the total amount of $CO_2$ that has crossed over through the membrane, the DIC concentration at the experiment (see Fig S5.3) was converted from mol $l^{-1}$ to a flux, knowing that the anolyte concentration was 10 ml.

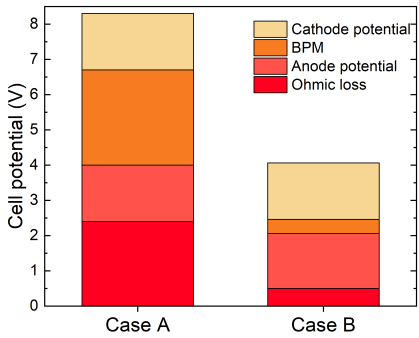


Supplementary Figure S5.4: Potential breakdown for the setup with reverse bias orientation (case A) and forward bias (case B). The experiments in triplicate to cancel out sample-to-sample variation; cell voltage of reverse bias has a standard deviation of 0.43 V and forward bias of 0.24 V.



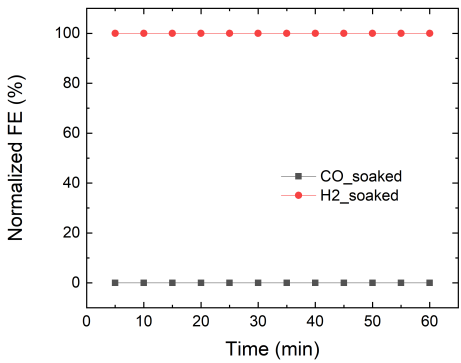


Supplementary Figure S5.5: Effect of preconditioning the BPMEA on the normalized Faradaic efficiencies by soaking the membrane with catalyst for 24 hours in demi water, at 25 mA $cm^{-2}$ in reverse bias mode.

## REFERENCES

[1] M. A. Blommaert, R. Sharifian, N. Shah, N. T. Nesbitt, W. A. Smith, and D. A. Vermaas, *Orientation of bipolar membrane determines the dominant ion and carbonic species transport in membrane electrode assemblies for CO2 reduction,* Journal of Materials Chemistry A **9**, 11179 (2021).

[2] S. Hernández, M. A. Farkhondehfal, F. Sastre, M. Makkee, G. Saracco, and N. Russo, *Syngas production from electrochemical reduction of CO2: Current status and prospective implementation,* Green Chemistry **19**, 2326 (2017).

[3] D. S. Ripatti, T. R. Veltman, and M. W. Kanan, *Carbon Monoxide Gas Diffusion Electrolysis that Produces Concentrated C 2 Products with High Single-Pass Conversion,* Joule **3**, 240 (2019).

[4] C. M. Gabardo, C. P. O'Brien, J. P. Edwards, C. McCallum, Y. Xu, C.-T. Dinh, J. Li, E. H. Sargent, and D. Sinton, *Continuous Carbon Dioxide Electroreduction to Concentrated Multi-carbon Products Using a Membrane Electrode Assembly,* Joule **3**, 2777 (2019).

[5] C. Xia, P. Zhu, Q. Jiang, Y. Pan, W. Liang, E. Stavitsk, H. N. Alshareef, and H. Wang, *Continuous production of pure liquid fuel solutions via electrocatalytic CO2 reduction using solid-electrolyte devices,* Nature Energy **4**, 776 (2019).

[6] Z. Yin, H. Peng, X. Wei, H. Zhou, J. Gong, M. Huai, L. Xiao, G. Wang, J. Lu, and L. Zhuang, *An alkaline polymer electrolyte CO 2 electrolyzer operated with pure water,* Energy & Environmental Science **12**, 2455 (2019).

[7] B. Kim, F. Hillman, M. Ariyoshi, S. Fujikawa, and P. J. Kenis, *Effects of composition of the micro porous layer and the substrate on performance in the electrochemical reduction of CO2 to CO,* Journal of Power Sources **312**, 192 (2016).

[8] C. Delacourt, P. L. Ridgway, J. B. Kerr, and J. Newman, *Design of an electrochemical cell making syngas (CO+ H2) from C O2 and H2 O reduction at room temperature,* Journal of the Electrochemical Society **155**, 42 (2008).

[9] Y. C. Li, D. Zhou, Z. Yan, R. H. Gonçalves, D. A. Salvatore, C. P. Berlinguette, and T. E. Mallouk, *Electrolysis of CO2 to Syngas in Bipolar Membrane-Based Electrochemical Cells,* ACS Energy Letters **1**, 1149 (2016).

[10] D. A. Salvatore, D. M. Weekes, J. He, K. E. Dettelbach, Y. C. Li, T. E. Mallouk, and C. P. Berlinguette, *Electrolysis of Gaseous CO 2 to CO in a Flow Cell with a Bipolar Membrane,* ACS Energy Letters **3**, 149 (2017).

[11] A. Pătru, T. Binninger, B. Pribyl, and T. J. Schmidt, *Design Principles of Bipolar Electrochemical Co-Electrolysis Cells for Efficient Reduction of Carbon Dioxide from Gas Phase at Low Temperature,* Journal of The Electrochemical Society **166**, F34 (2019).

[12] M. A. Blommaert, J. A. H. Verdonk, H. C. B. Blommaert, W. A. Smith, and D. A. Vermaas, *Reduced Ion Crossover in Bipolar Membrane Electrolysis via Increased Current Density, Molecular Size, and Valence,* ACS Applied Energy Materials **3**, 5804 (2020).

[13] D. A. Vermaas, S. Wiegman, T. Nagaki, and W. A. Smith, *Ion transport mechanisms in bipolar membranes for (photo)electrochemical water splitting,* Sustainable Energy and Fuels **2**, 2006 (2018).

[14] M. A. Blommaert, D. A. Vermaas, B. Izelaar, B. in 't Veen, and W. A. Smith, *Electrochemical impedance spectroscopy as a performance indicator of water dissociation in bipolar membranes,* Journal of Materials Chemistry A **7**, 19060 (2019).

[15] D. A. Vermaas and W. A. Smith, *Synergistic Electrochemical CO2 Reduction and Water Oxidation with a Bipolar Membrane,* ACS Energy Letters , 1143 (2016).

[16] R. Pärnamäe, S. Mareev, V. Nikonenko, S. Melnikov, N. Sheldeshov, V. Zabolotskii, H. V. Hamelers, and M. Tedesco, *Bipolar membranes: A review on principles, latest developments, and applications,* Journal of Membrane Science **617**, 118538 (2021).

[17] J. Xia, G. Eigenberger, H. Strathmann, and U. Nieken, *Flow battery based on reverse electrodialysis with bipolar membranes: Single cell experiments,* Journal of Membrane Science **565**, 157 (2018).

[18] Y. Chen, A. Vise, W. E. Klein, F. C. Cetinbas, D. J. Myers, W. A. Smith, W. A. Smith, W. A. Smith, T. G. Deutsch, and K. C. Neyerlin, *A Robust, Scalable Platform for the Electrochemical Conversion of CO2 to Formate: Identifying Pathways to Higher Energy Efficiencies,* ACS Energy Letters **5**, 1825 (2020).

[19] L. Shi, Y. Hu, S. Xie, G. Wu, Z. Hu, and X. Zhan, *Recovery of nutrients and volatile fatty acids from pig manure hydrolysate using two-stage bipolar membrane electrodialysis,* Chemical Engineering Journal **334**, 134 (2018).

[20] R. S. Reiter, W. White, and S. Ardo, *Communication—Electrochemical Characterization of Commercial Bipolar Membranes under Electrolyte Conditions Relevant to Solar Fuels Technologies,* Journal of The Electrochemical Society **163**, H3132 (2016).

[21] M. Ünlü, J. Zhou, and P. A. Kohl, *Hybrid anion and proton exchange membrane fuel cells,* Journal of Physical Chemistry C **113**, 11416 (2009).

[22] M. Unlu, J. Zhou, and P. A. Kohl, *Hybrid Polymer Electrolyte Fuel Cells: Alkaline Electrodes with Proton Conducting Membrane,* Angewandte Chemie **122**, 1321 (2010).

[23] R. B. Kutz, Q. Chen, H. Yang, S. D. Sajjad, Z. Liu, and I. R. Masel, *Sustainion Imidazolium-Functionalized Polymers for Carbon Dioxide Electrolysis,* Energy Technology **5**, 929 (2017).

[24] J. J. Kaczur, H. Yang, Z. Liu, S. D. Sajjad, and R. I. Masel, *Carbon Dioxide and Water Electrolysis Using New Alkaline Stable Anion Membranes,* Frontiers in Chemistry **6**, 1 (2018).

[25] A. Alcaraz, F. G. Wilhelm, M. Wessling, and P. Ramirez, *The role of the salt electrolyte on the electrical conductive properties of a polymeric bipolar membrane,* Journal of Elec **513**, 36 (2001).

[26] A. V. Sokirko, P. Ramírez, J. A. Manzanares, and S. Mafés, *Modeling of Forward and Reverse Bias Conditions in Bipolar Membranes,* Berichte der Bunsengesellschaft für physikalische Chemie **97**, 1040 (1993).

[27] G. O. Larrazábal, P. Strøm-Hansen, J. P. Heli, K. Zeiter, K. T. Therkildsen, I. Chorkendorff, and B. Seger, *Analysis of Mass Flows and Membrane Crossover in CO2 Reduction at High Current Densities in an MEA-Type Electrolyzer,* ACS Applied Materials and Interfaces **11**, 41281 (2019).

[28] S. Z. Oener, M. J. Foster, and S. W. Boettcher, *Accelarating water dissociation in bipolar membranes and for electrocatalysis,* Science **369**, 1099 (2020).

[29] C. Shen, R. Wycisk, and P. N. Pintauro, *High performance electrospun bipolar membrane with a 3D junction,* Energy Environ. Sci. **10**, 1435 (2017).

[30] Y. Chen, J. A. Wrubel, W. E. Klein, S. Kabir, W. A. Smith, K. C. Neyerlin, and T. G. Deutsch, *High-Performance Bipolar Membrane Development for Improved Water Dissociation,* ACS Applied Polymer Materials **2**, 4559 (2020).

[31] J. Wrubel, Y. Chen, Z. Ma, and T. G. Deutsch, *Modeling Water Electrolysis in Bipolar Membranes,* Journal of the Electrochemical Society **167**, 114502 (2020).

[32] J. C. Bui, I. Digdaya, C. Xiang, A. T. Bell, and A. Z. Weber, *Understanding Multi-Ion Transport Mechanisms in Bipolar Membranes,* ACS Applied Materials & Interfaces **12**, 52509 (2020).

[33] W. J. van Egmond, M. Saakes, I. Noor, S. Porada, C. J. Buisman, and H. V. Hamelers, *Performance of an environmentally benign acid base flow battery at high energy density,* International Journal of Energy Research **42**, 1524 (2018).

[34] H.Strathmann, J.J.Krol, H.J.Rapp, and G.Eigenberger, *Limiting current density and water dissociation in bipolar membranes,* Journal of Membrane Science **125**, 123 (1997).

[35] X. Wang, W. Conway, R. Burns, N. McCann, and M. Maeder, *Comprehensive study of the hydration and dehydration reactions of carbon dioxide in aqueous solution,* Journal of Physical Chemistry A **114**, 1734 (2010).

[36] M. E. Leonard, L. E. Clarke, A. Forner-Cuenca, S. M. Brown, and F. R. Brushett, *Investigating Electrode Flooding in a Flowing Electrolyte, Gas-Fed Carbon Dioxide Electrolyzer,* ChemSusChem **13**, 400 (2020).

[37] B. Mayerhöfer, D. McLaughlin, T. Böhm, M. Hegelheimer, D. Seeberger, and S. Thiele, *Bipolar membrane electrode assemblies for water electrolysis,* ACS Applied Energy Materials **3**, 9635 (2020).

[38] A. H. Galama, J. W. Post, M. A. Cohen Stuart, and P. M. Biesheuvel, *Validity of the Boltzmann equation to describe Donnan equilibrium at the membrane-solution interface,* Journal of Membrane Science **442**, 131 (2013).

# 6

# ENERGY REQUIREMENTS FOR ELECTROCHEMICAL CO PRODUCTION FROM $CO_2$ IN A MEA WITH A BIPOLAR MEMBRANE VERSUS ANION EXCHANGE MEMBRANE

*Recent innovations in $CO_2$ electrolysers involve membrane electrode assemblies (MEAs). Typically, anion exchange membranes (AEMs) are used with a high conductivity in alkaline environment, but those suffer from unwanted $CO_2$ crossover, implying (indirect) energy consumption for generating an excess of $CO_2$ feed and purification of the KOH anolyte. As an alternative, bipolar membranes (BPMs) with their composition of two oppositely charged membrane layers have been suggested, which can mitigate that reactant loss. However, BPMs are associated with a higher cell voltage as they dissociate water. In this study, the direct and indirect energy consumption required to electrochemically produce CO was investigated in a MEA with BPMs or AEMs. While the BPM-run cell had a high stability and almost no $CO_2$ loss, the product selectivity of CO was low, making the energy requirement higher than the AEM-run cell. For the BPM to be of relevance in the $CO_2$ electrolysers, the cathode interface will have to be improved in future work.*

This chapter is in preparation for publication.

## 6.1. INTRODUCTION

To mitigate global warming, political and industrial stakeholders have embraced technologies that recycle emitted $CO_2$, such as the electrochemical reduction of $CO_2$. [1] Via this electrochemical reaction of $CO_2$ ($CO_2$ER), which can be coupled to a renewable energy source in order to be sustainable, (hydro)carbon building blocks (e.g. CO, $C_2H_4$) are produced for downstream processes. [2] However, to be industrial competitive with already existing processes based on fossil fuels, a higher efficiency should be achieved as the electricity dominates the operating costs. [2, 3]

To reach higher performances in terms of product selectivity, energy efficiency and stability, the reactor configurations for $CO_2$ER have progressed throughout the years. To overcome the mass transport limitations of $CO_2$ in this reactor configuration existing in aqueous environments, gas diffusion electrodes (GDEs) were introduced. With the GDE, a three order of magnitude reduction in diffusion transport to reach the catalyst surface is achieved, which enables us to operate at high current densities ($\geq$100 mA $cm^{-2}$). [4] In a GDE based setup, a membrane electrode assembly (MEA) or zero gap electrolyser configuration is attractive to reach higher current densities with the same cell potential, as it allows to further reduce the ion path. [5] In this configuration, an ion exchange membrane is sandwiched between two electrodes resulting in lower ohmic losses. The opposing electrode, the anode, requires a strong alkaline environment (e.g. KOH) to optimally perform the oxygen evolution reaction.



Typically, an anion exchange membrane (AEM) is used in such a MEA configuration for $CO_2$ reduction, as it has a high ionic conductivity (see Figure 6.1). Using an alkaline anolyte also enables us to use earth abundant materials like NiFe-based catalysts for the oxygen evolution reaction (OER). A disadvantage of this configuration is the reaction of gaseous $CO_2$ from the cathode feed with hydroxide ions in the membrane or from the anolyte, forming carbonate or bicarbonate ions. Those (bi)carbonate ions cross over to the anolyte via migration and diffusion. Even the use of a $KHCO_3$ electrolyte also does not circumvent this problem since the interfacial pH at the cathode is sufficiently high at high current densities [6], and disables to use NiFe-based catalysts for the OER. The carbonate formation (or carbon crossover) is unwanted since it reduces the chemical potential of hydroxide ions at the anode, which increases the required thermodynamic potential for oxygen evolution. This $CO_2$ loss also reduces the $CO_2$ utilization rate, which implies that the strong alkaline electrolyte should be either regenerated or disposed as waste.

The extent of the carbon crossover depends on the membrane properties. Although the new class of AEMs, such as like Sustainion [7] or PiperION [8], are highly conductive and have proven to reach high partial current densities for making CO, these membrane are strong carbonate ($CO_3^{2-}$) conductors as well. The diffusion coefficient of the carbonate species depends on the AEM, with the extreme case of

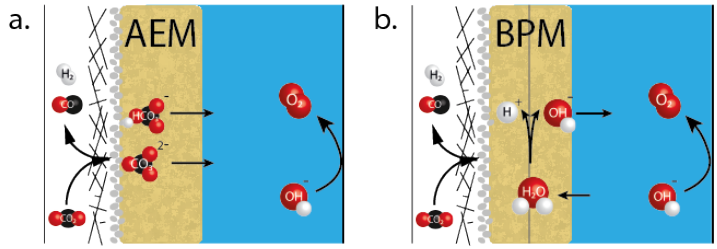


Figure 6.1: Schematic illustration of (a) an AEM-run cell versus (b) one with a BPM. $CO_2$ gas feed is presented on the left, where the $CO_2$ has to diffuse through the GDE in order to reach the cathode, where it can be converted into products (for example CO), with hydrogen evolution reaction as a competing side-reaction. The AEM-run cell will transport anions (e.g. $CO_3{}^{2-}$) towards the anode, where oxygen is generated. The BPM-run cell performs water dissociation reaction at the internal interface of the BPM, of which the produced proton will be transported to the cathode, and hydroxide ion towards the anode.

having no membrane (i.e., only a GDE) where the carbon crossover is maximised. [9, 10] Another type of ion exchange membrane are the cation exchange membranes, like Nafion, that strongly suffers from ion crossover in these conditions and is not suitable for $CO_2$ER at high alkaline pH. [11, 12]



The carbon crossover can be prevented with the use of a bipolar membrane (BPM), as it consists of two membrane layers with opposite fixed charges with in between an interface layer, where the water dissociation reaction (WDR) occurs (see Figure 6.1). The reaction, $H_2O \rightarrow H^+ + OH^-$, maintains an alkaline environment around the anode as the hydroxide ions is migrated towards the anode. To drive this reaction, a thermodynamic potential of 0.83 V is required. Although in theory this required water dissociation potential can be gained back in the created chemical potential (i.e., a pH gradient), previous work has shown that this does not fully balance out [13, 14], presumably because the environment of the cathode is not at pH 0. This leads to a higher cell potential, which has held back the use of bipolar membranes as serious competitors to be used in a $CO_2$ electrolyser.

Having established that both AEM-based and BPM-based $CO_2$ reduction cells face limitations in cell voltage and crossover, a comparison of those systems on a single metric would help to assess the potential for practical future potential. In this thesis, we perform a study to compare those system based on direct and indirect energy consumption. From an energy consumption point of view, we can weigh the loss of $CO_2$ and spent anolyte in an AEM-based MEA against the additional cell potential in a BPM-based MEA. Therefore, we studied two MEA systems for $CO_2$ to CO conversion, one with an AEM and one with a BPM, to quantify the direct and indirect energy required to produce CO and to determine whether the increase of potential in BPMs is justified as the $CO_2$ and $OH^-$ loss is minimized.

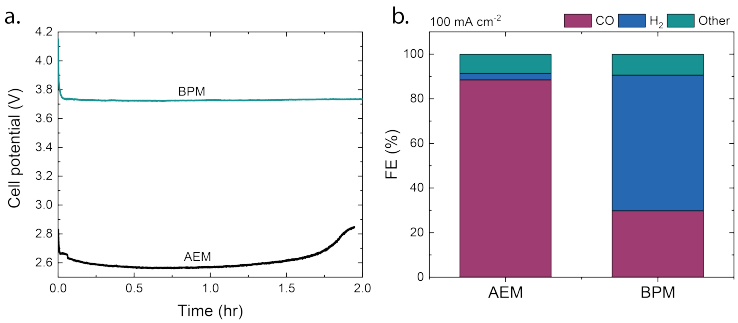


Figure 6.2: (a) Cell potential of MEA setup with AEM and BPM at 100 mA $cm^{-2}$, (b) Faradaic efficiency of MEA with AEM and BPM, where 'other' stands for liquid and at the anode decomposed carbon products.

## 6.2. RESULTS

To quantify the required energy for the production of CO, three contributions are considered: 1) cost to operate the electrochemical cell, 2) loss of $CO_2$ from the inlet stream, and 3) loss of $OH^-$ ions as the chemical potential of the system decreases. Each contribution is expressed in kJ per mol produced CO, which means the Faradaic efficiency is automatically taken into account.

To determine the cost to operate the electrochemical cell, constant current electrolysis experiments were performed in a MEA setup. In this setup, a GDE with Ag as catalyst was pressed on the AEM (Sustainion) with a Ni-mesh as anode surrounded by 1M KOH. The experiments were performed for two hours at 100 mA $cm^{-2}$. To compare its performance with a bipolar membrane, another series of experiments were performed with the same setup and the only difference being the use of a Fumatech BPM instead of the AEM. For further experimental details, see Supplementary Information.

Often a comparison in both configurations focuses on the applied potential and the product distribution. The total cell potential for the AEM-run cell reaches a minimum of 2.6 V, while the BPM-run cell (3.7 V) requires more than one volt extra to reach 100 mA $cm^{-2}$ (Figure 6.2a). The obtained products at the cathode depend on the membrane type (Figure 6.2b). The Faradaic efficiency (FE) for CO is nearly 90% for CO with the AEM-run cell, with little $H_2$ produced. In the BPM-run cell, a maximum of 30% for FE towards CO is achieved, with a $H_2$ production twice of the CO production (60%). For both cases, similar values have been reported previously. [9] Roughly, 10% of the FE remains undetected in both cases, as Ag is known to produce formic acid at this current density, which ends up being decomposed at the anode. [9]

In this batch-type experiment of Figure 6.2a, the cell potential of the AEM-run cell is not stable over time. This is due to the change in pH of the anolyte (initially 60 mL 1M KOH) caused by the carbon ($CO_3{}^{2-}$) crossover. The pH drops in almost 2 hours from 13.8 to 11.3 (Figure 6.3), after which the experiment was stopped to prevent degradation of the Ni-mesh. After 1.75 hour, a sudden jump is visible in the cell potential, indicating that the concentration of $OH^-$ becomes too low to perform the OER from the $OH^-$ pathway, and the reaction starts to shift to the pathway where $H_2O$ serves as $OH^-$ source. This requires a higher cell potential (as seen in Figure 6.2). At the cathode for the carbon formation to occur, $OH^-$ is required:

$$CO_2 + OH^- \rightarrow CO_3^{2-} + H_2O \tag{6.1}$$

Given the high alkaline environment, only carbonate is formed that requires two hydroxide ions. [15] These hydroxide ions can come from two sources; either from diffusion of $OH^-$ from the electrolyte to the gas-liquid interface, or via $CO_2$ER, where the produced $OH^-$ is immediately converted with an additional $CO_2$ molecule. The latter process of combined $CO_2$ER and $CO_2$ scavenging can be described by Equation 6.2 with $x = 1$ (for full utilization of the produced $OH^-$) or $0 < x < 1$ (for partial $OH^-$ consumption):

$$(1+x)CO_2 + H_2O + 2e^- \rightarrow CO + 2(1-x)OH^- + xCO_3^{2-} \tag{6.2}$$

To differentiate between the mechanisms, the pH was calculated if only the $OH^-$ production from the $CO_2$ER were to be consumed (i.e., $x = 1$, dashed line in Figure 6.3). For that case, the pH for the AEM-run cell would not drop below 13.2 in this experiment, indicating that additional carbon crossover also occurs. A carbon balance was determined, via the chemical equilibrium software VisualMINTEQ as presented in an earlier reported article [16], indicating that the total carbon concentration is 0.5 M at the end of the experiment or an average molar flux of 2.5 µmol $cm^{-2}$ $hr^{-1}$ (15% of the inlet $CO_2$ at 40 mL $min^{-1}$). Further analysis on the $OH^-$ source shows that 67% of the $OH^-$ comes from the $CO_2$ER and the remaining part from the electrolyte. If the same experiment would be performed in a steady-state continuous reactor, keeping the anolyte pH constant, the crossover is expected even higher, as the $CO_2$ crossover rate decreases over time in a batch-type reactor as the anolyte saturates. [16]

The pH drop in the AEM-run cell is in stark contrast with the pH of the anolyte in the BPM-run cell, which remains practically stable throughout the experiment (Figure 6.3). This indicates that barely any dissolved inorganic carbon is crossing over through the BPM. Recent literature has shown that, depending on the type of membrane and production method, some BPMs also suffer from $CO_2$ crossover. [16]

With the information presented so far, the energy consumption to produce CO via $CO_2$ER was calculated. The first component, the direct energy consumption coming from the electrochemical cell, was determined based on the cell voltage and

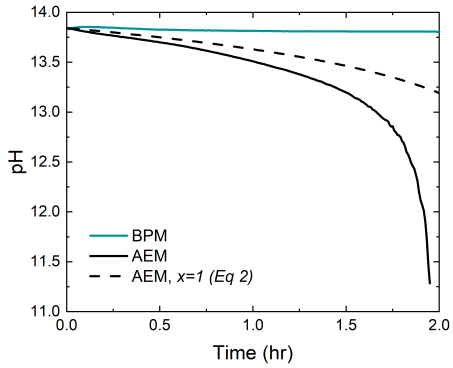


Figure 6.3: pH of the AEM- and BPM-run cell, with for AEM the simulation-based pH if the consumed $OH^-$ only was sourced from the $CO_2$ER.

Faradaic efficiency:

$$P_{electrolysis} = \frac{nFU}{FE_{CO}} 10^{-3} \ [kJ\ mol^{-1}] \tag{6.3}$$

Where $P$ is the energy required per produced mol of CO, $n$ is the amount of electrons required for $CO_2$ER, $U$ the cell potential, and $FE_{CO}$ the Faradaic efficiency towards CO. In this calculation, the contribution of hydrogen (side-reaction) or oxygen (anodic reaction) is ignored, as CO is of main interest for this study. $P_{electrolysis}$ is presented in the red bars in Figure 6.4, in which the red dotted portion indicates the minimal energy required if the FE would be 100%.

The second component to the total energy consumption is the neutralization of $OH^-$ by inorganic carbon, which implies the necessity of regenerating the $OH^-$ solution to operate in steady state. To regenerate these ions, the minimum required energy for this process is 0.83 eV per $OH^-$ ion, to drive the water dissociation reaction (Equation 6.3 with $U = 0.83\ V$). The third component is the loss of dissolved $CO_2$, which implies the need for a larger supply of $CO_2$ feed. The energy consumption for capturing additional $CO_2$ depends on the process to capture and purify the $CO_2$. The state-of-the-art requires at the moment around 200 kJ per mol $CO_2$, this value should then be converted to the amount of $CO_2$ that dissolves per mol produced CO by dividing with $FE_{CO}$. [17]

The total required (direct + indirect) energy is plotted in Figure 6.4, differentiated for each component. For the BPM-run cell, only the direct energy consumption from the electrolysis cell contributes. As no carbon crossover occurs, there is no $CO_2$ loss. Additionally, at this current density there is little (other) ion crossover, like $K^+$, and the selectivity of the water dissociation reaction is nearly 100%, which

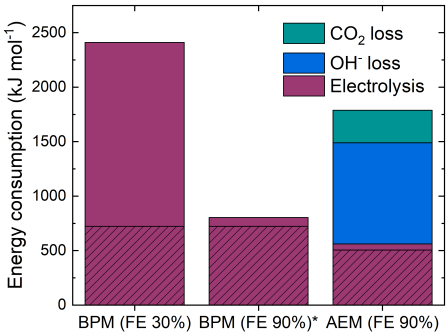


Figure 6.4: Energy consumption for the production of CO for a BPM- and AEM-run cell, for MEA-configurations operating at 100 mA $cm^{-2}$. The electrolysis component is separated into two parts, where the section with diagonal lines indicates the minimal energy needed to produce CO at a FE of 100%. *For comparison, the energy consumption is plotted at a similar FE as for the AEM-run cell.



allows to neglect $OH^-$ replenishment. The electrolysis component suffers in the BPM-run cell from the low FE towards CO (30%), leading to high values per mol CO. A substantial gain is therefore achievable in this configuration as the minimal required energy for the production of CO in these conditions is 720 kJ $mol^{-1}$. If a higher Faradaic efficiency were to be achieved, a lower energy consumption can be obtained. This would require a BPM-catalyst interaction that is designed for this specific reaction and environment. Recent literature reports have shown promising results by inserting a buffering layer [18, 19], which prevents the formation of hydrogen via the acidification of the cathode environment.

If the FE of the BPM-run cell would be 72%, the total energy required for the production of CO, would be similar as the (direct + indirect) energy needed in the AEM-run cell (at a FE of 90%). The impact of the $OH^-$ and, more importantly, $CO_2$ loss, reduces the energy efficiency of the AEM-run cell with 45%. For every mol of CO produced, 1.5 mol of $CO_2$ diffused into the electrolyte, leading to energy consumption of 300 kJ $mol^{-1}$ for the $CO_2$ loss. The gain in the AEM-run cell if the FE were further increased up to 100% would only lead to a 5% reduction in energy consumption. When the Faradaic efficiency is equal in both cases (FE 90%, Figure 6.4), the BPM-run cell is favoured due to the long stability of the electrolyte. This means that with a BPM-run cell, significant performance gains can be achieved for $CO_2$ER. With this comparison between two ion-exchange membranes, there is more than ever a need for new BPM configurations with a focus on the cathode-membrane interface.

## 6.3. CONCLUSION

In this study, the energy consumption required to electrochemically produce CO from $CO_2$ was investigated at a fixed current density with an anolyte (1M KOH) in a membrane electrode assembly with two ion-exchange membranes. To fairly address the indirect energy losses due to inorganic carbon crossover, anolyte degradation and side reactions such as hydrogen evolution, we propose to benchmark $CO_2$ conversion systems including the indirect energy costs for $CO_2$ replenishment and anolyte purification. Although the direct cell voltage required for this operation was lower for the anion exchange membrane, the $CO_2$ loss to $OH^-$ and consequent drop in anolyte pH resulted in poor stability of AEM when operated for 2 hours. In contrast, the MEA operated with a bipolar membrane showed a steady cell potential and no drop in anolyte pH over time indicating its relevance in minimizing the carbon crossover to the anode. For the present state-of-the-art BPMs, the poor product selectivity of CO for the BPM-cell (30%, against 90% for the AEM-based cell) brings the total (direct + indirect) energy consumption for BPM-based cells higher than that of AEM-based cells. However, the total energy required for the BPM would be the same as the AEM if it produces CO with 72% FE, leveraging its advantage in minimizing the $CO_2$ losses to electrolyte and increasing $CO_2$ utilization rate. While further research is required studying the carbon crossover in function of electrolyte and cell configuration, this specific case shows that the AEM-based cells suffers from the high energy losses linked to the carbon crossover. Indicating that the BPM-based cell can achieve significant energy reduction to produce CO if the FE is increased. Hence, future work on BPM-based cells should direct to increase Faradaic efficiencies, e.g. via adding a buffer layer on the cathode to minimize the hydrogen evolution and maximize CO production in a BPM operated MEA configuration.



## REFERENCES

[1] European Commission, *The European Green Deal*, Tech. Rep. (Brussels, 2019) arXiv:arXiv:1011.1669v3 .

[2] M. Jouny, W. Luc, and F. Jiao, *General Techno-Economic Analysis of CO2 Electrolysis Systems,* Industrial & Engineering Chemistry Research **57**, 2165 (2018).

[3] W. A. Smith, T. Burdyny, D. A. Vermaas, and H. Geerlings, *Pathways to Industrial-Scale Fuel Out of Thin Air from CO2 Electrolysis,* Joule **3**, 1822 (2019).

[4] B. Kim, F. Hillman, M. Ariyoshi, S. Fujikawa, and P. J. Kenis, *Effects of composition of the micro porous layer and the substrate on performance in the electrochemical reduction of CO2 to CO,* Journal of Power Sources **312**, 192 (2016).

[5] T. Zheng, K. Jiang, N. Ta, Y. Hu, J. Zeng, J. Liu, and H. Wang, *Large-Scale and Highly Selective CO 2 Electrocatalytic Reduction on Nickel Single-Atom Catalyst,* Joule **3**, 265 (2019).

[6] T. Burdyny and W. A. Smith, *CO2 reduction on gas-diffusion electrodes and why catalytic performance must be assessed at commercially-relevant conditions,* Energy & Environmental Science **12**, 1442 (2019).

[7] R. B. Kutz, Q. Chen, H. Yang, S. D. Sajjad, Z. Liu, and I. R. Masel, *Sustainion Imidazolium-Functionalized Polymers for Carbon Dioxide Electrolysis,* Energy Technology **5**, 929 (2017).

[8] B. Endrődi, E. Kecsenovity, A. Samu, T. Halmágyi, S. Rojas-Carbonell, L. Wang, Y. Yan, and C. Janáky, *High carbonate ion conductance of a robust PiperION membrane allows industrial current density and conversion in a zero-gap carbon dioxide electrolyzer cell,* Energy and Environmental Science **13**, 4098 (2020).

[9] G. O. Larrazábal, P. Strøm-Hansen, J. P. Heli, K. Zeiter, K. T. Therkildsen, I. Chorkendorff, and B. Seger, *Analysis of Mass Flows and Membrane Cross-over in CO2 Reduction at High Current Densities in an MEA-Type Electrolyzer,* ACS Applied Materials and Interfaces **11**, 41281 (2019).

[10] J. A. Rabinowitz and M. W. Kanan, *The future of low-temperature carbon dioxide electrolysis depends on solving one basic problem,* Nature Communications **11**, 10 (2020).

[11] J.-B. Vennekötter, T. Scheuermann, R. Sengpiel, and M. Wessling, *The electrolyte matters: Stable systems for high rate electrochemical CO2 reduction,* Journal of CO2 Utilization **32**, 202 (2019).

[12] M. Lin, L. Han, M. R. Singh, and C. Xiang, *An Experimental- And Simulation-Based Evaluation of the CO2 Utilization Efficiency of Aqueous-Based Electrochemical CO2 Reduction Reactors with Ion-Selective Membranes,* ACS Applied Energy Materials **2**, 5843 (2019).

[13] D. A. Vermaas, S. Wiegman, T. Nagaki, and W. A. Smith, *Ion transport mechanisms in bipolar membranes for (photo)electrochemical water splitting,* Sustainable Energy and Fuels **2**, 2006 (2018).

[14] Y. C. Li, D. Zhou, Z. Yan, R. H. Gonçalves, D. A. Salvatore, C. P. Berlinguette, and T. E. Mallouk, *Electrolysis of CO2 to Syngas in Bipolar Membrane-Based Electrochemical Cells,* ACS Energy Letters **1**, 1149 (2016).

[15] X. Wang, W. Conway, R. Burns, N. McCann, and M. Maeder, *Comprehensive study of the hydration and dehydration reactions of carbon dioxide in aqueous solution,* Journal of Physical Chemistry A **114**, 1734 (2010).

[16] M. A. Blommaert, R. Sharifian, N. Shah, N. T. Nesbitt, W. A. Smith, and D. A. Vermaas, *Orientation of bipolar membrane determines the dominant ion and carbonic species transport in membrane electrode assemblies for CO2 reduction,* Journal of Materials Chemistry A **9**, 11179 (2021).

[17] R. Sharifian, M. Wagterveld, I. A. Digdaya, C. Xiang, and D. A. Vermaas, *Electrochemical carbon dioxide capture to close the carbon cycle,* Energy & Environmental Science **14**, 781 (2021).

[18] Y. Chen, A. Vise, W. E. Klein, F. C. Cetinbas, D. J. Myers, W. A. Smith, W. A. Smith, W. A. Smith, T. G. Deutsch, and K. C. Neyerlin, *A Robust, Scalable Platform for the Electrochemical Conversion of CO2 to Formate: Identifying Pathways to Higher Energy Efficiencies,* ACS Energy Letters **5**, 1825 (2020).

[19] D. A. Salvatore, D. M. Weekes, J. He, K. E. Dettelbach, Y. C. Li, T. E. Mallouk, and C. P. Berlinguette, *Electrolysis of Gaseous CO 2 to CO in a Flow Cell with a Bipolar Membrane,* ACS Energy Letters **3**, 149 (2017).

# SUMMARY

Electrochemistry can be a useful technology to enable the transition toward renewable energy sources and to prevent further climate change. Some electrochemical applications are already industrially implemented, like water electrolysers, while others, like $CO_2$ reduction, need further development to be industrially competitive. Here, a bipolar membrane can provide the conditions for a step forward. It will not only separate (gaseous) products from the two electrodes in an electrochemical cell, but it will also allow the use of different pH and electrolyte at either side. This enables optimization of electrode compartments. As it is composed of a cation and anion exchange layer, no ion transport can theoretically occur across the entire membrane. To still provide the required charge transport, the BPM can dissociate water at the interface layer of the BPM, where often a catalyst is deposited to enhance this reaction.

An ideal bipolar membrane has highly conductive membrane layers, fast kinetics at the interface layer and therefore high water permeability to the interface, a long lifetime, and a low ion crossover. As the BPM can be implemented in various electrochemical energy applications, like water and $CO_2$ electrolysis, batteries, fuel cells and resource recovery, different specific requirements exist per application. For batteries and resource recovery a low ion crossover is crucial, while for fuel cells, water and $CO_2$ electrolysis fast kinetics are essential. Hence, for each application a specifically developed BPM is required for future applications. The development should be based on knowledge gained by studying the performance of BPMs in these conditions with techniques like electrochemical impedance spectroscopy.

Electrochemical impedance spectroscopy was used to study the resistance contribution in a bipolar membrane, allowing to differentiate the different components of the membrane. At the interface between the two membrane layers, which was of main interest, the water dissociation reaction was studied at various current densities. Interestingly, the electrochemical impedance response was different depending on the surrounding electrolytes. Therefore, two cases were studied; with and without co-ions. When co-ions were present, the i-V curve showed a plateau current density. With impedance, we showed that the environment changes once the plateau current density is passed, the ion transport is no longer dominated by co-ion transport but water dissociation starts to occur instead. The presence of the co-ions also has a reducing effect on the ageing of the BPM, which was successfully monitored via impedance spectroscopy.

Co-ion transport across the BPM reduces the efficiency of the water dissociation. This transport also reduces the stability of the electrolytes. Thus, the ion crossover of surrounding electrolytes can hamper the BPM. The crossover is affected by voltage, current density, pKa, valence, and ion size. Via these parameters, control over ion crossover is achieved. While at low current densities, diffusion is dominant, migration takes over at high current densities. However, the relative crossover compared to the total charge becomes very low at industrially relevant conditions. Also electrolytes with a high valence have a low ion crossover. Electrolytes with a high ion size also reduces the crossover, but that often comes at the expense of lower conductivity.

To study the effect as a function of the orientation of a bipolar membrane on the transport mechanisms of ions and carbonic species, a novel membrane electrode assembly was created. In this assembly, a catalyst was directly deposited on the membrane layer, which was exposed to gaseous $CO_2$. Two assemblies were made, one where the BPM was orientated in reverse bias, while the other was in forward bias. The dominant transport mechanism in the reverse bias case is water dissociation. While in the forward bias case the transport leads to a neutralization of ionic species at the internal layer. The orientation of the BPM leads to trade-offs with regards to potential, selectivity, and stability. Although in the forward bias case a significantly lower cell voltage can be achieved, the product selectivity tipped towards hydrogen production after 10 minutes and a higher salt accumulation at the catalyst was seen. The reverse bias case, which suffered more from $CO_2$ crossover, maintained a steady equal carbon monoxide and hydrogen production.

To compare the bipolar membrane to an anion exchange membrane, which is the benchmark in $CO_2$ electrolysis, an experimental study was established in a membrane electrode assembly. As expected, the total cell voltage of the AEM-run cell was lower than with the BPM, but the crossover of $CO_2$ through the AEM led to a poor stability of the electrolyte. The BPM, due to its water dissociation capabilities, mitigated the $CO_2$ crossover to the anode. Despite the $CO_2$ loss in the AEM, the required energy to produce carbon monoxide was lower than the BPM-run cell, due to the low product selectivity of the BPM-run cell. Future work should aim to increase that selectivity, by modifying the cathode interface, up to the same values as the AEM-run cell as the required energy would then reduce by more than 20%.

# SAMENVATTING

Elektrochemie kan een nuttige technologie zijn om de energietransitie naar hernieuwbare energie bronnen mogelijk te maken en zo verdere klimaatopwarming te voorkomen. Sommige elektrochemische toepassingen, zoals water elektrolyse, worden al toegepast in de industrie. Andere toepassingen, zoals $CO_2$ reductie, hebben verdere ontwikkeling nodig om concurrerend te zijn op industrieel vlak. Bij elektrochemie gebeurt er een chemische verandering door toevoeging van elektrische energie. Omgekeerd is het ook mogelijk om energie te creëren door een chemische verandering. Voor elektrochemie heb je minimaal twee elektroden en een ionengeleider (elektrolyt) nodig. Reacties vinden plaats waar de elektroden en het elektrolyt contact hebben. Bij twee elektroden zijn er ook twee reacties. Helaas is het moeilijk om de ideale omstandigheden voor een reactie te creëren in zo'n cel, omdat die verschillen per reactie. Een bipolair membraan (BPM) kan echter wel de juiste condities voorzien om in ideale omstandigheden te werken. Dit type membraan bestaat uit twee tegengestelde geladen membraanlagen. Aangezien het opgebouwd is uit een kationen- en anionen-uitwisselingslaag, kan er theoretisch geen transport van ionen gebeuren doorheen het hele membraan. Hierdoor zal het niet alleen (gasvormige) producten van de twee elektrodes in een elektrochemische cel scheiden, het laat ook toe om verschillende pH's en elektrolyten aan beide zijden te gebruiken. Om toch het benodigde ladingstransport te voorzien, kan het BPM water dissociëren aan de contactlaag tussen de twee lagen van het BPM, waar vaak een katalysator is geplaatst om de water dissociatie reactie te bevorderen.

Een ideaal bipolair membraan heeft lagen met een hoge geleidbaarheid voor de ionen, snelle kinetiek aan de contactlaag voor de water dissociatie en daarom een hoge water permeabiliteit (voor het transport van water), een lange levensduur, en een lage ion overdracht (doorheen het hele membraan). Als het BPM geïmplementeerd wordt in verschillende elektrochemische energie toepassingen, zoals water en $CO_2$ elektrolyse, batterijen, fuel cells (brandstofcellen) en resource recovery (herstellen van grondstoffen), zijn er verschillende specifieke benodigdheden per toepassing. Voor batterijen en resource recovery is een lage ion overdracht cruciaal, terwijl voor fuel cells, water en $CO_2$ elektrolyse snelle kinetiek essentieel zijn. Daarom is het nodig dat er voor elke toepassing een specifiek BPM wordt ontwikkeld, zoals beschreven staat in Hoofdstuk 2. Om hiervoor de juiste kennis op te bouwen heb ik tijdens mijn onderzoek BPMs in verschillende omstandigheden bestudeerd met technieken zoals elektrochemische impedantie spectroscopie.

In Hoofdstuk 3 staan de resultaten van onze studie met elektrochemische impe-

dantie spectroscopie naar de weerstand verdeling in het bipolair membraan. Deze techniek laat toe om tussen de verschillende componenten van het membraan te differentiëren, denk hierbij aan de weerstand van de membraanlagen, als ook de kinetiek voor de water dissociatie of de interactie tussen de co-ionen van het elektrolyt en de membraanlaag. Met co-ionen wordt hier verwezen naar alle ionen die geen product zijn van de waterdissociatie reactie (proton en hydroxide ionen). Op het contact tussen de twee membraanlagen, voor ons het interessantste, werd de waterdissociatie reactie bestudeerd op verschillende stroomdichtheden. Bijzonder was dat de resultaten afhingen van de omgevende elektrolyten. Daarom werden twee casussen bestudeerd; met en zonder co-ionen. Wanneer co-ionen aanwezig waren, vertoonde de i-V curve een plateau stroomdichtheid. Met impedantie, toonden we aan dat de omgeving veranderde eenmaal de plateau stroomdichtheid is gepasseerd. Het ionentransport wordt dan niet langer gedomineerd door co-ion transport maar juist door water dissociatie. De aanwezigheid van de co-ionen heeft ook een vertragend effect op het verouderen van het BPM, wat we succesvol konden observeren via impedantie spectroscopie.

Het transport van co-ionen doorheen het membraan vermindert de efficiëntie van de waterdissociatie. Dit zorgt dan voor een vermindering van de stabiliteit van de elektrolyten. Dus, ionoverdracht van de omgevende elektrolyten kan de prestaties van het BPM belemmeren. Daarom bestuderen we in Hoofdstuk 4 hoe de overdracht van ionen beïnvloed wordt door voltage, stroomdichtheid, pKa, valentie, en ion grootte. Via deze parameters is controle over ionoverdracht bereikt. Terwijl op lage stroomdichtheden diffusie dominant is, neemt migratie over op hoge stroomdichtheden. Echter, de relatieve overdracht in vergelijking met de totale lading wordt erg klein op industrieel relevante condities. Ook elektrolyten met een hoge valentie hebben een lage ion overdracht. Elektrolyten met een hoge ion grootte verminderen de overdracht ook, maar dat gaat vaak hand in hand met een lagere geleiding.

Aangezien het bipolair membraan bestaat uit twee tegengestelde membraanlagen, krijg je verschillende mechanismes. In reverse bias is de kationen uitwisselingslaag gericht naar de cathode en is er een transport vanuit het membraan naar buiten, bij forward bias is die laag gericht naar de anode en is het transport gericht naar binnen het membraan. Om het effect van de functie van de oriëntatie van het bipolair membraan te bestuderen op het transport mechanisme van ionen en koolzuur, werd een nieuw membraan-elektrode-montage gecreëerd. De resultaten van onze studie zijn gepresenteerd in Hoofdstuk 5. In deze montage, was een katalysator direct op de membraan laag aangebracht, die was blootgesteld aan het gasvormige $CO_2$. Twee montages werden gemaakt, een waar het BPM georiënteerd was in reverse bias, de andere in forward bias. Het dominante transportmechanisme in de reverse bias geval is waterdissociatie. Terwijl in het forward bias geval, transport resulteert in een neutralisatie van ionen aan de interface laag. De oriëntatie van

het BPM leidt tot afwegingen met betrekking tot voltage, selectiviteit en stabiliteit. Hoewel in de forward bias montage een aanmerkelijk lagere cel voltage werd bereikt, was de product selectiviteit na 10 minuten uitsluitend waterstofproductie en er werd meer zout accumulatie op de katalysator opgemerkt. De reverse bias montage, waarin meer $CO_2$ overdracht plaatsvond, had een stabiele gelijke koolstof monoxide en waterstof productie.

Om een bipolair membraan te vergelijken met een anion exchange membrane (anionen uitwisselingsmembraan, AEM), die de maatstaf is in $CO_2$ elektrolyse, is een experimentele studie uitgevoerd in een membraan-elektrode-montage, zie Hoofdstuk 6. Zoals verwacht, het totale cel voltage van een AEM cel was lager dan van een BPM cel, maar de overdracht van $CO_2$ doorheen het AEM leidde tot een lage stabiliteit van het elektroliet. Door de waterdissociatie capaciteiten, voorkwam het BPM die $CO_2$ overdracht tot de anode. Ondanks de verliezen van $CO_2$ in de AEM was de benodigde energie om koolstof monoxide te produceren lager dan in de BPM cel, vanwege de lage selectiviteit van het product van de BPM cel. De focus van toekomstig werk moet zich daarom richten op het verhogen van die selectiviteit. Dit kan door de kathode interface te veranderen, om vergelijkbare waardes met de AEM cel in omzetting van $CO_2$ te bereiken met als resultaat dat de benodigde energie 20% lager zou zijn.

# ACKNOWLEDGEMENTS

It is with mixed feelings that I start writing this section. On the one hand I feel emotional that my PhD journey is coming to an end, while on the other hand I realise all the lessons I learned, experiences I went through and people I got to know have made me a better person. This is something I will take with me as new adventures are awaiting. But before that, it goes without saying that I couldn't have done it without a significant number of people. Like Kailun once said while helping out with an experiment: 'I might not be able to help you reaching your PhD defense, but I can bring it one day closer', and many other people did so too, which has brought us here today and I would like to thank you all for that.

**Wilson** and **David**, thank you for supervising me throughout my PhD. Both of you share the same sense of perfectionism that enables to go further in a scientific project, which has led to these interesting articles.
Wilson, thank you for me believing in me from day one. You enabled my transition from engineer to scientist by always triggering me in asking scientific questions, while still encouraging me to follow my engineering gut. I really enjoyed our biweekly meetings. Often I would walk out with enormous positive energy after hearing you talk of all the endless possibilities we could investigate, which has also led to the different topics that we have addressed in this thesis. You have also taught me some valuable life lessons. Like a guy with a tattoo in his face once said: 'Everybody has a plan, until they get punched in the face', which we both did by prioritising our families when it was needed. I will cherish the fun moments we had on the summer course at DTU and at NREL and MRS. Thank you for learning to always look at the bigger picture.
David, thank you so much for your help throughout these years. You were always there to help me in the lab, find hypotheses or use your excellent knowledge on membranes to explain what initially seemed like odd results. In these years I have also seen you grow in your supervisor role as you are now leading a blossoming group and I am grateful that I was a part of that. Not only were you always supportive in the lab, you even helped me renovating my kitchen! Thank you for always expecting the best of me.

I also want to extend my gratitude to the committee (**Dr. Andreu**, **Prof. Van Der Bruggen**, **Prof. Urakawa**, **Prof. Padding** and **Prof. Koper**). Thank you for being a part of this PhD defense and assessing my work. Further, I would also like to thank the members of the DISCO project, especially **Ben** for the heart warming welcome I received whenever I was in need of help and visited Shell Amsterdam. Thank you

for all the fun lunches! **Giulia** and **Thierry**, thank you for your interest during the DISCO meetings and fun moments in between. I am glad that some of our results are continued to be used, thank you for that **Andrey** and I'm sure you'll do a good job.

The MECS-group also deserves a big thank you, I really enjoyed the group meetings but especially the coffee breaks and our Wednesday afternoon borrels. The group has changed a lot over the last few years and so I'll name only a few here. First to be thanked are my paranymphs, **Nienke** and **Sanjana**. You were always there when I needed help or a break. Nienke, thank you for giving me a real-life example of a model PhD student; working 8-to-5 hours from monday to friday and leaving your laptop behind at work, which is something I never managed. But of course also a big thank you for being my PhD mentor and asking me to join on two beam travels to Grenoble. Sanjana, as we both started our PhD at the same day (You one hour later!), you were like a sister to me and I am happy we had so many fun moments. Next on the list of surely to be thanked are **Herman** and **Joost**, the comical technician duo. I have learnt a great deal about the Dutch culture thanks to our breaks. You were always very helpful in the lab. I definitely learnt now how to ask a specific need or requirement (no more 'I need this tool to close this metal thingy with a fixed strength', a.k.a. a torque wrench). Thank you **Bernard** and now **Fokko** for leading the MECS group impeccably and always have your door open for questions and comments. Also **Noortje**, **Rajshree**, **Roos** and the other management assistants have been of great help throughout my PhD.
Thank you to my office mates: **Nienke**, **Fahimeh** (thank you for introducing me to the Persian culture), **Kai**, **Erdem** and **Hugo** (thank you for the filming). Also thank you to the members of the P3T group: **Wilson**, **Bernard**, **Divya**, **Anirudh** (thank you for the fun beam travels together with Nienke), **Sanjana**, **Kailun** (thank you for the badminton), **Tom**, **Nate**, **Recep**, **Mark**, and later **Erdem**, **Hugo**, **Siddhartha**, **Maryam** and **Aaron**. Tom, thank you for your friendship throughout the years, you had to take up a lot of responsibility but still managed to be there for everyone. The group is in good hands.
A big thank you also goes to the students that I supervised during their BSc or MSc thesis: **Mark**, **Boaz**, **Joost**, **Victor** and **Namrata**. I enjoyed working together and have learnt a lot from supervising your projects. Good luck in your future endeavours.

As a bipolar membrane expert, it is not more than logic to have two different research groups (although not oppositely charged), so I would also like to thank the TP group for their openness and interest in my research. Especially the EFS group deserves a big thank you: **David**, **Christiaan**, **Evert**, **Duco**, **Lorenz**, **Rose**, **Kosta**, **Matthäa**, **Jorrit**, **Nathalie**, **Andrey** and **Minu**. Rose, thank you for your kindness and bringing joy to our meetings, I love that you are always smiling! Jorrit, you started just over a year ago but you quickly became a good friend. I love that you

always have a good story up your sleeve. With your enthusiasm and fun activities you helped EFS to bond, even via Zoom-meetings. Keep up the good work and don't forget to once in a while think about the bigger picture.

A number of people also helped me to relax outside of work. Thank you **Tom Sassen**, **Danny** and **Ingrid** for the great evenings at bouwpub or playing board games. Merci beaucoup, Ingrid, pour tout les pauses et soirées. Thank you **Thijs**, for all the fun evenings in Delft, it is always nice hanging out with you! Also my great climbing friends cannot be left out this list: **Nienke**, **Peter**, **Nate**, **Katie**, **Giorgio** and later **Joram**. Thank you for all the boulder and top-rope sessions, trips to the Ardennes and of course the summum of our adventures, one week of climbing in Kalymnos, Greece. Last but not least in the leisure category, all my teammates from FC Tutor, thank you for all the futsal games and evenings afterwards at X or de Kurk!

En dan nu een paar woordjes in het Nederlands. Ik zou graag mijn vrienden willen bedanken om er te zijn voor mij de enkele keren dat ik de grens overstak terug naar België. De bean bag boys (**Tom**, **Sibren**, **Pepijn**, **Lucas** and **Toon**), mijn MSc thesis compagnons (**Ans** and **Charlotte**), het stenen tijdperk (**Bob**, **Loïc**, **Laurens**, **Hendrik** en de rest natuurlijk ook!), ons fietsgroepje (**Stefan**, **Robin**, **Jeroen**, **Jef**); bedankt allemaal!

Ook wil ik graag de familie Haers bedanken. **Jan**, je positivisme en sterke focus op het genieten van het leven zouden een voorbeeld moeten zijn voor iedereen. Enorm bedankt voor de interessante documenten over hernieuwbare energie. **Ludovic** en **Lorenz**, bedankt voor jullie hartelijke verwelkoming bij jullie thuis. Op nog vele mooie momenten samen!

**Hester**, bedankt voor je eeuwige steun en mij al op jonge leeftijd warm te maken voor een ecologische levensstijl, dit heeft er zeker ook aan toe bijgedragen om dit onderzoek te gaan doen. **Eline**, bedankt om de lat altijd erg hoog te leggen en mij te helpen met de keuze van een kleurenschema voor mijn figuren. **Opa**, bedankt voor de fijne telefoongesprekken het afgelopen jaar, daar heb ik erg van genoten. **Mama** en **Papa**, bedankt voor jullie hulp de voorbije jaren en bij deze thesis om bepaalde stukken na te lezen. Natuurlijk ook bedankt voor alle verwennerij in Heverlee! Ik ben blij dat ik jullie advies heb opgevolgd en naar Delft ben gekomen om dit onderzoek te voeren. Tenslotte wil ik ook **Anna** bedanken. Al jaar en dag ben je mijn beste maatje, en ik kan je niet genoeg bedanken voor alle steun die je me hebt geboden doorheen mijn doctoraat. Ik kan niet wachten om te ontdekken welke avonturen ons te wachten staan!

*Marijn*
*Delft, 19-08-'21*

# CURRICULUM VITÆ

## Marijn Antoon BLOMMAERT

| | |
|---|---|
| 09-11-1994 | Born in Delft, the Netherlands |
| 2012–2015 | BSc in Engineering Science<br>KU Leuven, Belgium |
| 2015–2017 | MSc in Engineering Science cum laude<br>Chemical Engineering Techniques<br>in Chemical and Biochemical Process Engineering<br>KU Leuven, Belgium |
| 2015 | Erasmus+ (UP de Madrid, Spain) |
| 2017-2021 | PhD in Chemical Engineering<br>Faculty of Applied Sciences<br>Delft University of Technology, the Netherlands<br>*Thesis:* Ion Transport Mechanisms in Bipolar Membranes for Electrochemical Applications<br>*Promotor:* Dr. W.A. Smith<br>*Copromotor:* Dr.ir. D.A. Vermaas |

# List of Publications

10. **Blommaert, M.A.**; Aili, D.; Tufa, R.A.; Li, Q.; Smith, W.A.; Vermaas, D.A. *Insights and Challenges for Applying Bipolar Membranes in Advanced Electrochemical Energy Systems.* ACS Energy Lett., **6**, 2539–2548 (2021)

9. **Blommaert, M.A.**; Sharifian, R.; Shah, N.; Nesbitt, N.T.; Smith, W.A.; Vermaas, D.A. *Orientation of bipolar membrane determines the dominant ion and carbonic species transport in membrane electrode assemblies for $CO_2$ reduction.* J. Mater. Chem. A, **9**, 11179 (2021).

8. Sharifian, R.; **Blommaert, M.A.**; Bremer, M.; Wagterveld, R.M.; Vermaas, D.A. *Intrinsic bipolar membrane characteristics dominate the effects of flow orientation and external pH-profile on the membrane voltage* J. Membr. Sci., doi: 10.1016/j.memsci.2021.119686 (2021)

7. Tufa, R.A.; **Blommaert, M.A.**; Chanda, D.; Li, Q.; Vermaas, D.A.; Aili, D. *Bipolar Membrane and Interface Materials for Electrochemical Energy Systems* ACS Appl. Energy Mater., doi: 10.1021/acsaem.1c01140 (2021)

6. **Blommaert, M.A.**; Verdonk, J.A.H.; Blommaert, H.C.B.; Smith, W.A.; Vermaas, D.A. *Reduced Ion Crossover in Bipolar Membrane Electrolysis via Increased Current Density, Molecular Size, and Valence.* ACS Appl. Energy Mater., **3**, 5804-5812 (2020).

5. **Blommaert, M. A.**; Vermaas, D. A.; Izelaar, B.; in 't Veen, B.; Smith, W. A. *Electrochemical impedance spectroscopy as a performance indicator of water dissociation in bipolar membranes.* J. Mater. Chem. A, **7**, 19060-19069 (2019).

4. Firet, N.J.; **Blommaert, M.A.**; Burdyny, T.; Venugopal, A.; Bohra, D.; Longo, A.; Smith, W.A., *Operando EXAFS Study Reveals Presence of Oxygen in Oxide-Derived Silver Catalysts for Electrochemical $CO_2$ Reduction.* J. Mater. Chem. A, **7**, 2597-2607 (2019).

3. Firet, N.J.; Venugopal, A.; **Blommaert, M.A.**; Cavallari, C.; Sahle, C.J.; Longo, A.; Smith, W.A., *Chemisorption of anionic species from the electrolyte alters the surface electronic structure and composition of photocharged $BiVO_4$.*, Chem. Mater., **31**, 7453-7462 (2019).

2. **Blommaert, M.A.**; Subramanian, S.; Yang, K.; Smith, W.A.; Vermaas, D.A. *High indirect energy consumption in AEM-based $CO_2$ electrolyzers demonstrates the potential of bipolar membranes* (in preparation)

1. Yang K.; Li, A; Subramanian, S.; **Blommaert, M.A.**; Smith, W.A.; Burdyny, T. *Enhanced $CO_2$ utilization driven by cation during electrochemical $CO_2$ reduction in bipolar membrane electrode assembly* (in preparation)